ABSTRACT

WESSELS, LAURA RENE. A Fluorescence Microscopy Study of the Dynamics of Low-pH Triggered Membrane Fusion. (Under the Direction of Assistant Professor Keith Weninger.)

Enveloped viruses employ membrane fusion during cell penetration in order to deliver their genetic material across the cell boundary. Large conformational changes in the proteins embedded in the viral membrane play a fundamental role in the membrane fusion process. Despite the tremendously wide variety of membrane containing viruses, it appears they all contain membrane fusion protein machinery with a remarkably conserved mechanism of action. The purpose of the research in this dissertation was to experimentally observe real time dynamic membrane fusion using fluorescence microscopy. An *in vitro* assay fusing viral membranes to supported lipid bilayers, triggered by the exposure to low pH and visualized with fluorescent dye molecules, was developed to observe viral membrane fusion. Studies of influenza and Sindbis virus were conducted with this assay. The intermediate structures of membrane fusion are too small to be spatially resolved with an optical microscope due to the diffraction limit, however fluorescence dequenching of dye molecules inserted into the viral membrane/lipid membrane system can provide information about the dynamics of membrane fusion as well as providing insight into the sequence of conformational changes of the lipid bilayer. Effects of adding the dye labels to the viruses are also investigated.

A fluorescence microscopy study of the dynamics of low-pH triggered Membrane Fusion

by
Laura Wessels

A dissertation submitted to the Graduate Faculty of
North Carolina State University
In partial fulfillment of the
Requirements for the Degree of
Doctor of Philosophy

Physics

Raleigh, North Carolina

2009

APPROVED BY:

Dennis Brown	Laura Clarke
Celeste Sagui	Keith Weninger Chair of Advisory Committee

DEDICATION

EJW II R.I.P.

BIOGRAPHY

Laura Wessels was born in Virginia. She received her Bachelor's degree in Physics and Mathematics from the University of Mary Washington in Fredericksburg, Virginia. She received her Master's degree in Mechanical Engineering from Vanderbilt University in Nashville, Tennessee.

ACKNOWLEDGEMENTS

I would like to thank my mother who instilled in me early on the desire to obtain the highest level of education possible. I would like to thank my father for being mellow. I would like to thank my adviser, Keith Weninger, whose help and insight allowed me to complete this work. I would also like to thank Raquel Hernandez and Dennis Brown for their assistance in the virus project. I would like to thank my friends Trey Walker and Matt Kerr for their compassion on rough days. Finally I would like to thank my brother for serenity.

TABLE OF CONTENTS

LIST OF TABLES

LIST OF FIGURES

INTRODUCTION

1.1 Motivation

Membrane fusion is the process whereby two lipid bilayers merge into a single continuous bilayer. Membrane fusion occurs in many biological situations including the entry of many viruses into cells. Much remains to be learned about viral membrane fusion. In order for a virus to replicate it must undergo fusion either at the cell surface or within the cell. Understanding of viral membrane fusion is of fundamental interest in science, because the mechanism is likely similar to other cellular membrane fusion phenomena, which are critical to life.

A virus reproduces by infecting cells & using the cell's machinery to replicate its genetic material. That genetic material is contained in a protective protein coat called a capsid, which may also be encased by a viral (lipid) membrane. In order for the genetic material to get into the cell it must pass both the viral membrane & the cell membrane. This can be achieved through membrane fusion. It has been established that enveloped viruses have highly efficient fusion proteins, but currently it is unclear precisely how membrane proteins mediate membrane fusion. Viral systems are some of the best-studied membrane fusion protein machines. In particular, enveloped viruses fusing to protein-free bilayers has allowed characterization of many biochemical properties of viral fusion.

The focus in this research is on the fusion between enveloped viruses and lipid bilayers. A better understanding of viral membrane fusion has potential applications in design of anti-virals for viruses that currently have no obstacles to infection or that mutate quickly, causing current anti-viral medications to lose their effectivity for halting the spread

of the virus. Single molecule imaging via total internal reflection fluorescence microscopy (TIRFM) is a relatively new technique, developed in the early 80's by Daniel Axelrod,(Axelrod 1989) that uses the total internal reflection of light to illuminate a ~200 nm depth beyond a glass-water interface. The intensity drops off exponentially away from the interface, thus background is reduced because fluorescent dye molecules beyond the thin layer at the surface cannot be seen. For this reason, TIRFM is the preferred method for single-molecule fluorescence imaging of plasma-membrane associated processes. The goal of the *in vitro* studies in this thesis of the fusion of viral membranes to lipid membranes using TIRFM is to image merging of lipid membranes followed by delivery of the viral DNA/RNA core. These measurements should provide information on specific lipids required for membrane fusion, time constants for the steps of membrane fusion and environmental factors necessary for membrane fusion to occur. System requirements as such experimental setups and biological probes useful in membrane fusion will also be determined.

1.2 Introduction to Membrane Fusion

Membrane fusion is a vital phenomenon that allows eukaryotic cells to transfer materials among their membrane-encased compartments. Biological membranes do not spontaneously fuse under normal physiological conditions, so proteins are critical to mediate biological instances of membrane fusion. Eukaryotic cells have a highly conserved system of proteins known as SNAREs (soluble N-ethylmaleimide-sensitive factor (NSF) attachment protein (SNAP) receptor) that control intracellular membrane fusion.(Brunger 2005; Jahn and Scheller 2006; Sudhof and Rothman 2009) Fertilization, fusion of mitochondria and cell-cell fusion processes during development each use distinct proteins for membrane fusion.(Chen

and Olson 2005; Hoppins and Nunnari 2009; Wassarman and Litscher 2008) One of the most easily studied biological occurrences of membrane fusion is infection of a cell by an enveloped virus.(Dimitrov 2004; Earp and others 2005; Lakadamyali and others 2003; Marsh and Helenius 2006; Sieczkarski and Whittaker 2005) Enveloped viruses commonly release their genomes into a cell by fusing with the plasma membrane or by fusing from within an endosome following endocytosis.

All instances of protein mediated membrane fusion require surmounting significant kinetic and energetic barriers. Membrane fusion proteins allow these barriers to membrane fusion to be traversed. The prefusion states of these proteins are metastable and are not at a global free energy minimum. The proteins mediate fusion by undergoing large conformational changes to lower energy states.(Basanez 2002; Chernomordik and Kozlov 2005; Harrison 2008)

The transition from the metastable state to the lower energy state for viral fusion proteins is triggered when a virus encounters a specific cue from a targeted cell. Viruses that undergo endocytosis by cells have evolved to use the endosomal acidification to trigger the conformational changes that lead to membrane fusion. Other viruses are triggered to fuse with the plasma membrane of cells by other signals, for example co-receptor binding. In either case, the nature of the actions of the viral fusion proteins is thought to be universal. First the proteins change into a more extended conformation that allows the exposure of a hydrophobic fusion peptide that is initially buried within the untriggered protein. This extended conformation allows the fusion peptide to insert and bury itself into an opposing membrane. Viral membrane fusion proteins are anchored in the virus membrane by a

transmembrane domain. Thus this extended, fusion-activated state, with the fusion peptide in the target membrane crosslinking the two membranes that are destined to fuse. The fusion protein then folds back on itself into a hairpin configuration, bringing the two apposing membranes into near contact. At this point a series of intermediate states is thought to form that involve various lipidic structures including a hemifusion stalk, a single bilayer diaphragm, and a fusion pore. The free energy of these intermediate structures depends on their geometry, the properties of the lipids in the membranes, the interactions of the lipids with the transmembrane domain and the fusion peptide of the proteins, and may be aided by cooperativity between several fusion proteins. (Chernomordik and Kozlov 2008; Martens and McMahon 2008; White and others 2008) The opening of the fusion pore allows the genetic material of the virus to enter the cell to initiate a possible infection. X-ray crystallography, electron microscopy, biochemical assays, genetic assays, computational/theoretical modeling and fluorescence microscopy have all contributed to this general picture of the process of viral fusion.

1.3 Fusion Protein Structure

Conformational changes are governed by the forces that control folding of proteins.(Nelson 2004) Proteins on the viral membrane that change shape at low pH are believed to aid in the fusion process. Proteins are made up of an oriented sequence of animo acids that start with an amino (N-) terminus and end with a carboxyl (C-) terminus. In general viral fusion proteins have a receptor binding site (HA1 in influenza) (Skehel and Wiley 2000) and a transmembrane subunit (HA2 in influenza). The surface subunit binds to protein receptors on cells. The transmembrane subunit includes a short sequence of

approxiamately 20 nonpolar amino acids that are can insert into the cell's membrane when exposed. This domain is known as the fusion peptide. The fusion peptide is sequestered on the interior of the fusion protein until the fusion process is activated by conformational changes induced by low pH exposure. Free energy is released at each conformational step during the protein rearrangements. These steps include extension of the N-terminal away from the viral surface, bending of the fusion protein into a hairpin and the transition to the final stable conformation. Free energy released in each of these steps can be coupled to the membrane to yield lipid rearrangements within the viral and cell membrane allowing for hemifusion, pore formation and pore enlargement.

Viral membrane proteins all share some common features. All are integral membrane proteins with transmembrane domains anchoring them in the viral envelope. Domains inside the virus particle adjacent to the transmembrane domain are often involved in virus particle assembly, but appear to play no significant role in membrane fusion. The larger, external domains of the viral fusion proteins fall into three classes of common structural paradigms, leading to the classifications class I, class II or class III (described below). Regardless of the class, a common feature of the external domains is the presence of a fusion peptide, which is essential for function. Critical interplay between the lipids in the bilayers, the transmembrane domains of fusion proteins, the fusion peptides, and possible cooperativity among multiple fusion proteins, along with interactions with other cellular proteins are all critical to achieve the efficient membrane fusion capability characteristic of viruses.

1.3.1 Class I Fusion Proteins

The class I proteins are characterized by a central, triple-stranded coiled coil region. Other domains of the proteins wrap this central spike with an anti-parallel orientation and associate with additional fusion protein molecules to form a homotrimeric helical hairpin assembly. High-resolution crystallographic studies of the class I fusion glycoproteins from influenza (HA)(Skehel and Wiley 2000), retroviruses (gp41 from Human immunodeficiency virus (HIV)(Freed and others 1990) and Simian immunodeficiency virus (SIV)(Yang and others 1999) and gp21 Human T-lymphotropic virus(Center and others 1998)) and gp2 from Ebola virus(Weissenhorn and others 1998) have all revealed similar structures. Class I proteins commonly exist on virus particles as trimeric spikes extending away from the particle membrane. The transmembrane anchor, the glycine rich fusion peptide (varies from 10-30 amphiphilic amino acids) and the external folded domains all contribute to membrane fusion in the class I family.

Table 1.1 Class I, II and III Fusion Proteins.

	Class I	**Class II**	**Class III**
Secondary Structure of Fusion Proteins(Martens and McMahon 2008)	Mainly α–helical	Mainly composed of β–sheets	Mixed secondary Structure
Location of Fusion Peptide(White and others 2008)	Mainly located on N-terminal	Located internally	Located internally
Fusion Peptide Structural Flexibility(Weise and Reed 2008)	Yes, between α–helix and random coil/turn structure	No, stable random coil & turn structure	Yes, between α–helix and random coil/turn structure
Post Fusion Structure(White and others 2008)	Trimer of hairpins	Trimer of hairpins	Trimer of hairpins

Influenza HA is a prototype for the class I fusion proteins due to the large body of research completed with this protein. It is responsible for much of our present knowledge of viral membrane fusion. Influenza particles bind to receptors on the exterior of a cell and then undergo endocytosis. Influenza has two proteins on its surface, haemagglutinin (HA) and neuraminidase (NA). Influenza's viral fusion protein HA has been well characterized thanks to x-ray crystallography of three separate HA conformations relevant to the fusion process. For this reason it has become the universal model for membrane fusion and a synthetic protein, sequentially designed and produced with heptad repeats containing hydrophobic residues at specific locations, has been designed that mimics HA's form and function.(Kashiwada and others 2008)

Influenza's viral membrane contains on average 375 HA spikes per virion with an average diameter of 120 nm. Influenza has intrinsic structural variability meaning its particles can appear spherical, elongated and in different sizes. The glycoproteins are closely but irregularly packed, with an average distance of 11 nm separation. The HA peptide extends approximately 12 nm out from the viral membrane surface. (Harris and others 2006) The single chain precursor, HA0 cleaves into HA1 and HA2, upon activation (Skehel and Wiley 2000) creating the amine (N-) terminus, which contains a hydrophobic region known as the fusion peptide and the (C-) terminus. The C-terminus anchors into the viral membrane. Once cleaved into subunits additional conformational changes take place in the transmembrane subunit leading to a state of metastability. HA1 and HA2 compose the metastable neutral pH conformation of HA found on mature virus, i.e. the prefusion conformation. Terminal sialic acids of glycoproteins and glycolipids (i.e. gangliosides) are

the cellular receptors for influenza. The hydrogen bonds and van der Waals contacts between sialic acid and the carbohydrate side chains of HA1 bind influenza to the cell. (Bergelson and others 1982; Carroll and others 1981)

From several crystal structures of the protein at different conditions along with biochemical studies, a model of the structural dynamics of HA that lead to membrane fusion has emerged. A loop to helix transition in HA2 is suspected to project the fusion peptide 100 Å towards the endosomal membrane where it anchors irreversibly, thus creating a metastable, extended conformation in which both membranes are crosslinked by HA. Next HA2's α helix performs a reverse turn and jackknifes back relocating the C-terminal by 100 Å towards the target membrane, thus bending the molecule in half like a hairpin (figure 1.1).(Bullough and others 1994)

Specifically three monomer transmembrane subunits intertwine to form a bundle whose core is composed of three N-terminal α-helices creating a triple-stranded "coiled-coil" (figure 1.2). Each monomer bends into a hairpin, creating a trimeric hairpin. Following fusion activation, 3 C-terminal segments pack into each α-helix anti-parallel to the N-terminals, creating a 6 helix bundle (figure 1.1 D). This six helix structure has only been seen in low pH post-fusion HA, not in neutral pH, pre-fusion HA. Experimentally it has been show that this 6 helix bundle forms surprisingly late, during the meta-stable state of HA(Chernomordik and Kozlov 2003). Thus conformational changes prior to the bundle formation must bring membranes together, allowing them to merge. The energy released by the formation of the bundle is used for pore enlargement.

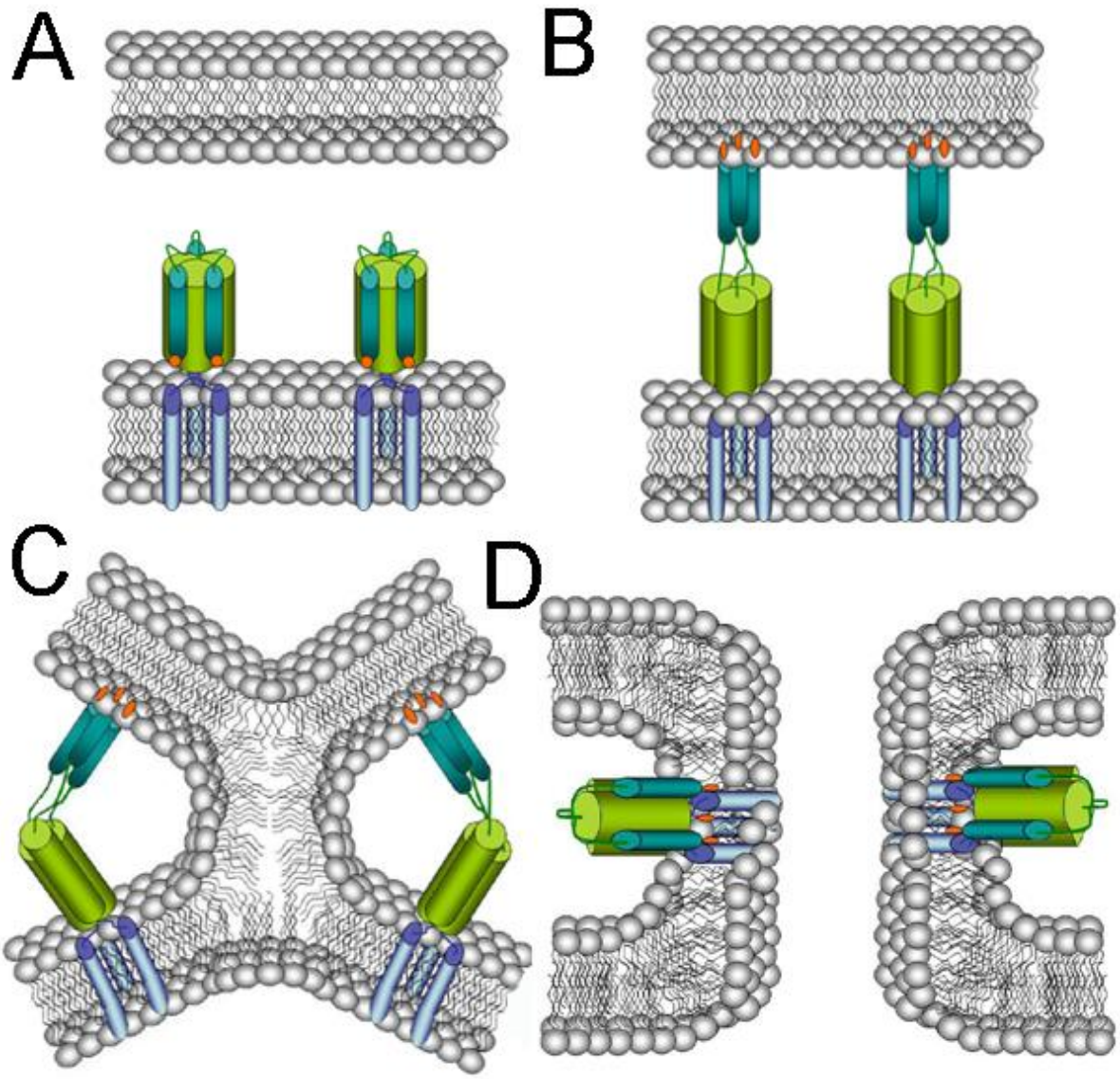

Figure 1.1 HA conformational changes. A) The trimeric membrane fusion protein spike assembly of influenza virus is anchored into the viral membrane in a pre-activated state. Shown schematically, the transmembrane domain is dark blue, the N-terminal fusion peptide is orange, the cylinders depict α-helical structures and thin lines are green cylinders. Upon acidification a hypothesized "extended intermediate" conformation is generated in which the hydrophobic fusion peptide is extended towards the targeted membrane. B) After anchoring into the endosome's membrane to crosslink the two membranes the fusion protein folds back (C.) into a hairpin positioning the transmembrane domain and fusion peptide in close proximity. D) This hairpin forces the two membranes close together and is essential for the process leading to full merging of the bilayers. Adapted from (Cohen and Melikyan 2004)

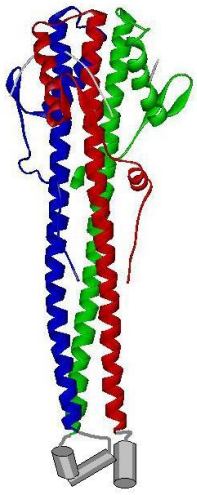

Figure 1.2. The low pH induced form of the homotrimeric influenza protein HA. The C-terminal transmembrane domains that anchor into the viral membrane are shown in gray.

With the N-terminus and C-terminus now adjacent to each other, membrane fusion can occur. This fusion-pH conformation is the lowest free energy state of HA. (Kielian and Rey 2006) These low pH conformational changes lead to large-scale movements of up to 10 nm in some domains. At low pH the central coiled-coil is elongated so that the N-terminus is near the fusion proteins and the C-terminus is near the membrane spanning domains. The bending and tilting of the outer monolayers bring the viral envelope and bilayer together. The membranes bend spontaneously when a lower energy can be achieved. Otherwise work by proteins is required.

As of yet there is no consensus on what conformations and entry angles of HA are necessary for the lipid membranes to become destabilized enough to undergo fusion. Early in the fusion process low pH induced conformational changes occur within a single HA, however late conformational changes may involve interactions between multiple copies of HA. Some studies suggest only 1 HA trimer is necessary for binding and fusion other studies

suggest a complex of three or six trimers is required.(Blumenthal and others 1996; Floyd and others 2008; Gunther-Ausborn and others 2000) Also the number and form of intermediate structures is still under debate. (Skehel and Wiley 2000) However the degree to which membrane structure is perturbed is determined not only by the number of proteins but also by the ability of these proteins to concentrate in the membrane. HA has an amphipathic helix, which can be oriented parallel to the lipid bilayer surface. This position makes it ideally situated to dwell at an interfacial location between the head groups and the hydrophobic core. This orientation allows for maximum cooperation between HA and lipids which to drive membrane curvature and thus fusion.(Farsad and De Camilli 2003)

Although all class I fusion proteins are thought to follow the general sequence of conformational changes seen in HA, not all of them use endocytosis to enter the cell or are triggered by exposure to acidic conditions. HIV, Avian sarcoma/leukosis virus (ASLV), Sendai virus and Murine leukemia virus (MLV) all fuse directly to the plasma membrane at neutral pH.(Earp and others 2003; Rawat and others 2003) Fusion of HIV-1 is triggered by the interaction of the virus fusion proteins with its receptor (gp120) and co-receptor (CD4). .(Furuta and others 1998; Kielian and Rey 2006; Markosyan and others 2005) When HIV-1 binds to a cell, the interaction of gp120 with CD4 changes gp120's shape. This in turn induces a conformational change in gp41 which initiates fusion between the viral membrane and the cellular membrane.(Kwong and others 1998) Conformational changes in gp41, like HA, expose an N-terminal fusion peptide, which will insert into the interior of the cellular membrane. The ability of a short peptide (T-20 or enfuvirtide) that binds to and stabilizes an enlongated form of gp41, inhibiting overall fusion, is the strongest evidence for the existence

of an extended intermediate conformation for all fusion proteins on the pathway to membrane fusion.(Furuta and others 1998; Munoz-Barroso and others 1998; Reeves and others 2002; Reeves and others 2005; Rimsky and others 1998; Wild and others 1994) The turn potential for the gp41 peptide is greater than for the HA peptide, but both proteins form a hairpin to bring the C and N termini together, and thus pull the membranes together.(Haque and others 2005)

1.3.2 Class II Fusion Proteins

Class II proteins are found in alphaviruses (E1 from Semliki Forest Virus (SFV)(Lescar and others 2001) and Sindbis Virus (SIN)(Zhang and others 2002)) and flaviviruses (E from tick borne encephalitis (TBE)(Rey and others 1995), dengue fever(Modis and others 2004) and West Nile virus(Nybakken and others 2006)). Class II proteins are expressed as a single polypeptide precursor that is cleaved prior to the virus' release from the infected cell and long before entering the endocytotic pathway. The cleavage of p62 yields E1 and E2 in alphaviruses and the cleavage of prM yields E and M in flaviviruses. The E and E1 glycoproteins fold into three domains primarily composed of β−sheets.(Schibli and Weissenhorn 2004)

Alphaviruses probably enter the cell via endocytosis(Helenius and others 1980), as shown by their ability to fuse with liposomes at low pH(White and Helenius 1980) although some evidence suggests alternate entry pathways.(Paredes and others 2004; Wang and others 2007) There is at least two possibilites for the Sindbis infection pathway. Endocytosis is the first possibility. The second possibility is that the viral envelope surrounding Sindbis may fuse with the cell's exterior plasma membrane in a pathway similar to HIV-1. If the viral

membrane fuses directly with the cell membrane then genetic material can enter the cell through either a lipidic pore or a protein pore. Membrane dye diffusion may or may not result during pore formation depending on the packing of proteins surrounding the fusion pore. If the proteins are tightly bound to each other they may prevent the lipid bilayers from mixing. However, if protein packing is not tight, then the bilayer may extend between the proteins and direct interaction between the viral envelope and cell membrane may occur with lipid molecules freely exchanging (described in more detail in section 1.4.8). (Blumenthal and others 1996) By comparing and contrasting results from experiments using both Sinbis and Influenza, an infection pathway for Sinbis may be determined.

Sindbis virus is very different from influenza structurally. Sindbis particles are very structured and rigid compared to influenza. In SV there are 240 copies of E1, capsid and E2 in the alphavirus virion. E1 and E2 form heterodimers that assemble into 80 trimeric assemblies, which are seen as 3 lobed projections on the viral surface. These 80 timers are linked together to form an icosahedral structure with an external diameter of 70 nm. These proteins are arranged with T = 4 quasi-symmetry (one heterodimer from the 3-fold spike and three heterodimers from a quasi-3-fold spike). At the base of each of these assemblies an E1 monomer lies on the membrane surface and forms a trimer around each of the icosahedral and quasi 3-fold axes, resulting in the formation of a surface lattice. The ability of class II proteins to support the icosahedral symmetry is a key difference with class I proteins. (Zhang and others 2002) Remarkably, recent structural investigations have suggested that the mechanisms of mediating membrane fusion appear nearly identical for class I and class II proteins.(Harrison 2008; Kielian and Rey 2006; Schibli and Weissenhorn 2004; Sollner

2004; White and others 2008)Functional studies support this conclusion of similar fusion mechanisms for class I and II proteins.(Wessels and others 2007; Zaitseva and others 2005)

E1 is responsible for cell fusion and E2 is involved in receptor binding and cell entry. E1's fusion peptide lies in domain II (the dimerization domain) and forms a large number of contacts with E2. The fusion peptide is located furthest from the viral membrane and buried within the domain. When low pH is encountered, E1 and E2 change their conformation. Fusion requires the dissociation of the tightly packed E1-E2 heterodimers, exposure of the fusion peptide and the formation of E1 homotrimers. The E1 molecule bends at the connection between domains I and II, also known as the "hinge" region. The hinge lies at the center of E1, with almost the same distance from the hinge to the fusion peptide as the hinge to the C-terminus leading to the membrane anchor. This hinge allows E1 to form an extended intermediate towards the target membrane then jackknife back to the viral membrane, bringing the snared target membrane with it (Cohen and Melikyan 2004; Jardetzky and Lamb 2004; Kielian and Rey 2006; Schibli and Weissenhorn 2004; Zaitseva and others 2005), just as HA does for influenza and gp41 does for HIV.

During the fusion process E1-E2 heterodimers rotate and disassemble, moving the bulky E2 molecules out of the center of the prefusion trimer and allowing the E1 homotrimer to form. Because the E1 fusion protein acts as the major assembly element of the prefusion icosahedral lattice, the movements of E2 result in the rearrangement of the viral surface. The final conformation of E1 leads to an arrangement of multiple fusogenic trimers that extend out from the viral surface as spikes. However it is not known whether these trimers keep lipids out of the fusion pore or allow interactions between the E1 molecules. (Mukhopadhyay

and others 2006) Fusion mediated by HA, a class I protein, is slower, more temperature sensitive and more leaky than fusion mediated by class II proteins such as E1. Lower pH values are needed to activate HA compared to E1 as well.

1.3.3 Class III Fusion Proteins

Class III proteins form trimers of hairpins by combining structural elements from class I and class II fusion protiens. The fusion domain of class III proteins contains two fusion loops at the tip of an elongated β sheet, similar to the structure of class II fusion proteins. However the post-fusion trimer shows an α helical trimeric core much like class I proteins.(Weissenhorn and others 2007). Baculovirus gp64(Kadlec and others 2008), vesicular stomatitis virus (VSV) G(Roche and others 2006) and herpes simplex virus type1 (HSV-1) gB (Heldwein and others 2006) proteins are suggested to be class III proteins.

Baculovirus gp64 is an envelope protein composed of mostly β-sheets with a central triple-stranded coiled coil that is involved in trimerization. The elongated trimer is composed of five domains. The fusion peptide resides at the tip of the β sheet domains in the trimeric postfusion state. This hydrophobic patch also acts as a receptor binding site. At low pH gp64 forms discrete glycoprotein spikes on the viral capsid that are ~10 nm tall on one or both poles of the virus. The low pH conformational change is reversible. Gp64 like other class III molecules remains trimeric during transformation to the fusion activated state.(Kadlec and others 2008)

Theoretically for most fusion proteins when a single envelope's trimer refolds enough energy is released to overcome the free energy barrier to fusion. This is not the case for rhabdoviruses where a pH dependent equilibrium between the pre- and post-fusion

conformations of G results in a higher energy requirement. (Gaudin 2000) Thus the energy released by the structural transition of just one trimer for rhabdovirus G is insufficient to catalyze fusion.(Weissenhorn and others 2007) Experimentally it has been shown that complex formation of multiple trimers precedes, rather than follows membrane merger.(Markovic and others 1998) Baculovirus gp64 forms aggregates containing up to 10 trimers.(Chernomordik and Kozlov 2003)

1.3.4 SNARE Proteins

Intriguingly, some of the same structural features seen in the viral fusion proteins are also present in the eukaryotic cellular fusion proteins: the SNAREs (soluble N-ethylmaleimide-sensitive factor (NSF) attachment protein (SNAP) receptor). (Bowen and others 2004; Brunger 2005; Jahn and Scheller 2006; Rizo and Rosenmund 2008; Sudhof and Rothman 2009) SNAREs are integral membrane proteins anchored to membranes by single pass transmembrane domains or palmitolyation. The heteromeric complex formed from SNARE proteins (the SNARE complex) is composed of two transmembrane containing SNAREs that bind to each other along with other SNARE proteins and possibly additional factors (e.g. Sec9, Munc18, complexin etc.). Formation of this complex brings two apposing membranes together in a manner very similar to viral membrane fusion (figure 1.3). SNARE proteins mediate fusion between cellular transport vesicles, e.g. synaptic vesicles, and the cell membrane. SNARE proteins are present in all eukaryotic cells on multiple compartments.(Wickner and Schekman 2008) Upon complex assembly, the transmembrane domains of SNAREs in each membrane crosslinks the membranes in close apposition, (Sutton and others 1998) similar to the configuration of viral fusion proteins with the

transmembrane domain and fusion peptides closely positioned in the jackknifed, folded-back conformation.

The crystal structure of the neuronal SNARE core complex revealed a twisted four α-helix bundle. The bundle is similar to post fusion virus protein structures. (Antonin and others 2002; Yoon and others 2008) Debates currently rage over the precise mechanisms connecting membrane fusion to the free energy of SNARE protein folding. Nevertheless, the similarities in structures between SNARE complexes and viral fusion proteins when crosslinking membranes destined to fuse suggest that the mechanism of achieving membrane fusion is common.

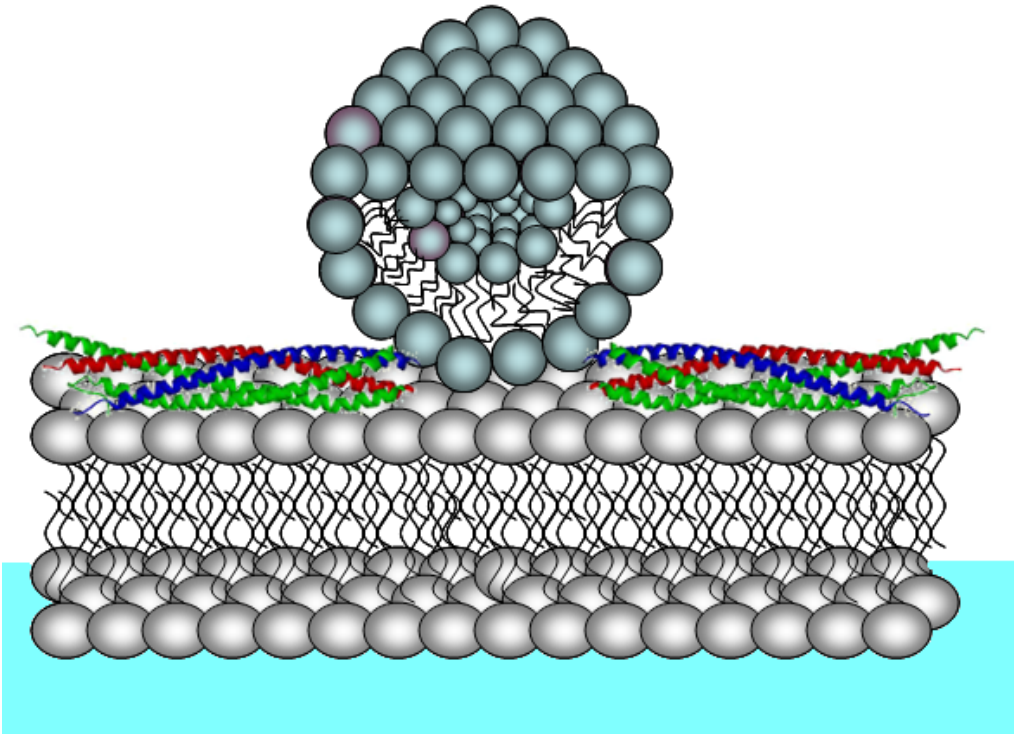

Figure 1.3. SNARE mediated fusion. A liposome with t-SNARE (blue helix, Sso1pHT in yeast, syntaxin in rats) and a planar bilayer supported by a glass substrate with v-SNARE (red helix, Snc2pF in yeast, synaptobrevin in rats) will form a 4 helix complex with t-SNARE (green helices, Sec9c in yeast, SNAP25 in rats) in solution. This helix when tightly bound will mediate fusion between the planar bilayer and liposome.

1.4 The Role of Lipids in Membrane Fusion

Membrane fusion proteins ensure close apposition of the membranes during fusion phenomena. Yet, simply forcing membranes into close proximity is not sufficient to yield membrane fusion. (Basanez 2002; Malinin and Lentz 2004) The properties of the lipids in the membranes play a crucial role in membrane fusion. The presence of certain lipid species and lipid derivatives within the bilayers can strongly promote or inhibit fusion, likely by modulating the spontaneous curvature of bilayers. (Farsad and De Camilli 2003; Lang and others 2008; Rawat and others 2003; Waarts and others 2002). Lipid composition may also be critical for recruitment of other proteins to the plasma membrane, organization of membrane domains for fusion and regulation of fusion protein complexes.(Lang and others 2008)

1.4.1 Introduction to Lipids

A lipid is a small molecule with a hydrophilic head, i.e. a polar head group, and a pair of hydrophobic tails. Lipids don't form stable structures of defined composition nor do they adopt conformations that are thermodynamically stable in isolation.(Lang and others 2008) When lipids are added to an aqueous solvent they form into 1) a micelle where the hydrophobic tails from several molecules come together, 2) a spherical structure with a lipid bilayer surface, called a liposome, where the solvent is caught inside (Sklodowaka and others 1999), or 3) a lipid bilayer (figure 1.4) on surfaces like glass and quartz where the hydrophilic head groups have a only a thin layer of water molecules separating them from the surface. Lipid bilayers are composed of two monolayers where the lipids orient so the polar

head groups are on the surface of the membrane sheet and the hydrophobic tails form the interior of the membrane. Lipid-like dye molecules can be incorporated into lipid bilayers or non-permeable soluble dyes can be trapped in the interior aqueous volume of liposomes. These soluble dyes will only be released if the liposome bursts (such as when a flat planar bilayer is formed on a substrate) or if the liposome fuses to other lipid membranes.

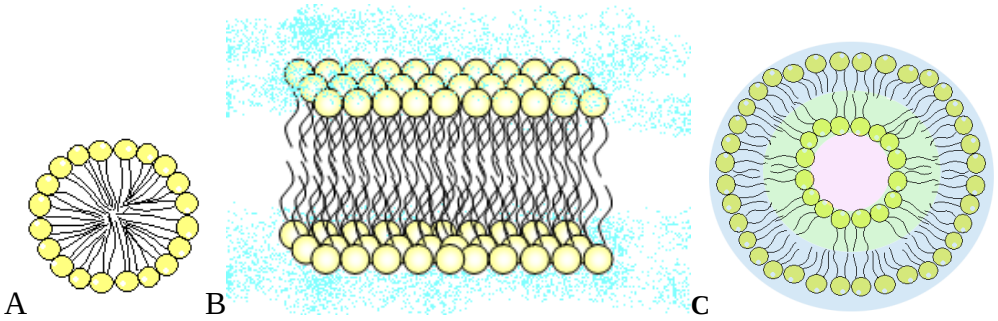

Figure 1.4. Self assembly of lipids in solution. a) A micelle shown in cross-section. The polar headgroups are in yellow and the nonpolar hydrocarbon tails are black. b) The structure of a bilayer membrane formed on a surface. Water molecules are in blue. When this bilayer forms the shell of a sphere, as shown in cross-section in c), the area highlighted in blue is called the outer monolayer, the green highlighted area is the inner monolayer and the pink highlighted area is the aqueous compartment. The tails of the inner and outer monolayer form the hydrophobic center of the bilayer.

The properties of the lipid molecules are determined by the specific polar headgroups as well as the chain length and degree of saturation of the hydrophobic acyl chains. Non-lipid molecules can become associated with the liposomes in various ways. Some molecules have covalent and electrostatic interactions with the polar head-groups of the lipids, allowing the liposomes to bind to other vesicles, viral membranes or membraneous surfaces. For example the addition of phosphatidylethanolamine (PE) provides an amine group on the liposome's outer leaflet whereas cholesterol provides a hydroxyl group.

A wide variety of hydrophilic molecules can be encapsulated within the aqueous cavity of a liposome including enzymes, DNA, vaccines and fluorescent dyes. The bilayer structure can shield encapsulated molecules from attack by other destructive enzymes or chemicals. Thus several pharmaceutical compounds use liposomes as a drug-delivery system (Kshirsagar and others 2005). Applications in membrane fusion have demonstrated that the contents of distinct liposomes mix following fusion. Several different reactants have been used in fusion studies, yielding a chemical transformation that can be tracked during experiments.(Edwards and Baeumner 2006)

1.4.2 The importance of lipids in membrane fusion

Membrane fusion is still not well understood in part because transitions during the fusion of membranes are very rapid. All cells have a plasma membrane which is a selectively permeable lipid bilayer coated by proteins. The plasma membrane controls access of nutrients into the cell while keeping the cell machinery separate from outside fluid that bathes the cell. Plasma membranes are on the order of 10 nm thick. Although some membrane fusion events are triggerable (like viral membrane-cell membrane fusion), in general, fusion occurs stochastically following exposure to triggering conditions. Membrane fusion is critical to many physiological processes such as intercellular communication, distribution of lipids and proteins to organelles, tissue building and spreading of infectious diseases.

Pores in PC bilayers are likely rounded and lined with lipid headgroups in order to reduce exposure of the hydrocarbon tails to water. (Rawicz and others 2008) Experimentally it is not currently possible to optically view the formation of a fusion pore in liposomes

between 50-400 nm. Structural transitions associated with fusion pore formation has been imaged in giant unilamellar vesicles, but these vesicles are over 20 micrometers in diameter (Haluska and others 2006) Similar experiments are not possible with sub-micron sized vesicles. Mixing between the outer (distal) monolayers of two membranes must occur before a lipidic pore can form. This outer leaflet mixing state is called hemifusion. This is the first step to forming a point-wise defect which is often referred to as a stalk due to its shape. When the stalk is formed, the outer monolayers are fused but their inner monolayers remain distinct. The stalk can take on a variety of shapes. Eventually, a pore will form to complete the fusion process. (Malinin and Lentz 2004)

The role of lipids in membrane fusion extends beyond continuous passive platforms that adapt their shape upon interaction with fusion proteins. Lipids influence the inclination of lipid bilayers to fuse. They may also recruit proteins to the plasma membrane by providing contact points for proteins localizing them to the fusion site. Lipids may organize membrane domains for fusion and direct regulatory effects on fusion protein complexes. (Lang and others 2008)

In the experiments in this thesis, I will present results using both liposomes and lipid bilayers. Bilayer experiments, in which a bilayer is formed on a quartz microscope slide and virus is injected over the bialyer, are viewed using total internal reflection fluorescence microscopy. The long narrow channel in the slide causes liposomes to form into lipid bilayers along the glass surfaces. Thus the virus particle fusing to the lipid bilayer is a fusion between a plane and a sphere. Bulk experiments use a spectrophotometer to measure fusion between two liposomes, or a liposome and a virus particle i.e. two spheres. The difference in

geometry is very important because liposomes are more or less likely to fuse based on their bending modulus. Lipids with highly positive or highly negative curvatures can't form stable structures like liposomes and bilayers, thus they are more likely to fuse in order to obtain these stable structures. However too much curvature will prevent structures from forming altogether, and are not usable for most experiments. (Nelson 2004)

1.4.3 Types of Lipids

Liposomes can also be charged positively or negatively in their headgroups. Most liposomes are Zwitterionic meaning they carry both a positive and negative charge. In general the thickness of the hydrocarbon region is on the order of 5-10 Å from one phosphate head group to the apposing phosphate headgroup. A higher percentage of virus particles are actively engaged in fusion when liposomes contain negatively charged phospholipids. The aggregation rate constant is also higher, thus leading to more interaction between liposome and virus. Cellular plasma membranes contain several different classes of lipids with different molecular shapes and charge distributions including PC, phosphatidylserine (PS), phosphatidylinositol (PI), PE, CH, and SM (Hung and others 2007; Simons and Vaz 2004) CH thickens the bilayer by as much as 4 Å when added to PC / PE bilayers. Cholesterol (figure 1.5) is a sterol (a combination of a steroid and an alcohol) that is minimally soluble in water and is found in the cell membranes of all body tissues. Saturated acyl chains of many phospholipids are straightened by cholesterol, thus bilayers with these kinked hydrocarbon chains will thicken more than bilayers with unsaturated hydrocarbon chains. CH is required to build and maintain biological function of most cells membranes by making the membrane's fluidity stable over wider temperature intervals. Cholesterol's solubility in lipid

bilayers is between 40-47%, but most natural membranes have less than 10% CH. In the electron density profiles of phospholipid bilayers the profiles vary, but with CH in the bilayers the profiles do not vary indicating a flatter more even bilayer surface. (Hung and others 2007)

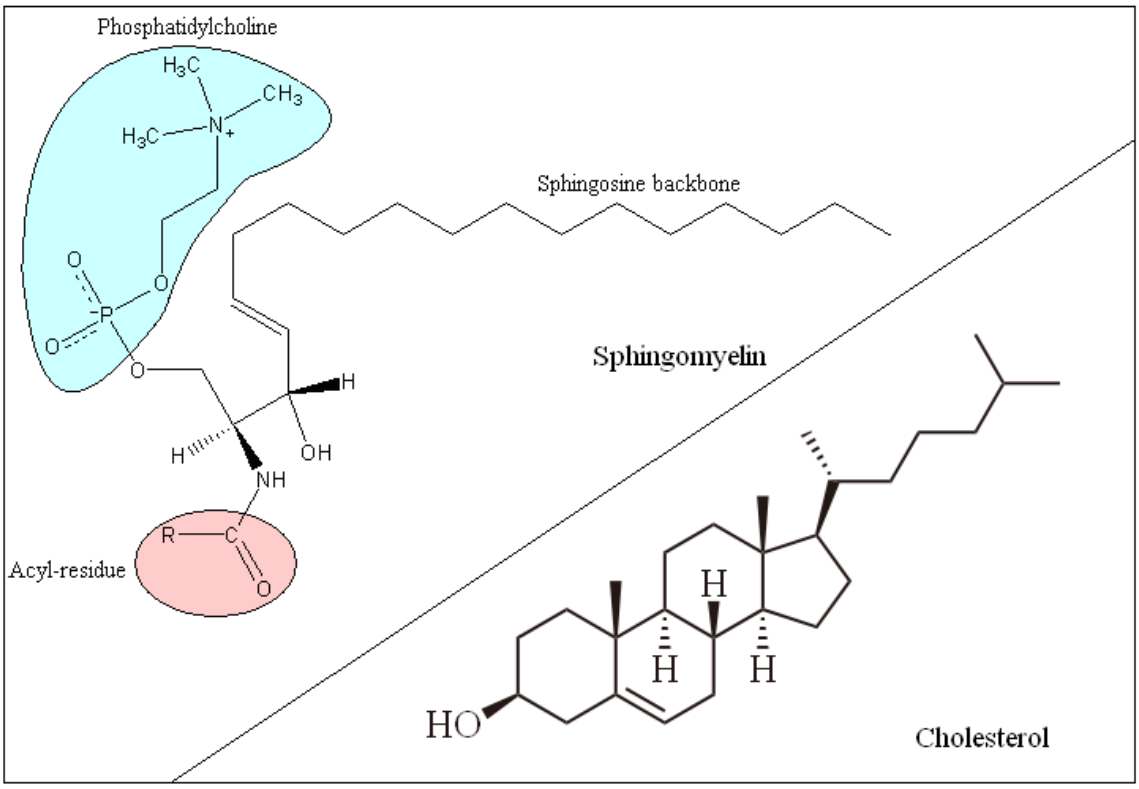

Figure 1.5 Structural formula of Sphingomyelin and Cholesterol. Images taken from Wikipedia: http://en.wikipedia.org/wiki/Sphingomyelin and http://en.wikipedia.org/wiki/Cholesterol, respectively.

Studies have been performed where lipid membrane fusion without proteins or other large biomolecules have been performed. Ohki and Arnold have theorized that the curved membrane area is more hydrophobic and possesses a higher surface energy than the less curved membranes. (Ohki and Arnold 2008) When Ca^{2+} is used to catalyze a fusion event, the Ca^{2+} binds to an acidic lipid membrane making the surface more hydrophobic resulting in

strong adhesion and structural changes in these membranes leading to membrane fusion. When membranes adhere together, they undergo different formations, starting with curvature at the edge of the adhered regions. Because these rim regions of the adhered membranes have higher curvature compared to the rest of the membrane, this rim area becomes the site of membrane fusion. The curved areas have higher surface energy compared to the rest of the membranes. When these curved areas fuse together the total surface energy of the membrane is decreased and the membrane becomes stable.

1.4.4 Lipid Rafts

Cholesterol doesn't work alone. Sphingomyelin (SM) (figure 1.5) is a type of lipid that increases the speed of transmission in the nervous system. Sphingolipids protect the cell surface against harmful environmental factors by forming a mechanically stable and chemically resistant outer leaflet of the plasma membrane. Sphingomyelin and cholesterol associate to form lipid rafts, (Nelson 2004) possibly due to the double bond in the monounsaturated long chain, which is known to have a large affect on the interactions between two phospholipids or a phospholipid and CH. These lipid rafts are involved in several cell functions beyond viral fusion. They are important for signal transduction, lipid sorting and protein trafficking because of their ability to sequester specific lipids and proteins. The size and shape of these rafts are dependent on temperature. Rafts exist in the bilayer's gel phase at 5^{o}C but as the temperature is raised, lipid order decreases. At 37^{o}C the bilayer is now in a fluid phase and rafts are no longer present (figure 1.6). (Giocondi and others 2007)

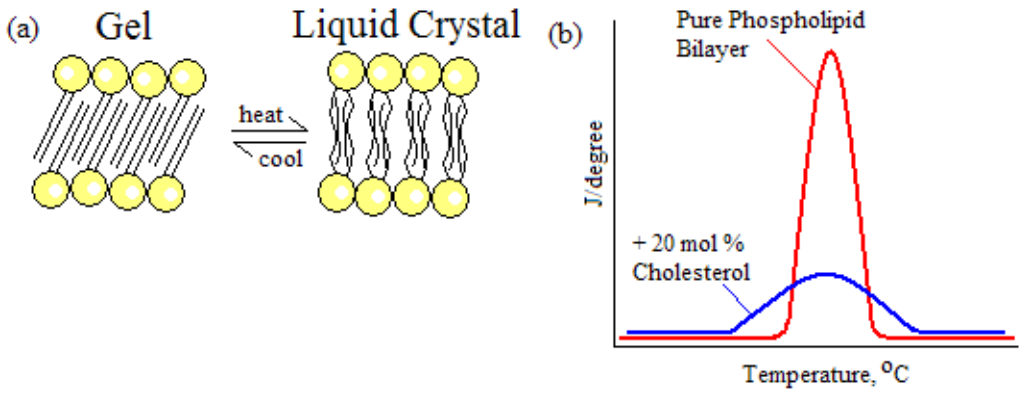

Figure 1.6 Lipid bilayer phases. A) The transition of a bilayer from gel at low temperatures to a liquid crystal at high temperatures. The gel phase features tightly packed head groups, regular tails and a thicker membrane. The liquid crystal phase had loosely packed head groups, disordered tails and a thicker membrane. B) The rate of heat absorption versus temperature shows the transition of the bilayer with and without cholesterol. (Garrett 1998)

Rafts in lipid bilayers also affect the elasticity, strength and water permeability of the bilayers. Bilayers with SM and CH resist stretching more than bilayers with just CH, and bilayers without CH and SM altogether are the most elastic. This elasticity is dependent on temperature as well, as shown is figure 1.6. Bilayers composed of just PC or PC and CH, exhibit little change in the elastic moduli when suction tension is applied with a micropipette (Rawicz and others 2008), but when SM was added the elastic moduli increases. Increasing temperature in all bilayers increases the water permeability of the bilayer and decreases the tension under which a bilayer will rupture. Bilayers with more CH are better able to withstand increases in tension and less likely to rupture. More specifically the thermal tension scale (σ_β), which is a parameter used to determine membrane strength and is derived from the ratio of the activation energy (the minimum energy necessary for a reaction to take place) (Nelson 2004) to the thermal energy (k_BT), describes the height of the energy barrier

that prevents the opening of an unstable hole and ability to increase membrane stress (see Table 1.2). For a rupture pore to form in a bilayer significant deformation of the lipid monolayers must occur. Bilayers with higher elastic-bending moduli can withstand stress better and are less likely to rupture. Bilayers with CH are more stable. Cholesterol's affect on its nearest neighbors' in a bilayer seems to force the hydrophobic chains of the phospholipids into an ordered state, creating condensed areas in the bilayer. The energy of a SM-CH interaction is much larger than the interaction energy between CH and a phospholipid with a hydrocarbon chain featuring a double bond, i.e. a phospholipid with a kinked tail, due to the van der Waals force between atoms. As temperature increases, the distance between the phospholipid and CH increases and the attractive force between them decreases. Also the addition of CH to PC lipid bilayers reduces the permeability of liposomes to water.(Rawicz and others 2008)

Table 1.2. Stretch moduli and lysis tension for bilayers. Average lipid stretch moduli, K_A, for various bilayers was measured at 15°C and 32-35°C and the lysis tension, σ_L, for these bilayers was measured at 15°C and 32-35°C. from (Rawicz and others 2008)

Bilayer Composition	K_A at 15°C	K_A at 32°C	σ_L at 15°C	σ_L at 32°C
SM:CH	3300 mN/m	2193 mN/m	33 mN/m	26 mN/m
SOPC:CH	1980 mN/m	1130 mN/m	26 mN/m	21 mN/m
SOPC:SM:2CH	2188 mN/m	1377 mN/m	26 mN/m	N/A
SOPC:SM:CH	1725 mN/m	880 mN/m	21 mN/m	17 mN/m
DOPC:CH	890 mN/m	870 mN/m	19 mN/m	16 mN/m
DOPC:SM:CH	655 mN/m	610 mN/m	15 mN/m	12 mN/m
SOPC	290 mN/m	290 mN/m	12 mN/m	N/A
DOPC	310 mN/m	N/A	10 mN/m	N/A

Lipid rafts are important because they are involved in the entry, assembly and budding of viral structural proteins for some enveloped viruses. Influenza, Ebola, Marburg,

Epstein-Barr and herpes simplex virus 1 all use membrane lipid rafts for entry into the cell. (Aizaki and others 2008; Carter and others 2009; Suzuki and Suzuki 2006) The sialic acid residues that HA binds are enriched in glycoconjugates in lipid rafts within the cell membrane. Interactions between the transmembrane domain and lipids causes HA to concentrate in lipid rafts.(Suzuki and Suzuki 2006) Flavivirus fusion is enhanced by CH, however CH is not absolutely required for fusion.(Kielian and Rey 2006) Alphaviruses require CH for cell entry, however they do not require lipid rafts for fusion. (Rawat and others 2003; Waarts and others 2002) Semliki Forest virus requires cholesterol to mediate an interaction between the virus and the target membrane before fusion. E1's binding and acid dependent conformational changes are both inhibited by a lack of cholesterol in the target membrane.(Smit and others 2002; Smit and others 2003; Vashishtha and others 1998; Wessels and others 2007)

1.4.5 Deforming Bilayers

Since a bilayer is composed of two monolayers positioned directly opposite from each other, if the monolyaers have the same compostion there will be no spontaneous tendency for the bilayer to bend. Also bilayers do not remember any previous bent configuration due to their fluidity. Although it is possible to deform a bilayer into a bent configuration there is an energy cost to do so. When a bilayer bends, one side is compressed and the other is stretched. In the monolayer that is stretched the polar headgroups will move apart. If they move apart far enough then water molecules can move into the nonpolar core. The free energy cost of bending a bilayer membrane into a sphere, which happens when liposomes are formed, is $8\pi\kappa$. With κ, the bending stiffness of the bilayer, estimated around 15 k_BT then $8\pi\kappa = 377$

k_BT. So the bending energy needed for large shape changes is a few hundred k_BT.

Only pure, artificial bilayers prefer to be flat. A real plasma membrane with compositional differences between the two monolayers will have a tendency to bend in one direction. Since bending a bilayer involves a combination of stretching the outer layer and squeezing the inner layer, the bilayer's elasticity is affected by the tails as well as the heads of the phospholipids. (Nelson 2004)

Membrane curvature may result from what is known as the bilayer-couple mechanism. In this case, lipids transfer into only one leaflet resulting in each monolayer having a different surface area. The inclusion of a small number of lipids through local invagination will result in asymmetry between the monolayers since lipids move laterally within a monolayer much more quickly than they transverse between monolayers in a bilayer. For lipids with large headgroups or single acyl chains, the monolayer will undergo positive curvature ($J\tilde{}_s > 0$), adopting a wedge-like geometry. For lipids with small headgroups, like PE, the monolayer will undergo negative curvature ($J\tilde{}_s < 0$) as shown in figure 1.7. Either way the relative increase in surface area of one leaflet will increase the spontaneous curvature of the bilayer. The monolayer with the larger surface area will be the side to which the bilayer will deform, taking on a positive curvature. (Farsad and De Camilli 2003) Assymetric bilayers can be achieved by imposing a pH gradient across the membrane.(Farge and Devaux 1992) Thus the bilayer-couple mechanism may be enough to promote membrane fusion alone for small highly curved vesicles,(Martens and McMahon 2008) but for viral fusion this mechanism must work in conjunction with the protein induced deformation mechanisms such as the local spontaneous curvature mechanism which will be

mentioned later.

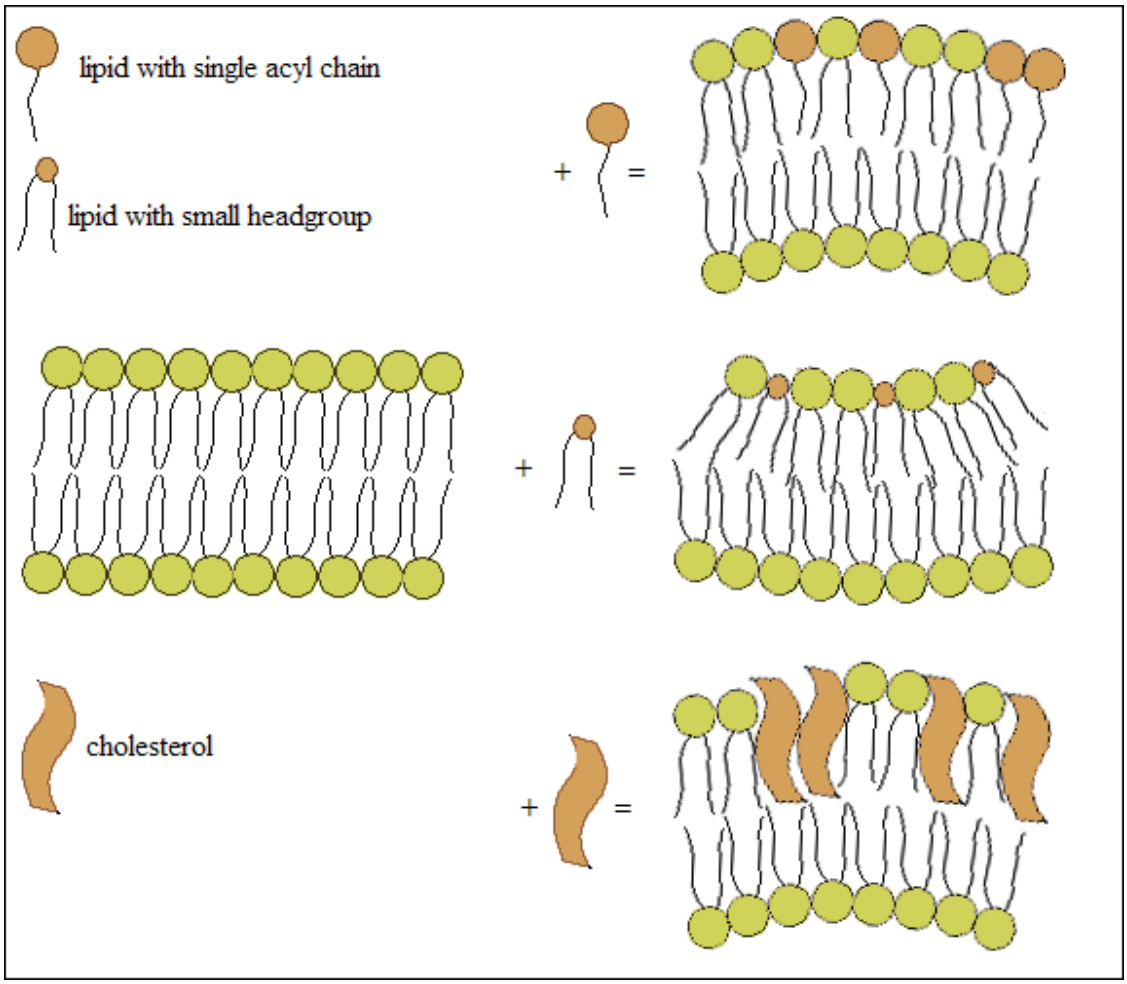

Figure 1.7. Spontaneous Curvature. A flat planar bilayer will undergo spontaneous curvature depending on its lipid composition. Lipids with single acyl chains produce positive curvature. Lipids with small headgroups induce negative curvature. CH induces positive curvature. Figure adapted from (Farsad and De Camilli 2003)

The curvature of bilayers affects membrane fusion processes. Each monolayer in a bilayer undergoes geometrical changes during stalk formation and expansion during fusion of closed vesicles of finite size. The high positive curvature of the outer monolayer of a vesicle provides more energy (that can be released during stalk expansion and pore formation)

compared to neutral curvature of flat membranes. Also the stress of positive curvature promotes fusion by restricting the changes possible in the monolayer's surface area, which is linked to the change in internal volume and osmotic conditions of the vesicle (discussed in section 1.4.7). (Malinin and Lentz 2004)

Monolayer bending is opposed by the cohesive hydrophobic interactions between the hydrocarbon chains of each leaflet. If spontaneous curvature is suppressed a curvature stress will build up in the bilayer. This curvature stress can be described as elastic energy stored in the membrane and can eventually destabilize the lipid bilayer structure. (Basanez 2002)

1.4.6 Effect of pH on Lipid bilayers

Both theoretical and experimental studies have shown that the pH of a solution affects cholesterol domain formation and membrane phase transitions. Changes in pH can affect a liposome's stability when the bilayer undergoes liquid to gel phase transitions, but characteristics of the gel phase do not show up in a lipid bilayer until pH 2 or lower.(Zhou and Raphael 2007) However the effects of protons and hydroxide ions can change the electric charge distribution at the membrane's surface. These ions can also affect the internal dipole potential of the membrane. Dipole potential is influenced by the external ions and the lipid headgroup composition. Since the dipole potential is positive inside a phospholipid bilayer core, these bilayers are more permeable to anions than to cations. The hydroxide ion is more polarizable and more hydrophobic than the proton so these hydroxide ions associate with PC lipids more favorably than protons. Thus partitioning of the anionic hydroxide ions potentially decreases the PC dipole potential. In other words, the dipole potential increases as the solution's pH decreases.

The phosphate and choline functional groups on Zwitterionic PC lipid molecules creates an electric charge distribution at the membrane surface, called the surface charge density, which is altered by the binding of protons and/or hydroxide ions. Changes in the ionic strength may also affect lipid packing which in turn changes the bending stiffness or membrane's elasticity. However the bending stiffness only increased at pH 4 and 9. (Zhou and Raphael 2007) This unusual result is due to the high concentration of protons at low pH increasing the surface charge density of the membrane and thus the bending stiffness, but decreasing the Debye length (the distance over which significant charge separation can occur) (Nelson 2004) and in turn the bending stiffness. Thus no change in the bending stiffness is seen except at moderate pH 4 and 9 where the change in surface charge density out-competes the decrease in Debye length yielding a larger overall bending stiffness. (Zhou and Raphael 2007)

1.4.7 Intermediate Structures of Membrane Fusion

For influenza and other viruses hemifusion stalk formation is promoted by cis-unsaturated fatty acids, which cause negative curvature when present in the outer monolayer. Hemifusion or stalk formation is inhibited by Lysophosphatidyl (LPC), which causes positive curvature when present in the outer monolayer. Conversely pore formation and expansion should be promoted by LPC when present in the inner monolayer and pore formation is inhibited by cis-unsaturated fatty acids when these lipids are present in the inner monolayer. In figure 1.7 positive curvature in a monolayer as shown in the top right illustration promotes pore formation. Chain length is very important. LPCs with 12-18 carbons in their hydrocarbon chains were tested.(Gaudin 2000) LPCs with smaller chain lengths are able to

move between the inner and outer monolayers more easily. The translocation of an LPC from the outer to the inner monolayer promotes pore formation and expansion at lower concentrations. For LPCs in the outer monolayer with 16-18 carbons in their chains, fusion was inhibited at lower concentrations than for LPCs with only 12-14 carbons. Varying the lipid composition of liposomes fusing to virus has demonstrated that events preceding membrane fusion are sensitive to the shape of the lipids in the membranes. In some cases, the transition from initial pore to full fusion is not completed, but rather the process stalls and reverses. In these cases, a pore flickering that opens and closes around the initial size without ever expanding is observed.

In vitro experiments using carefully designed blends of specific lipids can arrest fusion at a specific stage or inhibit fusion altogether providing critical insights into the fusion process, specifically fusion intermediates.(Chernomordik and others 1998; Chernomordik and others 1993) Inverted cone-shaped lipids like PS and lysophosphatidylcholine promote positive spontaneous curvature in the bilayer. These lipids inhibit fusion when present in the outer monolayers of membranes but promote fusion between these same membranes' inner monolayers, enhancing formation of a fusion pore. Conversely lipids which promote negative spontaneous curvature in the bilayer like PE enhance fusion between outer monolayers but arrest fusion between inner monolayers, leading to a hemifusion structure which resembles a stalk.(Basanez 2002; Chernomordik and others 1995; Zhukovsky and others 2006)

This stalk structure has been observed statically between bilayers composed of diphytanoyl phosphatidylcholine (DPhPC). (Gruner 2002; Yang and Huang 2002) The bilayers are first brought into contact by dehydration. Further reduction of the intervening

water results in the formation of stalks at the interbilayer contact points. There is a steep free-energy cost to exposing lipid hydrocarbon chain segments to water. The free energy of the stalk structure is dependent on its geometry and the properties of the lipid monolayer.(Gruner 2002; Yang and Huang 2002) In viral membrane fusion experiments where tracers have been placed both in the membrane as well as within the aqueous compartment of the liposome or red blood cell (RBC) ghost, it has been shown that outer lipid monolayer leaflets exchange molecules before aqueous compartments.(Bonnafous and Stegmann 2003; Floyd and others 2008; Gruner 2002; Nunes-Correia and others 2002; Razinkov and others 1997; Smit and others 2002) The actual form of the stalk structure is still under debate, although experimentally seen in a pure lipid system, (Yang and Huang 2002) no consensus on a protein-lipid hemifusion stalk model has been reached. Prior to evolution of the fusion pore, the inner monolayers may be separated by a void or may pucker inward and touch leading to transmembrane contact (TMC). This TMC may then move radially outward forming a hemifusion diaphragm (HD) (figure 1.8). (Malinin and Lentz 2004) Another possibility is the deformation of a planar bilayer by the partial insertion of the fusion loops and fusion peptides into the outer leaflet of the target membrane. This partial insertion displaces the lipid headgroups on the outer leaflet resulting in a difference in area between the inner and outer leaflet thus causing the bilayer to curve into a nipple like cap. For influenza the formation of a cap on the HA2 helical bundle would make pore formation irreversible. (Chizmadzhev 2004; Kozlovsky and others 2002)

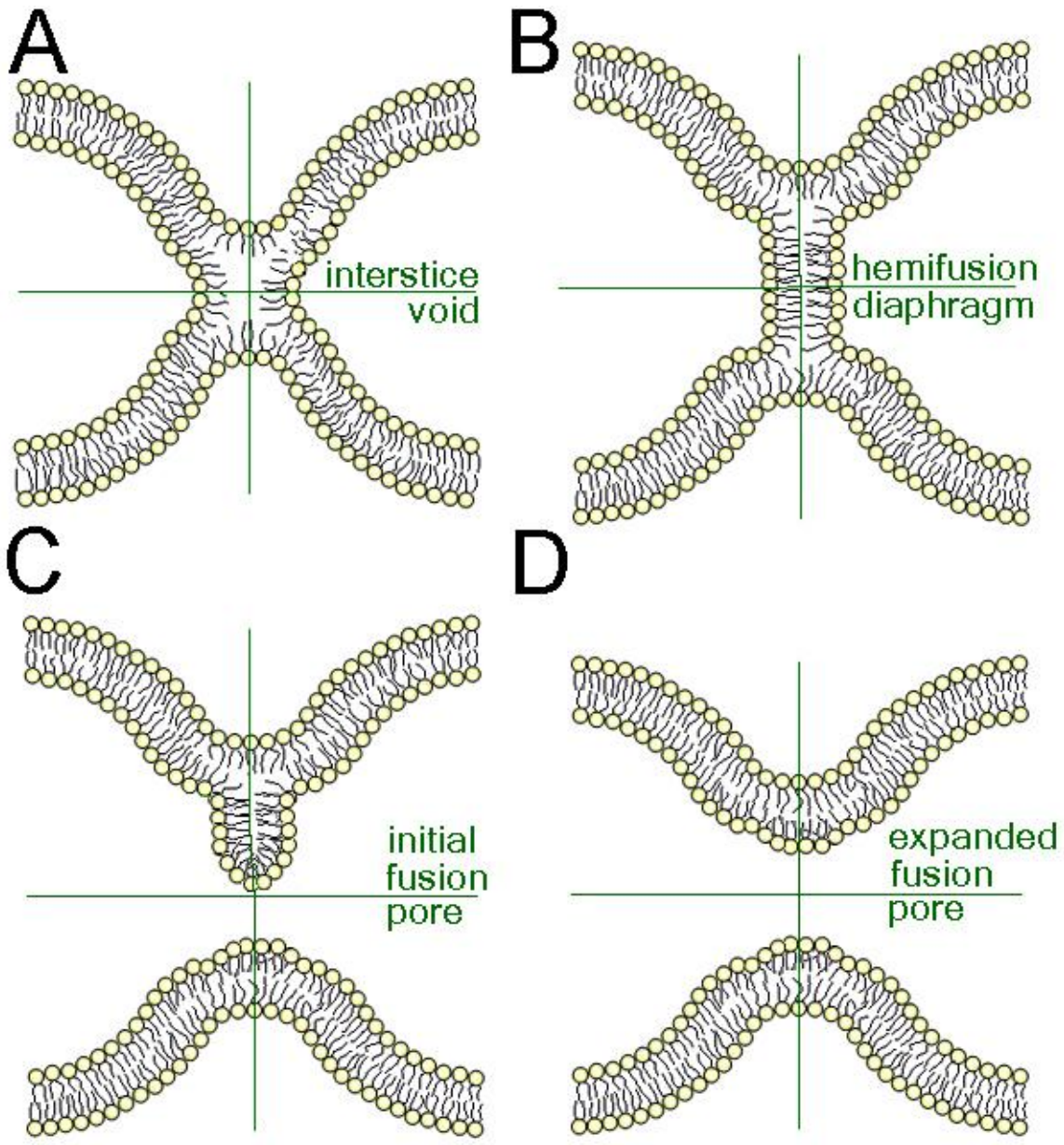

Figure 1.8. Membrane fusion via a HD. Vesicle radius to inner leaflet plane is 11nm. Each monolayer is 2nm thick thus the outer diameter is 26 nm. A. A void occurs when the inner monolayers do not come into contract prior to formation of the fusion pore. This void in the junction of fusing membranes creates a steep energy barrier. B. Membrane tilt and formation of a hemifusion diaphragm lower the energy barrier. C. Formation of a fusion pore begins when the HD's radius expands beyond the membrane's thickness generating a rupture near the HD's rim. This fusion pore may flicker in and out of existence before becoming stable. D. As the HD continues to expand the pore becomes large enough for the RNA/DNA to pass through it. Image adapted from (Chernomordik and Kozlov 2008; Malinin and Lentz 2004) .

After viral fusion proteins bring the membranes into near contact, the bending and void energy of the membranes become the next energy barrier that must be overcome. The bending energy and hydration forces of the membranes will prevent collapse of the extended protein intermediates that bridge them.(Floyd and others 2008) Once the TMC is formed, stretching or compression energy is required to bend the monolayers inward until they touch. This energy barrier can be exasperated or relieved by osmotic gradients.(Malinin and Lentz 2004) A compressive (negative) osmotic gradient will press lipid material from the inner or outer leaflet towards the void promoting pore formation. A swelling (positive) gradient has the opposite affect, pressing lipid material from the void toward the outer leaflet inhibiting pore formation. Lipids with natural tendencies toward membrane curvature, either positive or negative, can influence the energy balance in these intermediates. If the TMC is not stable and expandable then pore formation, if it occurs, may be unstable resulting in a flickering pore that will either open fully allowing for the exchange of material between aqueous compartments or collapse.(Malinin and Lentz 2004; Yoon and others 2008)

1.4.8 Pore Formation Fusion Models

There are three different models of lipid pore formation that have a pore originating from a hemifused stalk where the outer monolayers of the bilayer merge prior to pore formation. (Kozlovsky and others 2002) All of these stalk models contain three common points: first the membranes' bilayers must be brought into close contact, next merger of the outer or proximal monolayers of the lipid bilayers creates the stalk structure and finally the inner or distal monolayers merge to form a fusion pore. (Basanez 2002)

The models differ in the details of how the pore is formed. In the first model, the stalk pore hypothesis, the stalk radius grows until the distal monolayers form a single bilayer called a hemifusion diaphragm (HD) (figure 1.8 B). When the radius of the HD becomes larger than the lipid monolayer thickness, a pore will form along the rim of the HD where the 2 bilayers come together. Whether a HD continues to expand depends upon the spontaneous splay, $J^{\sim}_s$, of the contacting monolayers. Thermal fluctuations may provide enough energy for a fusion stalk to form, but not a HD. Temperature may speed up the fusion process by increasing the number of lipids flip-flopping between monolayers. Additional energy to form and expand the HD is provided by proteins in biological membranes. These fusion proteins provide a pulling force that is related to the HD's elastic energy. Real lipid bilayers can only be stretched 5% before they burst. It is estimated that one HA trimer does not generate enough pulling force to start HD expansion into a pore. Thus multiple trimers are needed to initiate stalk expansion.

A second model has a fusion pore forming directly from the stalk connecting the membranes. In this model the void (figure 1.8 A) is still present but lipids are free to move into and out of the void. This makes the free energy profile of the system dependent on the osmotic gradient. A negative osmotic gradient will promote fusion pore formation. (Malinin and Lentz 2004) In the third model the stalk grows anisotropically so that elongated connections between the contacting monolayers of the membranes are formed. Holes form in the stalk next to the fusing membranes. The holes eventually merge into a single large fusion pore. There is no experimental evidence that supports one model over another. However the formation of a HD is energetically lower than that of an elongated connection between

membranes. At the HD's rim, three bilayers form a junction. If θ is the tilt angle (figure 1.9) between monolayers than θ =π/6 at the HD rim. In the model where the stalk expands anisotropically, the elongated connection between bilayers creates a four bilayer junction. In a four bilayer junction θ =π/4. A smaller tilt angle requires less energy. (Kozlovsky and others 2002)

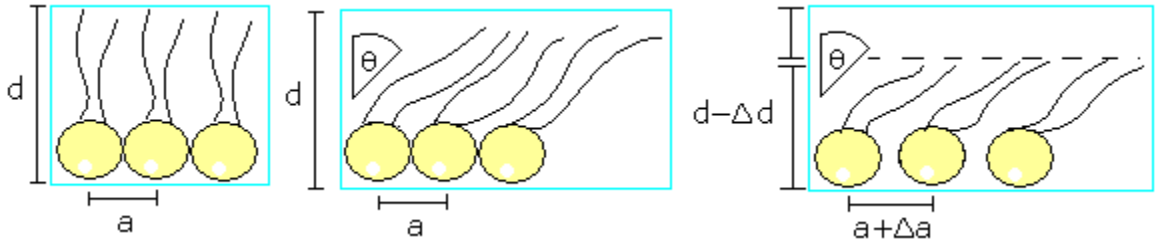

Figure 1.9. Bilayer Curvature. The three panels show lipid tilt. The phospholipid head area is a, the change in the lipid head area is Δa. The distance from the phospholipid head to the center of the bilayer is given by d, the change in monolayer height is given by Δd. In the first lower panel, lipids are neither bent nor tilted. In the middle panel lipids tilt, without changing the monolayer height, thus stretching the hydrocarbon chains. If the chains are compressed the monolayer would compress as well, as shown in the final panel. (Nelson 2004)

When the two monolayers are brought together both membranes experience positive curvatures, requiring a considerable amount of bending energy. This energy can be reduced if the membranes come together at a small solid angle, i.e. if instead of just two points touching;, a pair of large flat areas meet. However this decrease in bending energy will cause an increase in hydration energy, unless lipid tilting occurs along with membrane bending. (Cohen and Melikyan 2004) The repulsive hydration force is the main force opposing lipid bilayer approach at distances below 2-3 nm. (Basanez 2002)

Hydrophobic and hydration energies add up to an activation energy that can be overcome spontaneously to create a hemifusion stalk. In stalk formation the inner

monolayers do not deform but the bending of the outer monolayers requires energy. This energy is at a minimum when the positive curvature of the outer monolayer is balanced by the negative curvature of the inner monolayer. Once contact is made, the energy used to create the HD will be stored within the membranes and used again in the pore formation process. If the outer monolayers come together only via bending, voids will create energy barriers too large for the vesicles' inner monolayers to merge, thus preventing a HD from forming. To overcome this, lipids must bend and tilt, sometimes into sharp protrusions. Lipid tilt stretches the hydrocarbon chains at an angle, so the monolayer's thickness is not changed (figure 1.9). The hemifusion diaphragm is stable enough that additional forces are needed to create and enlarge a pore.To create the pore more energy is required. For a small fusion pore to grow into a large fusion pore, fusion proteins must not constrain the pore wall.

Theoretically it is not necessary for proteins to surround the hemifusion stalk or fusion pore.(Floyd and others 2008) Protein free pore formation has been observed in giant unilamellar vesicles (GUVs) where poly*(*ethylene glycol) and dehydration were used to fuse the GUVs without a hemifusion intermediate.(Estes and others 2006) SNARE mediated fusion has allowed for the measurement of the energy required for hemifusion between outer leaflets (1.4 kJ/mol) and pore formation between inner leaflets (5.5 kJ/mol).(Liu and others 2008) As predicted the energy required for pore formation is much larger than the energy required for hemifusion.(Malinin and Lentz 2004)

1.4.9 Fusion Protiens Affect on Lipid Membranes

The actions of the fusion peptide on the lipid bilayers are as important to the overall membrane fusion process as the role of the lipids and the lipid-transmembrane domain

interactions. Membrane curvature is affected by interaction between proteins and membrane lipids and the physical forces that are applied to the membrane surface. In viral membrane fusion, fusion proteins may deform membranes as well as bring them together. Proteins that bind to a membrane's surface can change the membrane curvature by applying pulling and bending forces to the surface. Two different mechanisms have been proposed to explain how fusion proteins can deform membranes. Proteins can form scaffolds that impart their own intrinsic curvature onto the membranes to which they bind. These proteins must be rigid or the lipid bilayer will relax to its native conformation. The energy of protein-membrane binding must be larger than protein-membrane bending; otherwise the bilayer will not fit the shape of the protein. The second mechanism is known as the local spontaneous curvature mechanism. In this mechanism the local deformation of membranes occurs when the hydrophobic functional groups of the proteins' insert into the lipid bilayer shallowly like a wedge as seen in figure 1.10. These wedges perturb the packing of the lipid polar headgroups causing a local monolayer deformation.(Zimmerberg and Kozlov 2006) Since voids can't exist in the membrane the hydrophobic lipid chains respond by tilting, resulting in the local bending of the monolayer towards the insertion and consequently bending the whole bilayer. (Martens and McMahon 2008) Both the scaffold building and local spontaneous curvature mechanisms require a feedback system in which the proteins can sense curvature. The effective energy consumed for binding and for bending can provide the necessary feedback. It is also possible for these mechanisms to work together. (Zimmerberg and Kozlov 2006) For example, curvature may be induced by the shallow insertions of protein moieties acting as wedges in the membrane in a coordinated fashion where these multiple molecules are held

in close proximity by a scaffold. (Martens and McMahon 2008) In the case of HA, at low pH the fusion peptide forms a V-shaped structure that buries into the outer monolayer of the membrane. This may increase the lateral pressure at the lipid hydrocarbon region resulting in the outer monolayer experiencing a negative curvature stress. (Basanez 2002)

A direct role for the transmembrane domain (TM) in the mechanism of membrane fusion has been revealed by experiments using engineered HA in which the transmembrane domain has been replaced by a glycosylphosphatidylinositol (gpi) lipid anchor.(Kemble and others 1994; Kemble and others 1993) In these experiments without the TM, membrane fusion is arrested at the hemifusion state with no fusion pore forming even after very long times. Whether the TM serves to couple forces created by protein folding into the bilayer, disrupt the lipid packing, or contributes structurally to the transmembrane pore remains a point of debate.(Kemble and others 1994; Kemble and others 1993; Melikyan and others 1995; Schroth-Diez and others 2000)

A.

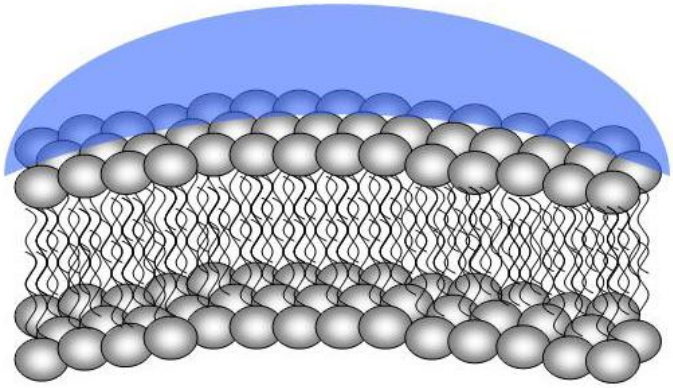

B.

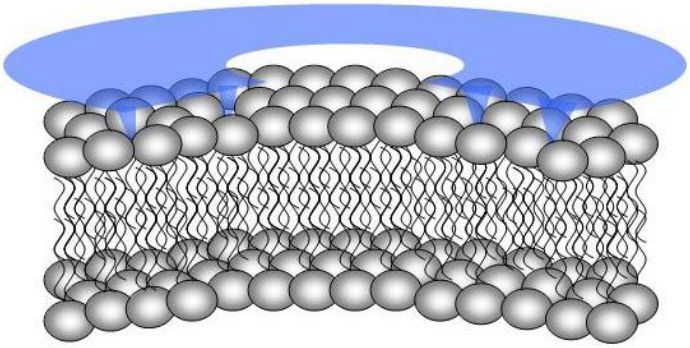

C.

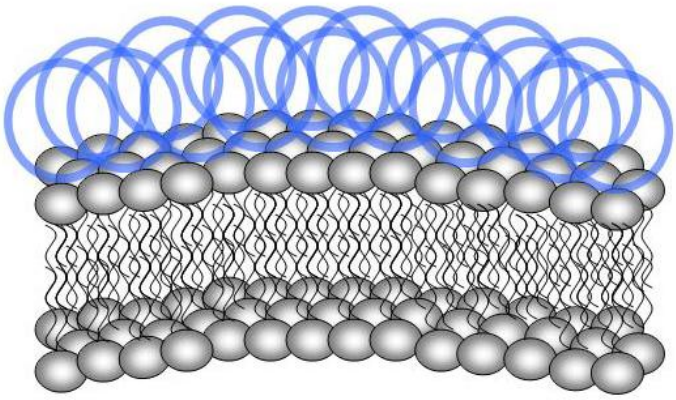

Figure 1.10. Membranes curved by interactions with proteins. A. The protein has intrinsic curvature that after binding the membrane's surface bends it. B. The protein has amphiphatic moieties that insert into the bilayer between the polar headgroups. C. Several proteins bind to the membrane surface forming structures that stabilize membrane curvature. Adapted from (Zimmerberg and Kozlov 2006)

Mutations in the short fusion peptide have a very large effect on the efficiency of fusion.(Duffus and others 1995; Kielian and others 1996) Our current mechanistic picture of the molecular level activity of the fusion peptide in disrupting the membranes is incomplete. One hypothesis about the mechanisms of the peptide is the 'spring-loaded boomerang' model which theorizes that energy gained by HA2's formation, extension and embedding of the coiled coils into the target membrane is used to dehydrate and bend the membranes so they can fuse by removing the remaining distance between the two proximal leaflets to allow for lipid mixing.(Chernomordik and Kozlov 2003; Tamm 2003; Weise and Reed 2008; White and others 2008) The fusion peptides will act as lipid mixers and interact directly with the transmembrane domains to open the fusion pore via a hemifusion intermediate.(Tamm 2003)

Cooperative interactions of the membrane contacting domains of the fusion proteins may also be fundamental to membrane fusion. As mentioned previously, Baculovirus gp64 requires cooperativity between viral proteins for membrane fusion to proceed. In other fusion proteins, like HA, cooperativity is likely, though not energetically necessary. This cooperativity leads to speculation of whether lipid interaction in the hemifusion stalk is restricted by a ring-like complex of glycoproteins. If proteins form a loosely packed ring around the TMC then lipids will be able to mix within the stalk allowing for lipid mixing without content mixing (figure 1.11 B). If proteins are packed tightly in a ring around the TMC then lipid flow will be restricted between outer leaflets and content mixing may precede lipid mixing(figure 1.11 A).(Chernomordik and Kozlov 2005) Protein cooperativity has also been suggested for many other membrane fusion protein phenomena including SNARE mediated fusion. (Hua and Scheller 2001)

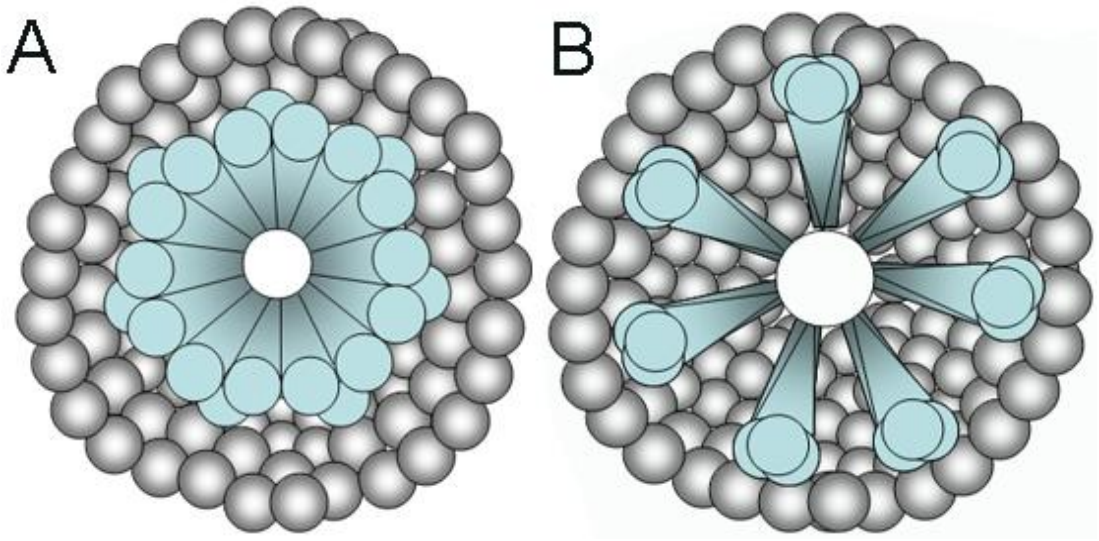

Figure 1.11. Top view of two models of details of the fusion pore in a lipid bilayer. Proteins are the light blue and lipids are the gray circles. A. Lipids are prevented from mixing between the two membranes by a tight collar assembled from the transmembrane domains of several fusion proteins. B. The assembly of transmembrane domains of multiple fusion proteins at the fusion pore are loose enough to allow lipids to diffuse between the two membranes. Image adapted from(Blumenthal and others 1996).

1.4.10 Lysis During Pore Formation

Molecular Dynamic simulations show that when lysis occurs it happens after stalk formation but before fusion pore formation. In the first model adjacent holes in the bilayer were formed by the stalk intermediate, the stalk encircled the holes and then the holes expanded to form fusion pores. Lysis would occur if the holes expand faster than the stalk can encircle them. In the second model the HD did not rupture. Instead a rupture in the bilayer adjacent to the HD formed due to stress (figure 1.12). The final model showed lysis prior to stalk formation due to very high membrane curvature leading to membrane instability. This model shows the importance of lipid composition, though modifications in lipid composition affected lysis probability in all models. Also both SNARE mediated and viral protein mediated fusion showed lysis. It is the general consensus that influenza and

other viral proteins work together during the fusion process, forming a ring. If the proteins are not geometrically coordinated then lysis may occur. Without the ring, hole expansion proceeds beyond the HD and the membrane is essentially torn in the simulation. (Engel and Walter 2008)

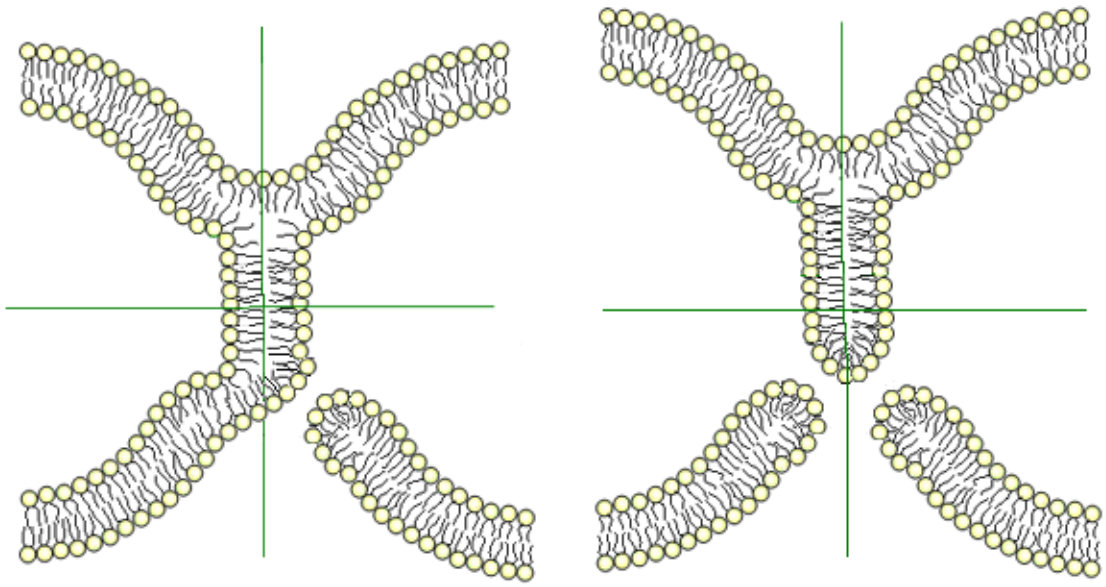

Figure 1.12. Membrane lysis during biological membrane fusion. Formation of the HD can result in nucleation holes next to the hemifusion stalk. The stalk will eventually encircle the holes to form a fusion pore in which content is lost. (Engel and Walter 2008)

1.5 Background of Dynamic Experimental Techniques

The importance of X-ray crystallography to our understanding of membrane fusion cannot be overstated. Landmark structures of HA (Bullough and others 1994; Wilson and others 1981), E1 (Bressanelli and others 2004; Gibbons and others 2004; Jardetzky and Lamb 2004; Modis and others 2004; Rey and others 1995) , gp41 and gp120 (Freed and others 1990; Furuta and others 1998; Kwong and others 1998)in a variety of pre and post activated states have not only given direction to the field of membrane fusion but also were critical

milestones in the field of structural biology. Electron cryo-microscopy and X-ray crystallography have provided insights into the overall virus particle composition.(Mukhopadhyay and others 2006; Skehel and Wiley 2000; von Bonsdorff and Harrison 1975; Zhang and others 2002) Both techniques can achieve near Å resolution, but provide only static images. Even with images such as the pre-fusion and post-fusion configuration of HA, the actual intervening folds of the protein and the steps of the membrane fusion process are unknown, creating the need for dynamic measurements.

Incorporation of fluorescent labels into the virus particles has allowed the most detailed studies of the dynamics of membrane fusion. For these measurements fluorescent lipid-like markers are added to the lipid bilayer of viruses, cells and liposomes or aqueous fluorescent labels are added to the interior of the compartments (figure 1.13). Often these fluorescent labels are added at high enough concentrations to self-quench so that upon fusion, they mix into the target compartment and dilute, relaxing the quenching and increasing the fluorescence. (Chen and others 1993; Hoekstra and others 1984; Nunes-Correia and others 2002; Smit and others 2002) Variations of this assay use resonant energy transfer between two distinct fluorophores to report concentration.(Struck and others 1981) Bulk fusion studies using this method have helped determine the lipid composition, pH conditions and temperature necessary for binding and fusion to occur. (Nunes-Correia and others 2002; Ohki and others 1998; Peisajovich and Shai 2003; Smit and others 2002; Smit and others 2003; Thongthai and Weninger 2008; Tsao and Huang 1985; Waarts and others 2002)

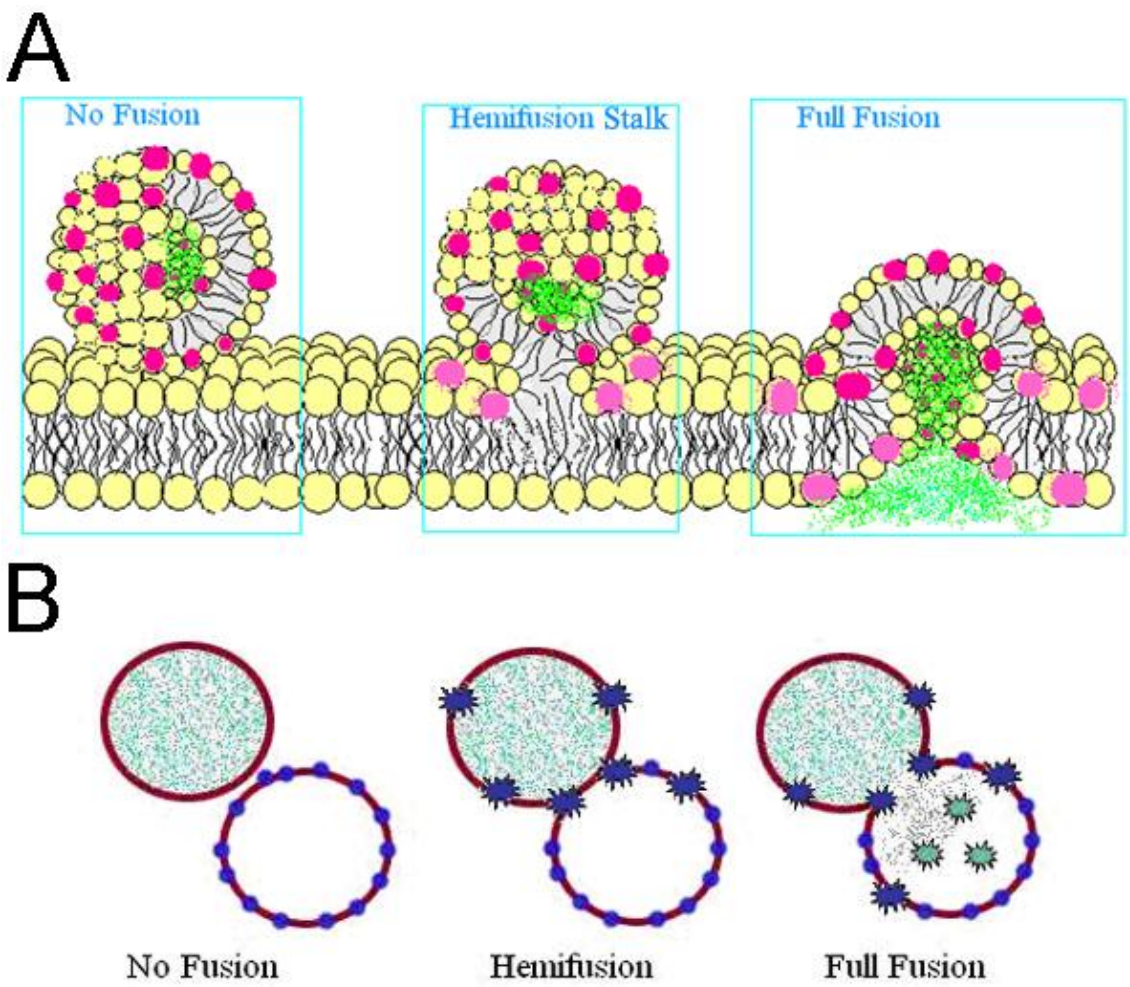

Figure 1.13. Fluorescent dyes in liposome. Fluorescent lipid dyes incorporated into a virus membrane can report on lipid-mixing occurring during hemifusion, but detection of content mixing is required to confirm pore formation and full fusion. A) Fusion of a vesicle with membrane and content dye to an unlabeled planar bilayer. B) Fusion of a membrane labeled vesicle to a content labeled vesicle.

Greater details of the kinetics of membrane fusion intermediates can be gleaned by using a microscope capable of imaging the fluorescence of individual dye-labeled virus particles. For example, using the single particle approach the times between binding and fusion (when no hemifusion intermediate is detectable), between binding and hemifusion and between hemifusion and full fusion have all become measurable. (Floyd and others 2008; Hinterdorfer and others 1994; Markosyan and others 2005; Melikyan and others 2005; Niles

and Cohen 1991; Wessels and others 2007; Yoon and others 2008) A recent single particle fluorescence study of individual influenza particles fusing under acidic conditions with lipid bilayers discovered the existence of three intermediate steps between low-pH activation and the quasi-stable hemifusion stalk state. One further single kinetic step was required to proceed from hemifusion to opening of the fusion pore.(Floyd and others 2008) The use of the single particle approach to resolve the details of membrane fusion dynamics holds great promise for the future.

The single particle fluorescent microscopy imaging techniques can be adapted to a number of different configurations. By using streptavidin coated surfaces, individual biotinylated vesicles can be immobilized on surfaces for imaging.(Boukobza and others 2001) The presence of the surface may affect the free energy of the system, but the ability to make extended observations of a single virus-liposome complex provides an approach that can overcome the limitations of bulk fusion assays due to the stochastic nature of each fusion event and the difficulty in synchronizing fusion of large ensembles of particles. With all fluorescent labeling experiments, careful consideration of the potential artifacts due to the presence of the label or products of photobleaching the dye labels is important.(Thongthai and Weninger 2008)

The single particle fluorescence tracking approach has been used to observe individual virus particles interacting with living cells (For reviews see (Brandenburg and Zhuang 2007; Damm and Pelkmans 2006; Greber and Way 2006; Marsh and Helenius 2006; Pelkmans and Helenius 2003) and also see (Brandenburg and others 2007; Finke and others 2004; Seisenberger and others 2001; Vonderheit and Helenius 2005)). Protein dye labels,

membrane dye labels and Green Fluorescent Protein (GFP) have been used to track viruses as they enter the cell and after entry into the cell as they moved towards the nucleus.(Finke and others 2004; Seisenberger and others 2001)

For enveloped viruses, labeling the viral membrane with self quenched concentrations of fluorescent dye has allowed membrane fusion with cellular membranes to be detected during single particle tracking experiments. (Lakadamyali and others 2003; Markosyan and others 2005; Melikyan and others 2005; van der Schaar and others 2007) For some viruses, the moment of membrane fusion has been correlated with a sequence of well defined active transport steps following endocytosis that move the virus to specific locations in the cell.(Lakadamyali and others 2003; Lakadamyali and others 2004; van der Schaar and others 2007) Double labeling of viruses with pH sensitive dyes demonstrated fusion followed endosomal acidification.(Lakadamyali and others 2003) In influenza, single particle tracking revealed that fusion occurs during late endosomal acidification near the perinuclear region of the cell typically about 8 minutes following the initial binding of the virus to the cell. During this interval, the virus is endocytosed, transported toward the perinuclear region where it undergoes intermittent movement by plus- and minus-end-directed microtuble-based motilities until acidification. (Lakadamyali and others 2003) HIV-1 is not endocytosed but single particle tracking techniques have been used to show that aqueous contents never transfer before the spread of lipid dye. The time between lipid dye spread and aqueous content transfer is stochastic, sometimes occurring several minutes after the membrane label has disappeared, and is dependent on the target cell.(Markosyan and others 2005)

Unfortunately, dye-labeling to allow dynamic observations using florescence microscopy can also perturb the virus functions. Dye molecules must not be reactive. The constant bombardment of photons will cause photobleaching (an irreversible chemical change to a non-fluorescent state) of the dye molecules. The bleaching of live cells with laser-light to reduce autofluorescence is known to change normal physiology over time.(Hoebe and others 2007) Experiments have shown that R18, a lipid membrane dye, adversely affects SV infectivity lowering it by up to 4 magnitudes. R18 does not affect SV's fusion capabilities.(Thongthai and Weninger 2008) Calcein, a soluble non-permeable dye, does (data presented later in section 3.2.1).

1.6 Preview of Upcoming Chapters

For my experiments, I use fluorescent lipid dyes in the virus or liposome membranes and sometimes aqueous content dye in the liposomes. Using bulk solution experiments, single virus particle experiments with bilayers and single virus particle experiments with immobilized liposomes, I look for dequenching of the fluorescent dyes to signal lipid mixing indicative of either hemifusion or pore formation. In the next chapter, Materials and Methods, I discuss how to prepare my virus and liposomes as well as my experimental setup and the errors that can affect my data. In subsequent chapters I will present results from my bulk and single particle experiments. Finally I include a brief discussion of my experimental results.

MATERIALS AND METHODS

2.1 Virus

Influenza (A, X:31, A Aichi/68, H3N2) grown in fertilized chicken eggs and purified by density-gradient ultracentrifugation was purchased from Charles River Laboratories (Wilmington, MA) and used as provided (2mg/ml viral protein). Sindbis was grown in baby hamster kidney cells (BHK-21) cultured by standard methods in minimal essential media with Earl's salts containing 10% fetal bovine serum, 5% tryptose phosphate broth, and 2mM glutamine. Cells were inoculated with Sindbis virus (SV) and incubated for 12h at 37^{o}C. Supernatant was then collected and clarified by low-speed centrifugation. Sindbis virus was purified from the clarified supernatant by ultracentrifugation on a step density gradient followed by a continuous density gradient in phosphate-buffered saline (PBS, 10 mM phosphate, 140 mM sodium chloride, pH 7.4), containing variable amounts (15-35%) of potassium tartrate to adjust the density. Purified Sindbis solutions were adjusted to a concentration of 2×10^{12} particles/ml as calibrated by BCA Assay (Pierce Biotechnology, Rockford, IL). Mosquito produced SV was grown in U4.4 cells (Paredes and others 2004) in Mitsuhashi and Maramorosch media. Cells were inoculated with Sindbis virus and incubated for 12 hours at 37^{o}C. Supernatant was collected and clarified by low speed centrifugation. Sindbis was used immediately or stored at -80^{o}C without noticeable loss of fusion capacity.

Both Sindbis and influenza were dye-labeled with the hydrophobic fluorescent dye R18 (octadecyl rhodamine B chloride), DiD (1,1'-dioctadecyl-3,3,3',3'-tetramethylindodicarbocyanine, 4-chlorobenzenesulfonate salt), DiI (1,1'-dioctadecyl-3,3,3',3'-tetramethylindocarbocyanine perchlorate) or DiR (1,1'-dioctadecyl-3,3,3',3'-

tetramethylindotricarbocyanine iodide) from Molecular Probes (Invitrogen, Carlsbad, CA). Aliquots of virus (100μl each, Sindbis at 2×10^{12} particles/ml, influenza at 0.2 or 2 mg/ml viral protein) were rapidly mixed at room temperature with 3μl of dye dissolved in ethanol at 1.4 mM. The dye-virus mix was incubated on ice for 2h. Virus was purified from unincorporated dye by gel filtration (NAP 5, G.E. Biosciences, Piscataway, NJ) at room temperature in PBS (for Sindbis) or Hepes-buffered saline (HBS, 45mM Hepes, 100mM NaCl, pH 7.4) (for influenza). We estimate that gel filtration in NAP 5 columns diluted the samples to ~1/3 the starting concentration (0.7×10^{12} particles/ml (Sindbis) or 0.07 or 0.7 mg/ml viral protein (influenza)).

When undyed virus was used, it was diluted to this same concentration. For experiments with calcein encapsulated liposomes undyed virus was put in high-salt HBS (17.5 mM Hepes, 625 mM NaCl, 0.15 mM EDTA) via gel filtration with a NAP-5 column.

2.2 Liposomes

2.2.1 Undyed Liposomes

All lipids (including total liver extract, brain phosphatidylethanolamine (PE), egg phosphatidylcholine (PC),brain phosphatidylserine (PS), 1,2-Dipalmitoyl-*sn*-Glycero-3-Phosphoethanolamine-N-(Cap Biotinyl), brain sphingomyelin, and cholesterol) were purchased from Avanti Polar Lipids (Alabaster, AL). Chloroform was removed from solutions of lipids and cholesterol (mixed at ratios indicated in the text) under flowing argon leaving a film on the surface of a glass tube. The lipid films were placed in vacuum for at least 2 hours and then hydrated with either Tris-buffered saline (TBS, 25 mM Tris-HCL, 150 mM NaCl, pH 7.3) or Hepes-buffered saline (HBS, 5 mM Hepes, 150 mM NaCl, 0.1 mM

EDTA) or high-salt HBS. Small unilamellar vesicles were prepared by extrusion through 100-nm-pore filters (miniextruder, Avanti Polar Lipids) at 5 mg/ml (liver extract), 4 mg/ml (mixes), or 20 mg/ml (PC).

2.2.2 Liposomes with Membrane Dye

Rhodamine PE (Avanti Polar Lipids) and DiD stored in choloroform were added to the lipid mixtures at 5% molar ratio for virus to vesicle experiments or protein free bilayer experiments and 1-2% molar ratio for FRET experiments. The chloroform was evaporated from the dye/lipid mixtures using flowing argon. Otherwise the protocol was the same as listed in section 2.2.1.

2.2.3 Liposomes with Gangliosides

Two types of gangliosides were used in these experiments: total gangliosides extract or GD1a. Total ganglioside extract from porcine brain (Avanti Polar Lipids) was stored in choloroform, and was added to the lipid mixtures in chloroform at the indicated molar ratios prior to evaporation of chloroform under argon flow. Otherwise the protocol was the same as listed in section 2.2.1. GD1a, purchased from Sigma-Aldrich (St. Louis, MO), was stored in dimethyl sulfoxide (DMSO). DMSO does not evaporate as easily as chloroform. Therefore to form mixtures of GD1a and lipids, GD1a was tranasfered to an empty glass tube and then the DMSO was evaporated under flowing argon. The tube was then placed in a vacuum until no visible liquid remained in the tube. The argon and vacuum steps were repeated as many times as was necessary. Then additional lipids in chloroform were added to the glass tube. The rest of the protocol to remove chloroform and form liposomes was the same as in section 2.2.1.

2.2.4 Liposomes Encapsulating Calcein Dye

Calcein was purchased from Sigma-Aldrich (St. Louis, MO). Liver extract was purchased from Avanti Polar Lipids (Alabaster, AL) at 25 mg/ml in chloroform. The chloroform was evaporated using argon gas to leave a lipid film on the test tube which was placed in a vacuum for a minimum of 2 hours, then rehydrated with buffer augmented with either 200 mM or 55 mM calcein dye (5mM Hepes/ 0.1 mM EDTA) adjusted to pH 8.0. After brief sonication, the solution was incubated at room temperature for at least 30 minutes. The solution was then extruded through a 0.1 micron filter (miniextruder, Avanti Polar Lipids) to create vesicles of the desired size. Calcein dye in the solution outside the liposomes was removed by passing the sample over a CL4B gel filtration column in buffers (either HBS or high-salt HBS) at pH 7.4.

2.3 Bulk Experiments

2.3.1 Experimental Setup

Bulk fluorimeter testing of florescent dyes, liposome compositions and buffers was performed in parallel with TIRFM experiments in order to ascertain the combination of dyes, liposomes and buffers that would produce the most fusogenic system. Bulk fusion experiments were performed on a Hitachi (Kyoto, Japan) F-4500 fluorescence spectrometer (figure 2.1). A quartz cuvette is placed in the excitation beam path. The cuvette holds between 100 μl to 200 μl of sample. Emission of the fluorescent dye is recorded. The slit width for excitation and emission wavelength was adjusted depending on the dye used in the experiment. The spectrophotometer's PMT voltage was 950 V and the response time remained set to 0.5 seconds for all experiments. A water bath was used in some cases to

regulate the temperature of the cuvette by pumping heated/cooled water through tygon tubing attached to the fluorimeter. Most experiments were performed at room temperature unless otherwise noted.

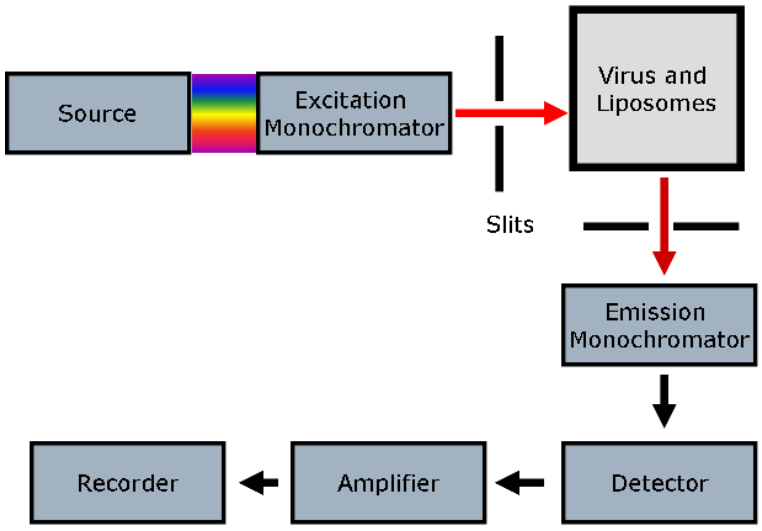

Figure 2.1 Schematic diagram of a Photospectrometer.

2.3.2 Calibration of Fusion curves

For testing fusion, 50 µl of virus (~0.7 x 10^{12} particles/ml) and 50 µl of liposomes (0.25 mg/ml), both stored in neutral pH are placed in the cuvette and an initial intensity, I_o, is recorded, then 100 µl of buffer at either the same (control) or lower pH is added. When the pH of the buffer is changed, the final desired pH is obtained by adding a pretested lower pH to the sample. The sample is always stored in neutral pH. Equal volumes are added to simplify the calculation of final concentrations. The emission intensity as a function of time,

I, is recorded for twenty minutes. At the end of each measurement, a small amount (1% volume fraction) of 100 mM dodecyl-maltoside is added to the cuvette to dissolve liposomes and viral membranes. Liposomes are dissolved to determine the intensity of the dye when it is completely unquenched, I_f. The final fusion percentage is calculated using the equation (fusion %) = 100 * (I - I_o/2)/I_f. Only the portion of the curve between the addition of buffer to control the pH and the addition of detergent is retained. The moment of addition of pH controlling buffer is set to zero time. The calibration process is illustrated in figure 2.2. The intial intensity, I_o, is halved because at time zero, for I, the volume in the cuvette is doubled. The sudden rises in the curve are due to the lid of the instrument being opened to allow buffer/detergent to be pipetted into the cuvette. The photospectrophotometer was also used to test the fluorescent dye properties. Either the excitation wavelength can be set and the emission wavelength recorded or vice versa. These curves were not calibrated. The specific units the intensity is recorded as are not specified so they are listed as arbitrary units (A.U.) on the graph axes in section 3.1.

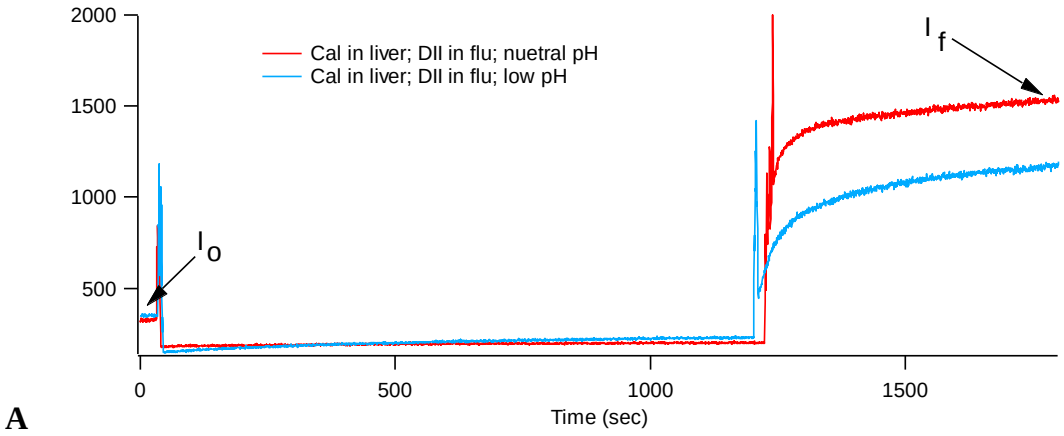

A

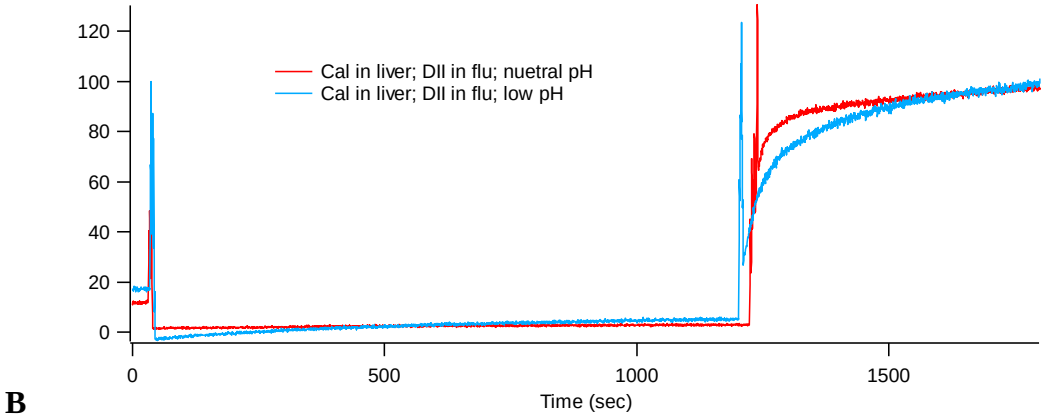

B

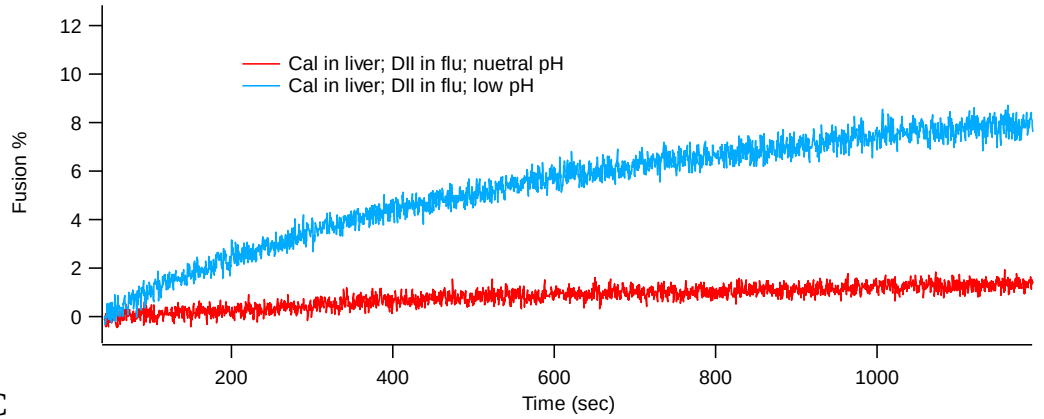

C

Figure 2.2. Calibrating fusion curves. A) Raw data. The spikes up in intensity occur when the instrument door is opened allowing white light from the room to filter in when buffer or detergent is pipetted into the cuvette. B) The curve is now calibrated so the final intensity after detergent is added is 100%. B) The last step is to zoom in on the middle portion of the curve and initialize the curves to zero.

2.4 Total Internal Reflection Fluorescence Microscopy

2.4.1 Emission Measurements Using a Single Dye

Single virus particles were observed with a prism-type total internal reflection florescence microscope (figure 2.3). Samples were illuminated with 8−10 mW laser light (532 nm). Fluorescence emission was collected by a water immersion objective lens (PlanApo 60X, NA 1.2, Olympus, Melville, NY), filtered by long-pass filter (HQ545lp, Chroma Technologies, Rockingham, VT), and detected with an electron multiplied CCD camera (Cascade 512B, Photometrics, Roper Scientific, Tucson, AZ) at 10 or 67 frames/s and electron multiplication set to 3000 (Roper Scientific ADC units in manufacturer supplied dynamic link library). Custom programs written in MATLAB (The MathWorks, Natik, MA) identified individual spots within movies resulting from single, isolated virus particles. Intensity time traces were extracted from the movies at those locations by integrating the background-subtracted signal from a 7-pixel-diameter circle (1.8 μm in the sample plane) centered on the identified spots and averaging by the integrated number of pixels. Virus solutions with low pH were injected into the flow cell while movies were recorded. For injection into flow cells, virus solution at neutral pH (~0.7×10^{12} particles/ml for Sindbis; 0.07 or 0.7 mg/ml viral protein for influenza) was contained in one syringe and acidic buffer was held in a second syringe. A motor actuated both syringes when the injection was triggered. The two solutions mixed in a T (mixing time < 1 second) and then traveled to the entrance of the flow cell. We measured a 1 second delay between solution leaving the tee and appearing in the field of view in a flow cell mounted on the microscope. The virus was acidified 1-2 seconds before it was exposed to the lipid bilayer. Enough solution was

perfused to ensure that 2.5 channel volumes were injected through the flow cell within 5 seconds (20 μl/s) during each experiment. Particles then encountered the bilayer at random times after their free diffusion in the flow cell.

Quartz microscope slides were cleaned with a sequence of bath sonication steps (soapy water, acetone, ethanol, 1 M potassium hydroxide, and water), and dried in a propane flame immediately before use. Flow-cell chambers were built by attaching glass coverslips to the quartz microscope slides, with channels defined by double-sided tape. The ends of the channels were sealed with 5-minute epoxy. Fluid was introduced into the channel through holes drilled in the quartz slide at either end of the channel. To form supported bilayers on the walls of the channel, liposomes were incubated in the chamber for 5 minutes and then rinsed away. A second incubation with 20 mg/ml of PC liposomes for 1 hour improved overall experimental reproducibility.

Sindbis virus will stick to many surfaces. We minimized surface adsorption by constructing the buffer exchange apparatus using PEEK (polyetheretherketone) tubing and fittings from Upchurch Scientific (Oak Harbor, WA) and disposable syringes (Norm-Ject, Henke Sass Wolf, Tuttlingen, Germany). Clear Tygon tubing was used immediately before the flow-cell entrance to diagnose the presence of air bubbles.

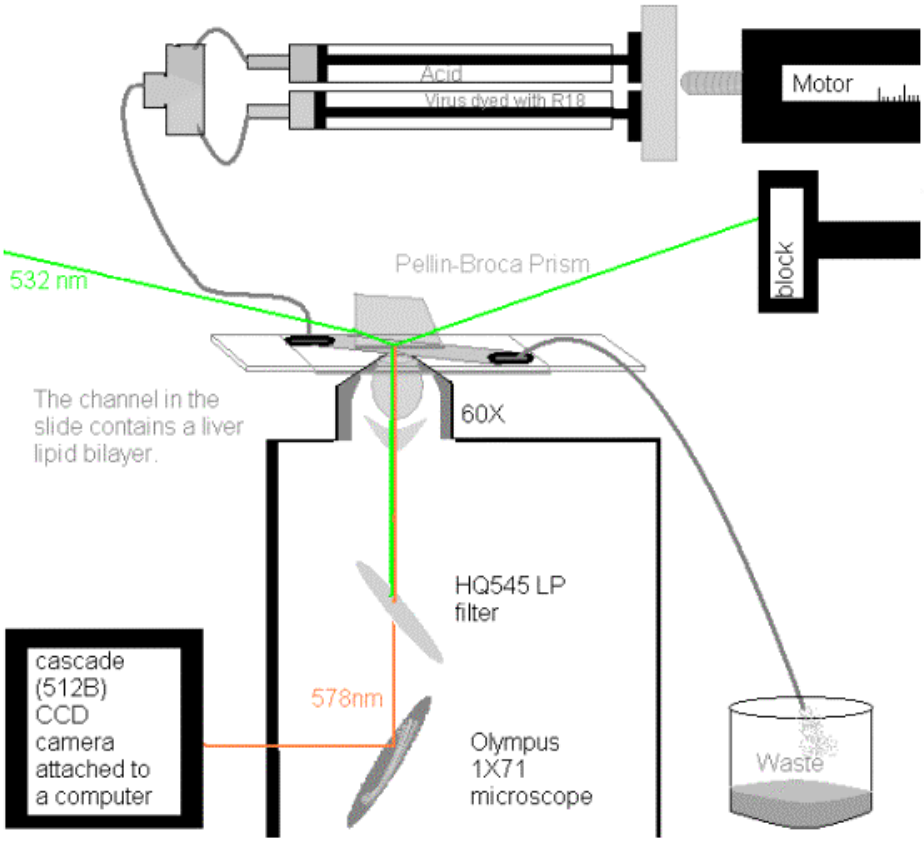

Figure 2.3. TIRFM's experimental setup. A motor pushes two syringes simultaneously. One syringe holds virus labeled with R18 membrane dye and the other syringe holds low pH used to trigger fusion. The virus and acid are mixed in a T before entering the channel. The lipid bilayer is preformed on the slide. R18 is excited by a 532nm laser. It fluoresces at 578 nm. A long pass filter allows the emission wavelength to pass through while it blocks the laser's wavelength. The emission wavelength is directed to a CCD camera where emission intensity is recorded.

2.4.2 Emission Measurements Using Two Dyes

For experiments in which two fluorescent dye molecules needed to be imaged simultaneously during data collection a Dual-View splitter (Optical Insights, New Mexico) was inserted between the microscope and the CCD camera to split the emission spectrum into two separate channels. The HQ545 LP filter was not inserted in the microscope to allow all collected light to pass into the dualview splitter. A 645 nm dichroic was used when imaging

DiD and DiI/R18. A 645 nm dichroic was used when imaging calcein and DiD/DiR. A 565 nm dichroic was used when imaging calcein and DiI. The dualview splitter allows for the bandpass filters to be placed in each channel to filter laser light out. The bandpass filter for the calcein channel was 550/100 nm. The bandpass filter for the DiD channel was 700/75 nm. Two bandpass filters were used in different experiments in the DiR channel: 750/30 and 805/50. The bandpass filter used for the DiI channel was 585/70 nm.

Flow cells in quartz microscope slides were constructed as described in section 2.4.1. These liposomes were bound to a quartz slide by infusing the slide's channel with 1 mg/ml Biotinylated Bovine Serum Albumin (Sigma Aldrich, St. Louis, MO) for five minutes followed by 0.00007 mg/ml Molecular Probes Streptavidin (Invitrogen, Carlsbad, CA) for five minutes then introducing the liposomes (0.0006 mg/ml) for five minutes. Either undyed SV or undyed influenza (~0.7×10^{12} particles/ml for Sindbis; 0.07 or 0.7 mg/ml viral protein for influenza) was used to fuse with the liposomes. If undyed influenza was used then the channel was infused with the flu for 5 minutes as a final step. After each step the channel was rinsed with buffer. With both viruses the double syringe pump was loaded with virus in one syringe and buffer in the other. The buffer was pretitered to yield a final pH of 7.4, 5.1 or 4.6. In control experiments where virus was not used, the second syringe was loaded with the high-salt HBS buffer at pH 7.4.

2.5 Creating Microfluidic Flowcells with PDMS

Polydimethylsiloxane (PDMS) (Sylgard 184 from Dow Corning) was used to make microfluidic channels that could sit upon a coverslip. (Fu and others 1999; McDonald and others 2000) First a transparent film was made using Adobe Illustrator

which contains the flow channel design. This pattern was printed using a commercial laser printer with 20,000 dpi resolution. Next a four inch silicon wafer with photoresist SU-8-2100 applied at 2000 rpm and baked at 95^{o}C for two hours was covered with the pattern mask and exposed to ultraviolet light for two minutes. The resist was developed, etched and removed to produce the five channel pattern as raised features on the silicon. PDMS was poured over the silicon mold and allowed to cure for 50 minutes at 150^{o}C until it became crosslinked. After crosslinking, the polymer was peeled off the mold. The surface of the polymer that was in contact with the mold was left with an imprint of the mold topography, defining the channels that form the microfluidic system. Five channels with dimensions 25 mm X 150 μm X 167 μm were designed on a single chip (figure 2.4). Holes were punched into the ends of the channels to allow introduction of solutions into the channels.

2.6 Discussion of Sources of Error Precision and Accuracy in the Experiments

Errors introduced by limitations in the accuaracy, precision and stability of the instruments (laser illumination sources, microscope optics, emCCD detection) are insignificant in these experiments compared to the batch-to-batch variations in the properties of the biological samples. The dominant sources of error in these experiments are related to quantitiative variation in the fusion behavior of the viruses and the bilayer structures formed by the lipids, which will be discussed in more detail below.

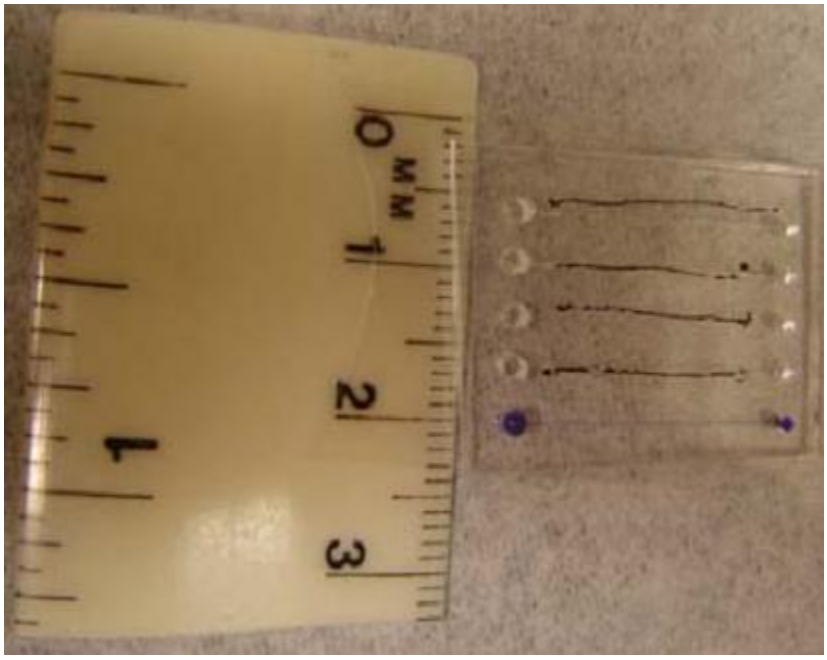

Figure 2.4. Microfluidic slide with five channels. A microscope coverslip lies under a rectangle of PDMS with five microscopic channels etched in it. The first four channels have been marked out to indicate they have already been used. The last channel has blue dye through it.

2.6.1 TIRFM Bilayer Experiments

The precise values of our ensemble measurements of single-particle behavior were variable over the months of experimentation of this project. Different purifications of Sindbis virus or different manufacturer lots of influenza virus exhibit different infectivity and fusion capacity. Different substrates and different manufacturer lots of lipids generate heterogeneity in the properties in the supported bilayers. To minimize the effects of the variability of our samples on the ensemble measurements presented here, all data for any given figure was acquired from the same sample, on the same day, on substrates prepared in batch with identical cleaning treatment and using the same supply of lipids. Despite variation in the

precise values of the experiments using different batches of materials, the trends from which conclusions are drawn were consistent in every experiment.

To estimate the expected variability in the quantitative values from our experimental protocol, we simulated multi-experiment runs all in one day, but instead of scanning parameter space, as was done to generate the data in the figures of the Biophysical Journal article (section 4.1.2), we repeated one condition in parameter space many times. From these repeated measurements of a single parameter space point, we estimate the fraction of standard deviation divided by average value for number of fusions at 44% (Sindbis) and 36% (influenza). The fraction of standard deviations divided by the average value for the median residence times are 25% (Sindbis) and 21% (influenza). The fact that both Sindbis virus and influenza have similar quantitative variability in this set of experiments repeating one point in parameter space using a single batch of reagents suggests that these effects are random. The spread in our parameter-space scanning data generally agrees with this variability in regions of parameter space where previous bulk solution experiments suggest there should be no systematic variation. The main ensemble effects that we claim in the article (increased fusion at low pH and increased residence time for Sindbis at pH below 5 for cholesterol containing target membranes) are effects substantially larger than these random run-run variations. The standard deviation of the final dequenching percentages, upon multiple attempts at identical bulk solution virus-liposome fusion experiments, was 10% for both viruses in our lab.

2.6.2 TIRFM Testing of Gangliosides

After lipid bilayers with gangliosides were placed in the flowcell as per section 2.4.1 membrane dyed virus was prepared as per section 2.1 and flowed into the flowcell at varying temperatures and for varying incubation times. The virus was rinsed out of the flowcell with approximately 1 ml of buffer before imaged on the microscope. The number of bound virions in the image was counted using a custom program written in MATLAB (The MathWorks, Natik, MA) for at least ten spots per slide for a minimum of three slides. Error bars represent statistical standard deviation. The error bars do not alter the overall results when testing various incubation times and temperatures, even at the lowest measurement there was more binding at 37^{o}C for 5 minutes compared to other tested combinations of incubation times and temperatures. Unfortunately the variability in testing the percentage of added gangliosides was much higher. The highest measurement of 5% GD1a is higher than the lowest measurement of 1% GD1a creating a lot of uncertainty. Fortunately by knowing the proper temperature and incubation time for maximum binding, the addition of gangliosides is shown to be an improvement compared to not incorporating gangliosides at all. The variability of the specific molar ratio is unimportant since the actual molecular weight of lipids from liver extract is unknown, the incorporation of GD1a can not be precisely calculated, only estimated.

2.6.3 TIRFM Fusion with Calcein Liposomes

After liposomes and, in the case of influenza only, prebound undyed influenza were anchored to slide as per section 2.4.2, a movie of the liposomes was taken to record the unperturbed system. The next movie was taken at a different spot on the slide during buffer

exchange (either pH 4.6, 5.1 or 7.4) with virus. At least two more movies were taken at different spots after buffer exchange. Each experiment has a minimum of four movies. The number of bound liposomes in each movie was counted using a custom program written in MATLAB. Each bound liposome was classified as dequenching, undocking, bursting or non-reacting. Some error in assignment is expected because in some cases the difference between bursting and dequenching is difficult to define. In a bursting event once the dye escapes there is very little intensity left. The decline in intensity after a bursting event should be similar to undocking, a sudden and complete loss. In dequenching events the sudden rise is followed by normal decline in intensity due to photobleaching. In events where there is a sudden rise followed by photobleaching that occurs over tens or even hundreds of frames, this is clearly dequenching. When the sudden rise is followed by an intensity decline of 7-8 frames or less this is clearly bursting. In events where a sudden rise is followed by intensity loss in less than 20 frames an event is usually categorized as bursting though the slow loss of intensity doesn't follow the model well, it still occurs more quickly than photobleaching. Bursting in general is rare. If the bursting and dequenching values are combined the overall pattern for dequenching would not change. The total number of liposomes in each classification was tallied, and divided by the total number of liposomes in that movie to determine the percentage for that classification. Each experiment was performed at least 3 times. Error bars represent statistical standard deviation of the average percentage for a minimum of 3 experiments. Each experiment has a minimum of 3 movies each, so the average and standard deviation are over a minimum of 9 movies.

2.6.4 TIRFM Fusion with Two Dye Emission

Using custom software programs written in MatLab, the bound liposomes were counted and traces were analyzed to identify dequenching events in both colors. Seven slides, with 27 movies total were analyzed. The total number of traces showing a double dequenching event was divided by the total number of bound liposomes to determine the percentage of liposomes that undergo full fusion. The percentage of fusing liposomes for each movie was determined and the standard deviation is the statistical standard deviation of all movies.

2.6.5 Error Bulk Fusion Percentage

The initial slope of the intensity for the time interval 20 minutes (5 minutes in bulk experiments listed in section 4.1.1-4.1.4) immediately after buffer is added into cuvette (time=0, start of figure 2.2 C) until detergent is added, is determined for a minimum of 3 trials. These slopes were averaged and the statistical standard deviation was calculated. Run to run variation in these values is dominated by the inhomogenity of the percentage of dye incorporated into the virus in each labeling reaction. Membrane dye is incorporated into the virus by incubating virus and dye together at specific concentrations for a defined amount of time at a constant temperature. Despite these controlled labeling conditions for each trial, the amount of dye entering the virus was not constant. Looking at uncalibrated data, figure 2.5 shows the red curve has a final intensity starting at 620. The blue, green and black curves all have final intensities between 910-1000. The slope of the curves between 15-250 seconds is a clear indication of which samples underwent fusion and which did not. The red curve when calibrated using the method outlined in section 2.3.2 gives a final fusion percentage of 5%,

but when using the original intensity in the following equation 100 * ($\Delta y/I_f$) a fusion percentage of 7% is found. In comparison the green curve when calibrated using both the method outlined in section 2.3.2 and 100 * ($\Delta y/I_f$) gives a final fusion of 3%. The amount of dye in the virus membrane influences the dequenching signal because the quenching is not strickly a linear function of concnetration. Thus the indicated percentage of fusion is not the percentage of virus particles fusing to liposomes, instead it is the percentage of membrane dye dequenching.

Fusing of two identical liposomes will lead to a doubling of the membrane surface area. Assuming the surface area of the new spherical liposome remains conserved, this predicts a 2.8-fold increase in volume compared to the sum of the two initial volumes. Under this assumption that the surface area is conserved, this model predicts that the content dye will decrease to from its initial 50 mM concentration to 50 mM/2.8 = 17.8 mM. Thus the content dye concentration decreases by more than a factor of 2, whereas the membrane dye is diluted by a factor of two. These geometric issues predict that the lipid and content signals will not track each other precisely.

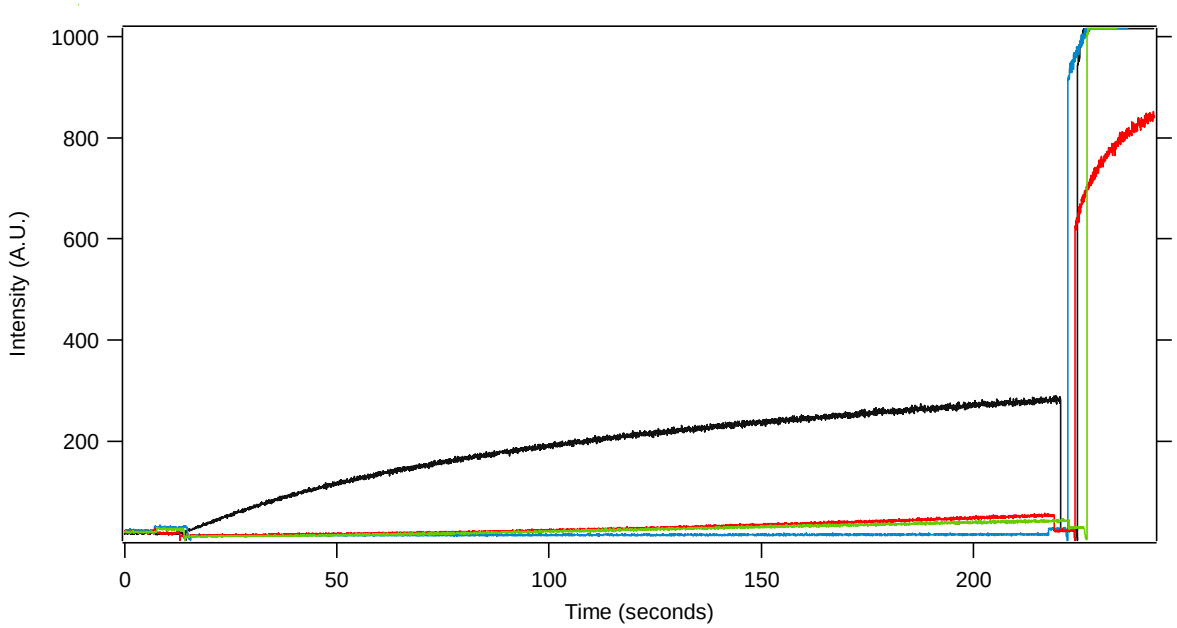

Figure 2.5. Raw data for figure 3.7. In this uncalibrated data, it is clear to see less dye was incorporated in the virus used in the sample for the red curve compared to the other 3 samples that make the green, blue and black curves.

A futher limitation in content dye experiments is that calcein dye leaks from the liposomes and becomes free dye in solution, causing an increase in intensity that mimics fusion under non-fusogenic conditions (section 3.1.1). We estimated the importance of this effect by adding calcein labeled liposome samples to cuvettes without added virus to determine the magnitude of leaking effects. Addition of neutral pH buffer to the cuvette will dilute free dye in solution, which will increase its emission intensity if it is present in a self-quenching concentration regime, but will increase the intensity of free dye in the solution. When the volume in the cuvette is doubled, the overall intensity should be halved. However in the experiments in figure 2.6, the total resulting intensity (red, black and green curves) after dilution is greater than the initial intensity (purple curve).

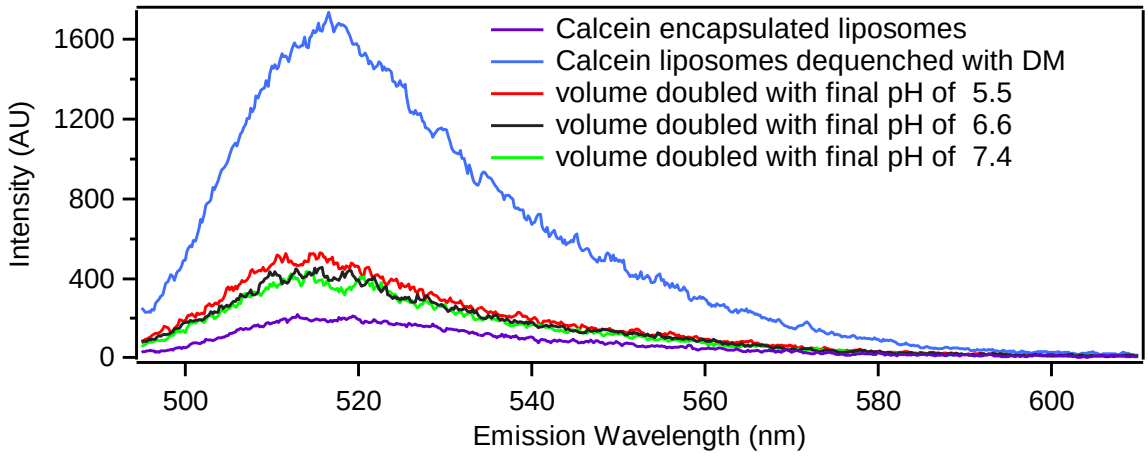

Figure 2.6. Emission curves of calcein encapsulated in liposomes. The same amount and concentration of calcein dyed liposomes was added to the cuvette. The purple curve represents the emission wavelength for 100 μl of liposomes dyed with 222mM calcien (0.25 g/l). 100 μl of neutral pH buffer were added to the cuvette and the emission was recorded again by the green curve. Despite the doubling in volume the intensity increased indicating free calcein dye had leaked into the extravesicular buffer and was dequenched in the now larger volume. The addition of dodecyl-maltoside (DM) to dissolve the liposomes, represented by the blue curve, shows that plenty of dye was still encapsulated by liposomes. This dye dequenches when the liposomes are dissolved, thus the increase in intensity. The process is repeated replacing neutral pH with low pH (6.6 pH black curve and 5.5 pH red curve).

Another source of variability in the experiments is the natural aging of the virus samples. The time the influenza virus was stored at 4^{o}C following thawing from –80^{o}C storage along with the precise buffer used for storage also affect the fusogencity of virus. (Smit and others 2002) After receiving infleunza from Charles River Laboratories (North Franklin, CT) or Sindbis from collaborators the virus was dethawed (in the case of influenza) and aliquotted, then re-frozen with liquid nitrogen. This freezing process causes difficult to quantify degredation to the virus. As mentioned earlier, these sorts of variations in the properties of the biological samples were the largest source of variability in the experiments.

BULK FUSION EXPERIMENTS

3.1 Measuring the Properties of Fluorescent Dye Molecules

3.1.1 Calcein

Calcein is a water soluble dye that is relatively impermeable to cell membranes. It is excited by 495 nm light and emits fluorescence at 515 nm light. Calcein emission is affected by the pH of the solution. Calcein will fluoresce more intensely at low pH (figure 3.1). The wavelength of the peak emission of calcein is much more dependent on the concentration of calcein than on its pH (figure 3.1). As the concentration is increased from 6 mM to 33 mM, the peak location moves to higher wavelengths by as much as 25 nm. The pass bands of the filters used in the TIRFM dualview splitter are typically in 30-50 nm wide, so a 25 nm drift can be significant. For the measurements in figure 3.1 calcein is not encapsulated into liposomes but rather is in solution in a buffer.

Osmotic balance can be assessed using the fluorescence spectrometer to determine the degree of calcein leakage from the liposomes. The addition of neutral pH buffer to samples in the cuvette will not dilute the calcein encapsulated inside liposomes but does dilute the overall liposome concentration. Thus emission from dye within liposomes should decrease. As mentioned in section 2.6.5 the dye emission increased. Calcein molecules have a negative charge of -4 at pH = 7.0. Physiological buffers outside the liposome are hypotonic relative to the liposome interior, causing water to pass through the membrane into the liposome, causing calcein to dequench and increase its emission intensity. (Sears 1983) Eventually the liposome will swell too large and leak or burst, releasing the calcein dye altogether.

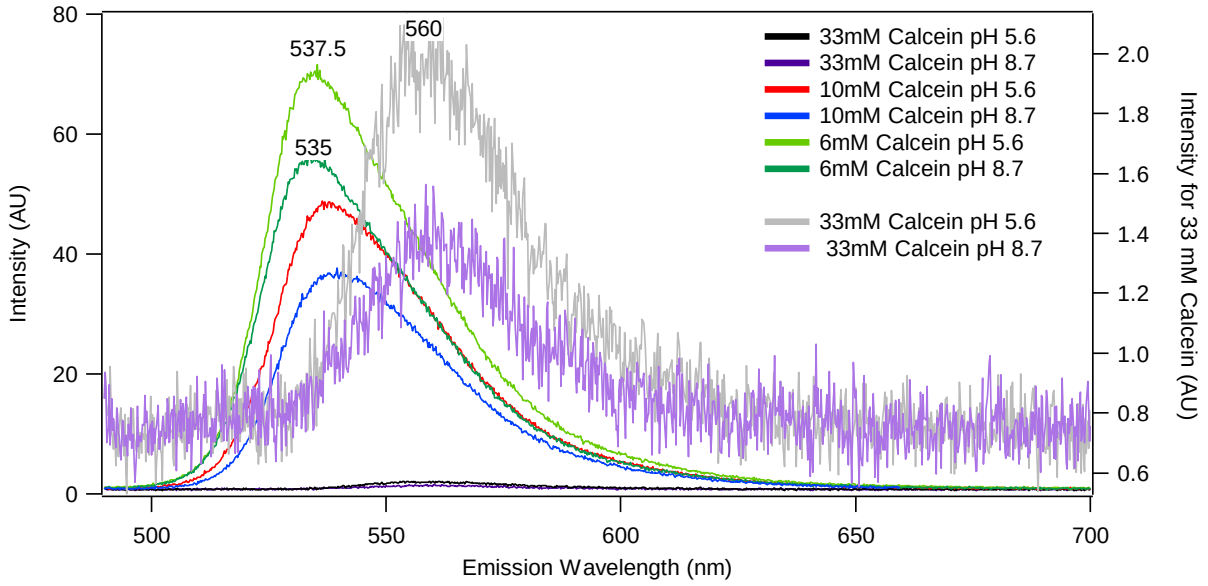

Figure 3.1. Emission peak drift of Calcein. The intensity of fluorescence for calcein is given by the left y-axis in arbitrary units. The 33mM concentration has low intensity compared to 6 mM and 10 mM calcein and so the bottom curves of 33mM calcein were enlarged and given by the right y-axis.

For unperturbed samples, calcein leaks out from the interior of the vesicle very slowly as shown in Figure 3.2. Within three hours, little leakage of calcein dye has occurred. After 20 hours, enough dye has leaked out of the vesicles and dequenched in the larger extravesicular volume resulting in close to a 10% increase in intensity. Initial dilution of calcein containing liposomes in HBS showed more than a 100% intensity increase with the addition of neutral pH. The bulk fluorimeter results were due to free dye that remains following gel purification of the sample. When the liposome sample was passed over the CLB4 column a second time the amount of free dye outside the liposomes was reduced to undetectable levels. Unfortunately this double purifcation diluted the sample, decreased the bulk fluorimeter intensities (initial, fusion and dequenching) and increased noise in the measurements.

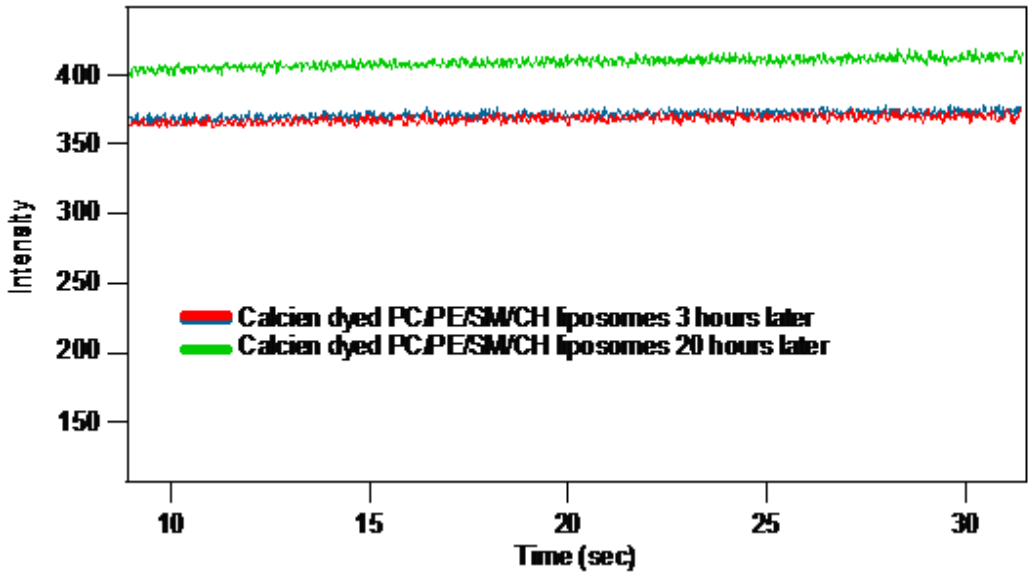

Figure 3.2 Calcein Leakage from liposomes. Calcein is a content dye impermeable to the membrane. Still some leakage of encapsulated dye is observed from liposomes.

Leakage of calcein from the liposomes is dependent on osmolarity, liposome composition, saline viscosity and the choice of buffered saline salts. An osmometer (Wescor 5100, USA) was used to balance the salt concentration outside of the liposome to the calcein concentration inside the liposomes (figure 3.3). Measured points are indicated in color. Red shows measurements for solutions with increasing concentrations of calcien, and blue shows results for calcein-free solutions with increasing NaCl. Using linear fits to the data (shown in black) for calcein of y = 297 (± 204) + 14 (± 4)*x, we predict that 222 mM calcein will have an osmolarity of 3405 mOs/kg. Using the fit to the NaCl data, y = x*(1.67 ±0.1) +196 ± 85, we see that the buffer required to osmotically match calcein requires a concentration of 2M NaCl.

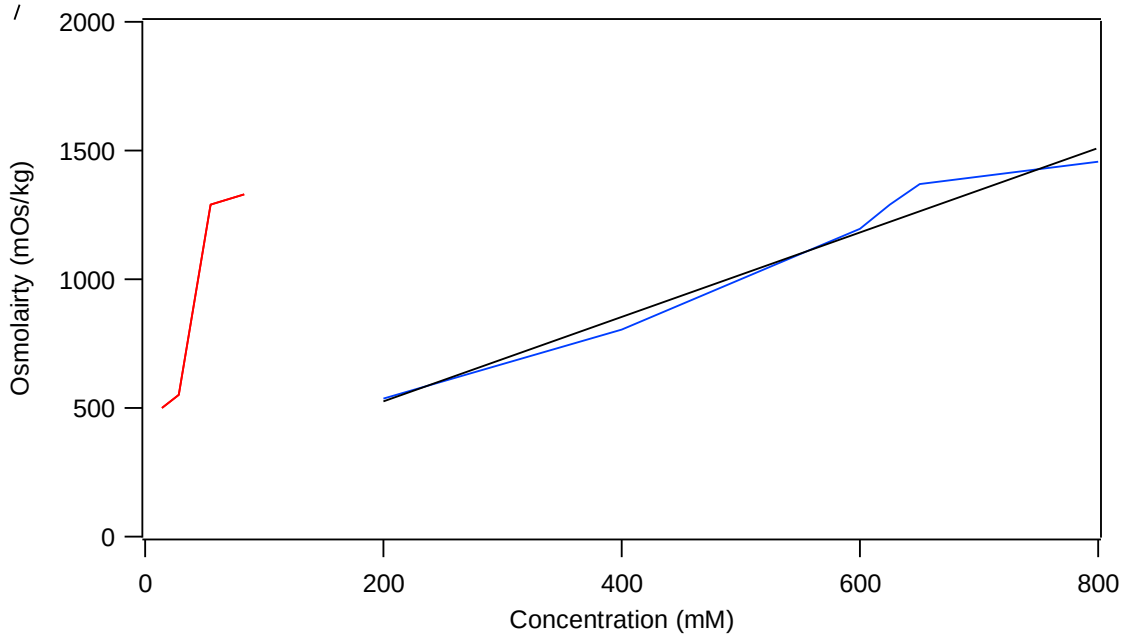

Figure 3.3. Calcein is highly ionic. The red curve shows the rapid increase in osmolarity for calcein. The highest molarity recorded was for 83mM. At 111mM calcein the reading was > 2000 mOs/kg, the osmometer's limit. The blue curve is for NaCl.

3.1.2 DiD

The hydrophobic fluorescent dye DiD (1,1'-dioctadecyl-3,3,3',3'-tetramethylindodicarbocyanine, 4-chlorobenzenesulfonate salt) partitions directly into the lipid bilayer. It is excited by 650 nm light and fluoresces at 670 nm. As shown in figure 3.4, DiD can be excited by 532 nm laser light, resulting in two emission peaks at ~560 nm and ~670 nm. The peak at 670 nm is the expected emission peak for DiD and is usually a result of 635 nm excitation light. The peak at 560 nm is not expected based upon published information for the dye from the manufacturer (Invitrogen). One possible explanation for this extra peak is that it arises from DiI that remains as a byproduct of the synthesis of DiD, which involves chemically altering DiI. Another possibility is that DiD at self-quenching concentrations might form dimeric or other multimeric structures that have altered

fluorescence properties. Such dimers are likely involved in the self-quenching phenomena. For these experiments, the presence of this blue-shifted peak makes FRET experiments using the dye pairs of DiD and DiI, R18 or Rho-PE inconclusive because the 560 nm peak will occur for both dyes under excitation at 532 nm.

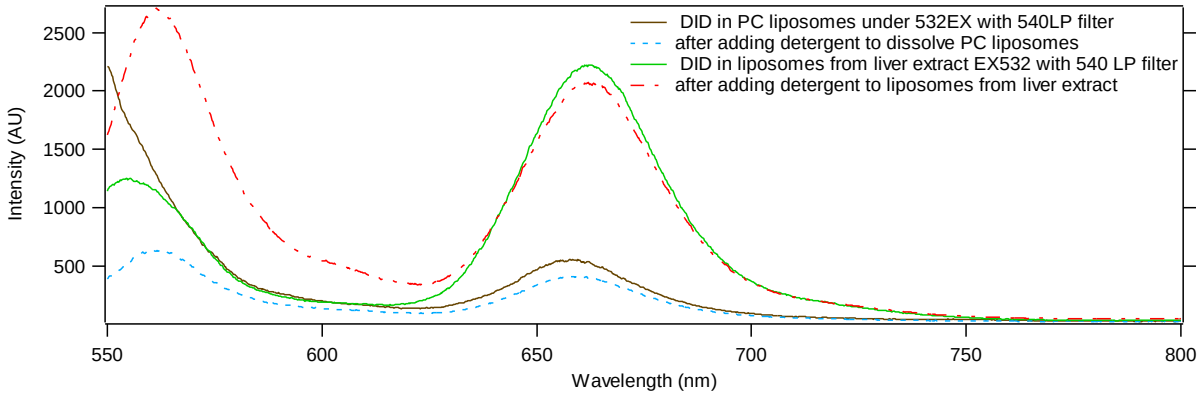

Figure 3.4. Emission Peaks of DiD. Liposomes from extracted liver lipids have cholesterol. Membrane labeling dyes quench at very low percentages when cholesterol is present. In PC liposomes, the dye remains unquenched, no peak is seen at 560nm. The y-axis' intensity is in units not specified by the machine. The 540 LP filter in the emission detector's path filters out excitation light scattered from the liposomes.

3.1.3 DiR

DiR (1,1'-dioctadecyl-3,3,3',3'-tetramethylindotricarbocyanine iodide) is also a hydrophobic fluorescent dye that partitions directly into the lipid bilayer. DiR has an excitation wavelength of 750 nm and an emission wavelength of 780 nm. The Hitachi F-4500 fluorescence spectrophotometer loses detection sensitivity for the far red-infrared wavelengths and thus testing of primary DiR fluorescence properties in bulk experiments was inconclusive. DiR is weakly excited by 635 nm light but its optimal excitation wavelength is 750 nm. DiR is not expected be excited by 532 nm light based on its manufacturer supplied

excitation spectrum measured for dye solublized in organic solvent. However testing of our samples incorporated into liposomes found that 532 nm light excite DiR (figure 3.5).

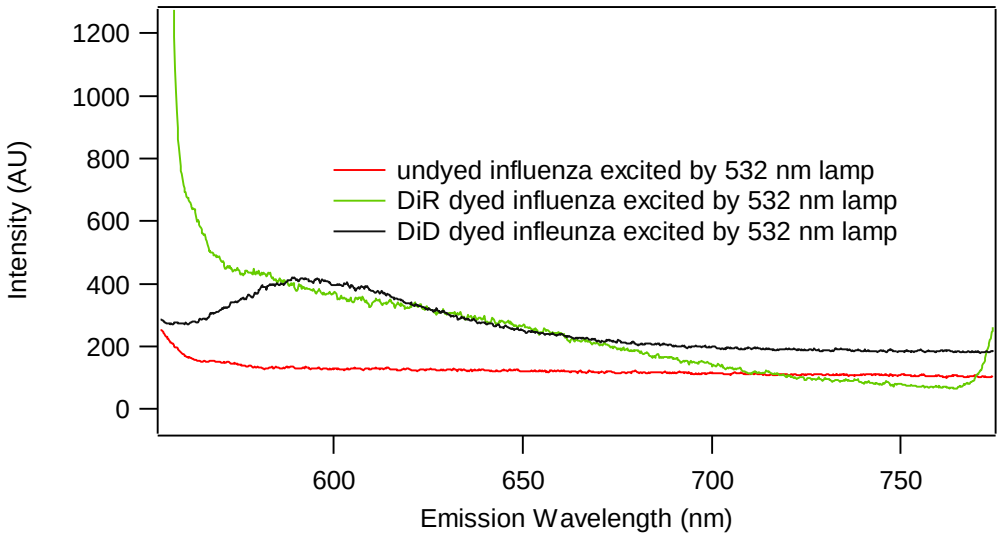

Figure 3.5. Emission Peaks of DiR. DiR was incoporated into influenza which has CH in the viral membrane. The expected emission peak at 750 is weak due to limitations of the instrument. DiR should not be excited by 532nm light but it is. DiR under TIRFM clearly shows up both with a 750/30 and 805/50 bandpass filter under 532nm laser light. DiD was also excited by 532 nm light.

3.1.4 DiI

DiI (1,1'-dioctadecyl-3,3,3',3'-tetramethylindocarbocyanine perchlorate) is also a hydrophobic fluorescent dye that partitions directly into the lipid bilayer. DiI has an excitation wavelength of 550 nm and an emission wavelength of 570 nm. The amplitude of the emission peak is affected by the pH of the buffer as well as the self-quenching. Some conditions result in shifting of the wavelength of the emission peak, which can result in an increase or decrease in recorded emission if only a fixed wavelength or narrow wavelength band is monitored.

DiI's emission peak does not shift when neutral pH buffer is replaced with low pH buffer. The emission peak does shift approximately 5 nm towards higher wavelengths, when detergent is added to the liposomes allowing the dye to dequench as shown in figure 3.6. This shift will not be enough to result in misrepresentative intensity changes for the spectral ranges defined by the optics in our instruments. Similarly DiD and DiR did not have wavelength shifts due to pH changes when incorporated in liposomes or as free dye in the cuvette.

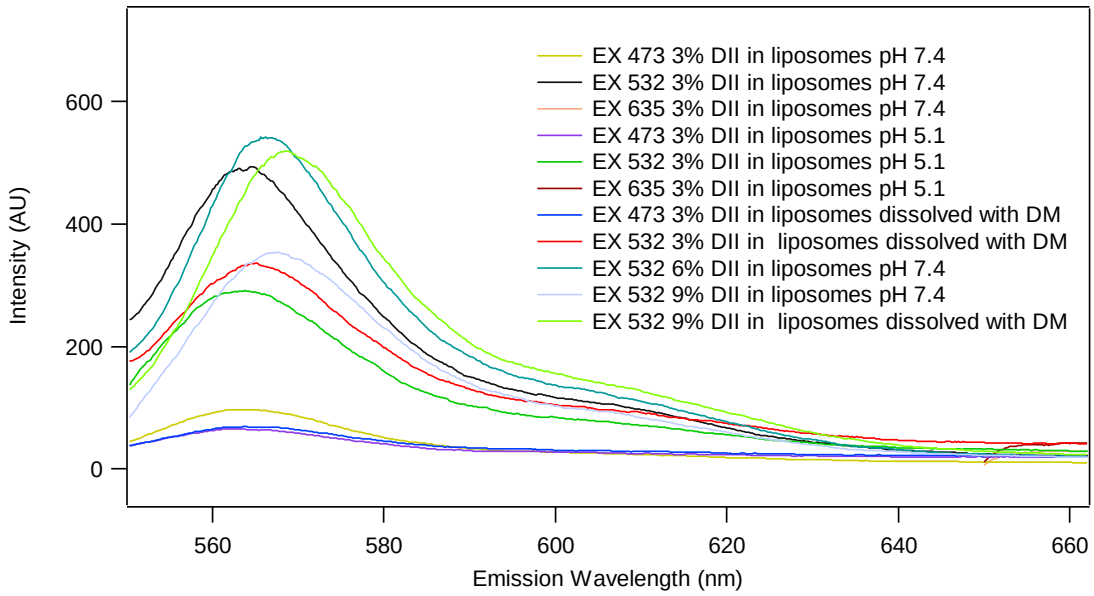

Figure 3.6. DiI Emission curves. The addition of low pH did not affect DiI's emission peak. There is little drift in the peaks, regardless of whether looking at DiI emission under 473 nm excitation or 532 nm excitation or whether 3, 6 or 9 % molar dye had been incorporated into lipsomes composed from liver extracted lipids. The detergent used to dissolve the liposomes was dodecyl-maltoside (DM).

3.2 Bulk Measurements of Fusion

Using methods described in Materials and Methods, (section 2.3) the fusion of influenza and Sindbis virus to liposomes was measured using a bulk fusion assay. For these

experiments, lipid-like dyes were incorporated in membranes of either the virus or the liposomes or calcein was incorporated into the interior of liposomes. Mixtures of virus and liposomes were placed in a fluorescence spectrometer cuvette and acidified. As fusion occurred between labeled and unlabeled particles the dyes dilute and the emission intensity increases due to release of the self-quenching dye. The effect of changing different experimental parameters on average membrane fusion was tested using this assay before attempting more challenging single particle observations (described in later chapters).

3.2.1Calcein's Affect on Membrane Fusion

In figure 3.7, we observed that replacing undyed liver liposomes with calcein loaded liver liposomes inhibited, but did not prevent fusion. For DiD labeled Sindbis virus (SV) fusing with undyed liver liposomes the final dequenching fraction was 25% , but when 222 mM calcein was excapsulated in these liposomes the final dequenching of the DiD signal was decreased to 5%. For DiD labeled influenza the final dequenching fraction was 6% when using unlabeled liver extract liposomes, but when 222 mM calcein was excapsulated in these liposomes then the dequenching percentage drops to only 1%. Despite calcein's inhibition of fusion, calcein is preferred over carboxyfluorescein for SV and influenza because it reportedly doesn't cross the liposomal membrane at the pH of experiment. (Bonnafous and Stegmann 2003)

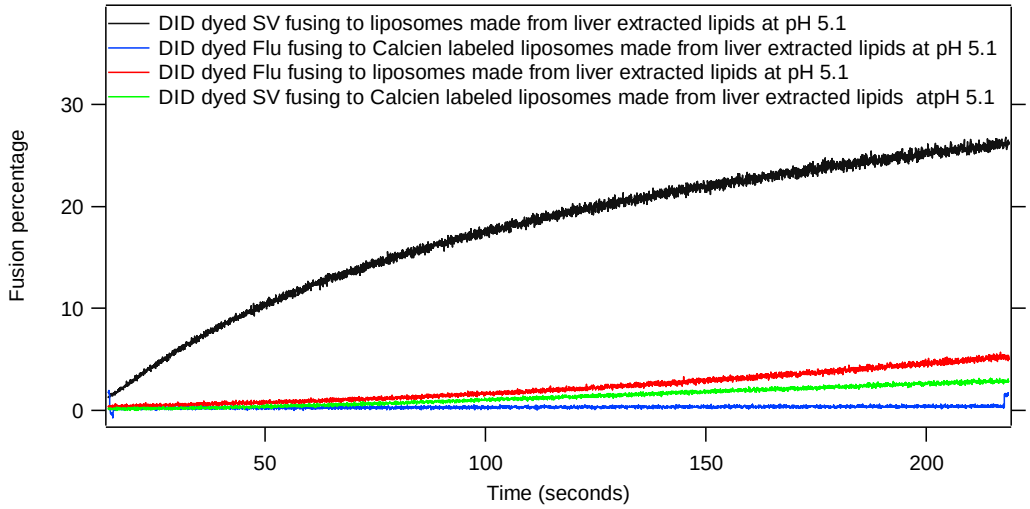

Figure 3.7. Calcein lowers fusion Percentage. DiD in virus is being measured, so 635 nm light is used to excite the sample and 670 nm emission is being recorded. For both Sindbis (green and black curves) and influenza (red and blue curves) virus the addition of 222 mM calcein to liposomes composed from liver extract lowered the final fusion percentage calculated from the DiD dequenching signal.

The fusion experiments in figure 3.7 were performed using 'physiological' salt concentrations of approximately 150 mM (Pritzen and Herrmann 1988) as the extravesicular buffer. The strong ionic character of calcein inside the liposomes needs to be osmotically balanced with an increased ionic strength salt buffer outside the liposomes as discussed previously in section 3.1.1. We used 55 mM calcein, which is strongly self-quenched. We determined as described in section 3.1.1 that the buffer concentration necessary in the exterior buffer to osmotically balance these calcein loaded liposomes is 17 mM Hepes, 625mM NaCl and 0.1 mM EDTA (figure 3.3). Literature reporting the affect of increased NaCl concentrations on influenza fusion is somewhat inconsistent but generally suggests decresed fusion efficiency. Some studies observe a decline in fusion as a result of raising the salt concentration (Korte and others 2007; Pritzen and Herrmann 1988), while others have reported an absence of fusion at low salt (hypotonic) concentrations (Citovsky and Loyter

1985). In our experiments, use of an osmotically balanced buffer with higher NaCl resulted in increases in both content mixing and lipid mixing signals of virus fusing to calcein loaded liposomes in bulk fluorescence experiments (figures 3.8 and 3.9). For these experiments the liposomes contain GD1a at 1 molar % to bind them to influenza. The liposomes were preincubated with virus for five minutes at 37^{o}C and the fluorescence spectrometer's cuvette was adjusted to 37^{o}C throughout the experiment to increase the possibility of fusion.

The curves were calibrated according to figure 2.2, but for calcein under 473 nm excitation, the low concentration of calcein led to only small dequenching increases when detergent was added. Due to the very small levels of fusion, for these experiments we instead report the change in initial slope to measure relative fusion efficiencies. Repeating experiments used to make figure 2.2 with lower calcein concentration and high-salt HBS removed calcein's inhibiting affect on fusion (figure 3.8). However the fusion percentage slope for influenza remained low; at pH 5.1 it rose twice as much compared to the slope at pH 7.4. The experiment was repeated using 473 nm excitation to observe dequenching of calcein in the liposomes instead of DiD in the virus (figure 3.9). In figure 3.9 it is clear that at low pH about twice as much fusion occurs compared to neutral pH for SV.

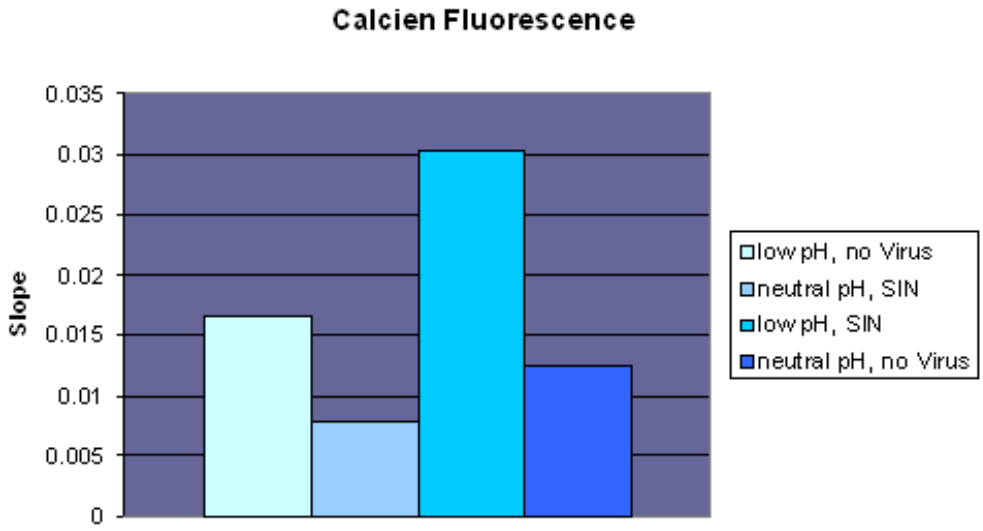

Figure 3.8. Fusion under blue lamp. Liver extracted liposomes with 55mM calcein fusing to Sindbis virus (SV) at low pH (5.1) and neutral pH (7.4) conditions under 473 nm excitation. Liver refers to either undyed liver liposomes or 20% calcein loaded liver liposomes and 80% undyed liver liposomes. Both liposomes and virus are in high-salt HBS to match calcein osmolarity.

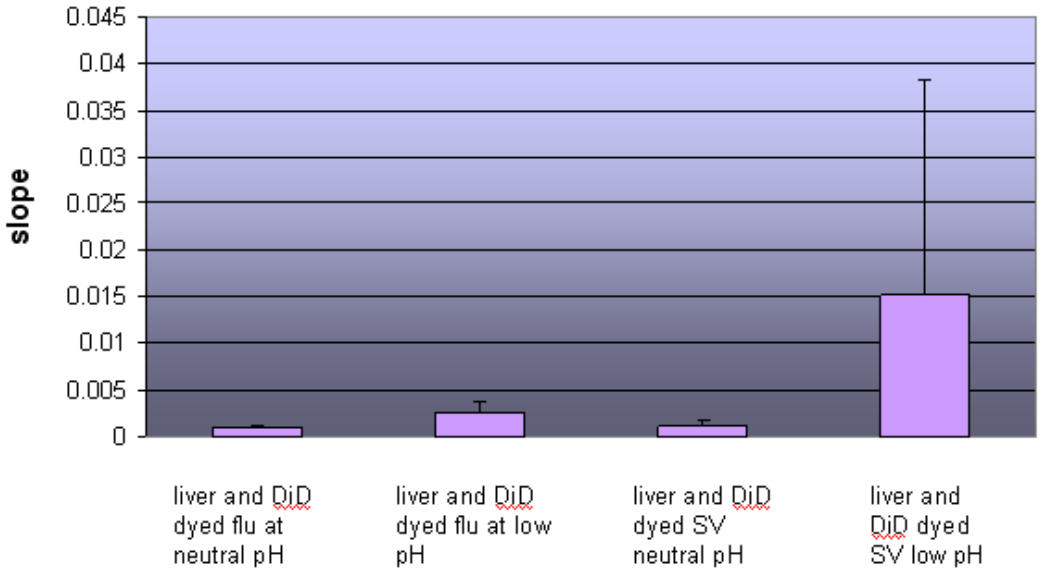

Figure 3.9. Fusion under red lamp. Liver extracted liposomes with 55mM calcein fusing to DiD labeled virus at low pH (5.1) and neutral pH (7.4) conditions under 635 nm excitation. Liver refers to either undyed liver liposomes or 20% calcein loaded liver liposomes and 80% undyed liver liposomes. Calcein didn't inhibit fusion. Both liposomes and virus are in high-salt HBS to match calcein osmolarity. Due to hardware failure, I was not able to obtain 3 trials of each measurement; however the low pH with virus showed the highest change in slope which is expected. Thus calcein didn't inhibit fusion.

3.2.2 Fusion with Gangliosides Incorporated

As mentioned in section 1.4 the composition of the liposomes has a very large effect on fusion. It was found that liposomes created from liver extract were most likely to fuse with influenza. Liver is a natural extract with molar ratio of lipid species reported by the manufacturer to be PC:PE:CH:PI:Other (2:1:0.7:0.6:1) (manufacturer datasheet, Avanti Polar Lipids, Alabaster, AL). In order to bind liposomes to influenza at neutral pH, gangliosides were added to the lipid mixture to provide a receptor for the HA to bind. The addition of gangliosides to liposomes affected fusion only slightly. Specifically it decreases the final dequenching percentage by 1% (absolute value, 20% relative value) (figure 3.10). The membrane dye used to label liposomes affects the system as well. In tests with Sindbis virus, R18 and DiI did decrease the virus' final dequenching percentage by 3% and 4% respectively. (Thongthai and Weninger 2008) However when R18 underwent photobleaching, the infectivity of Sindbis virus was compromised although the fusion capability (i.e. lipid mixing due to membrane fusion) was not. DiD and DiI did not further inhibit either infectivity or fusion when photobleached. (Thongthai and Weninger 2008)

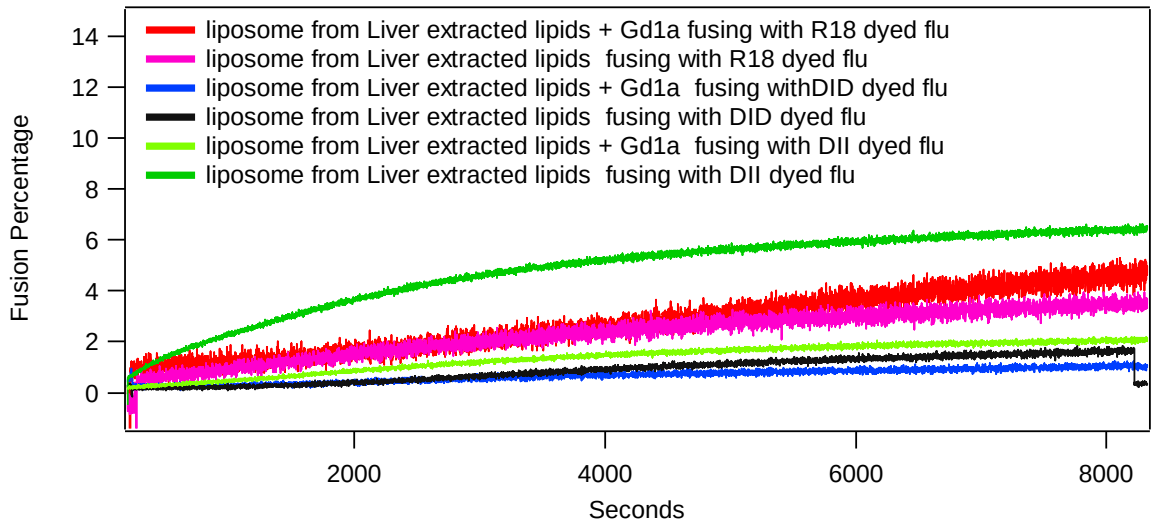

Figure 3.10. Affect of GD1a on fusogencity. Gangliosides are necessary to prebind influenza to liposomes but in liver they seem to inhibit fusion.

3.2.3 Fusion without Cholesterol Incorporated

In liver extract, the most fusogenic lipid tested in our lab, cholesterol is listed at 7% by weight, but we have also used lipid mixtures with as much as 25% cholesterol (molar percentage). Inclusion of cholesterol into the lipid bilayer suppressed calcein leakage but only at high concentrations of cholesterol, 20 (molar)% or higher.(Tsao and Huang 1985) Thus the liposome composition most efficient for fusion leads to increased calcien leaking from the liposomes.

Initially when a second emission peak was seen in spectrum curves for DiD and DiR (sections 3.1.2 and 3.1.3) the second peak was assumed to be the result of quenching. Since dyes will aggregate in the lipid rafts and suffer dramatically increased self-quenching effects, a lipid composition that does not contain CH but is still fusogenic was tested. Fusion of liposomes composed of PS:PC:PE (1:1:1) was studies both on the spectrophotometer and

using TIRFM. These PS:PC:PE bilayers were fusogenically similar to liver (figure 3.11). The membrane dye, DID, incorporated at quenching concentrations into liposomes with PS:PC:PE did not show the additional peaks (figure 3.12) that were present in the liver bilayer (supporting the idea that the additional peak is due to a dye aggregate associated with lipid rafts). The additional peak was only observed in cholesterol containing experiments. Nonetheless in virus to vesicle fusion, there will be cholesterol in the system due to the native cholesterol in the viral membrane so complications from the extra emission peak are unavoidable. Another difficulty with switching to a PS:PC:PE liposomes system for fusion experiments is that fusion using this composition is highly influenced by the liposome's curvature. PS:PC:PE is more likely to form only a hemifusion stalk instead of a fusion pore due to the high negative curvature in the bilayer.

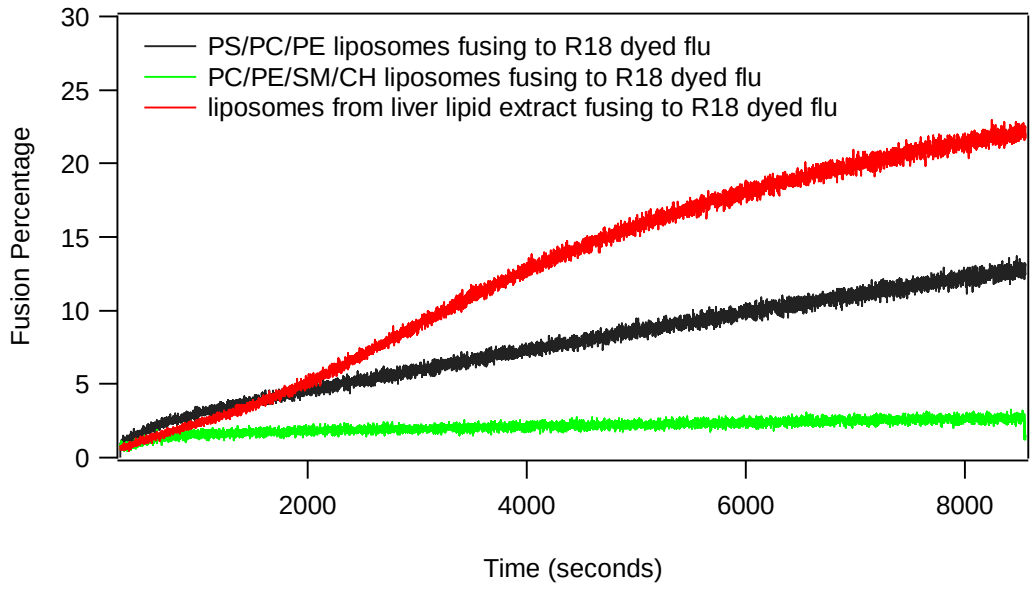

Figure 3.11. Affect of Lipid composition on fusogencity. Final pH is 5.1 for all curves.

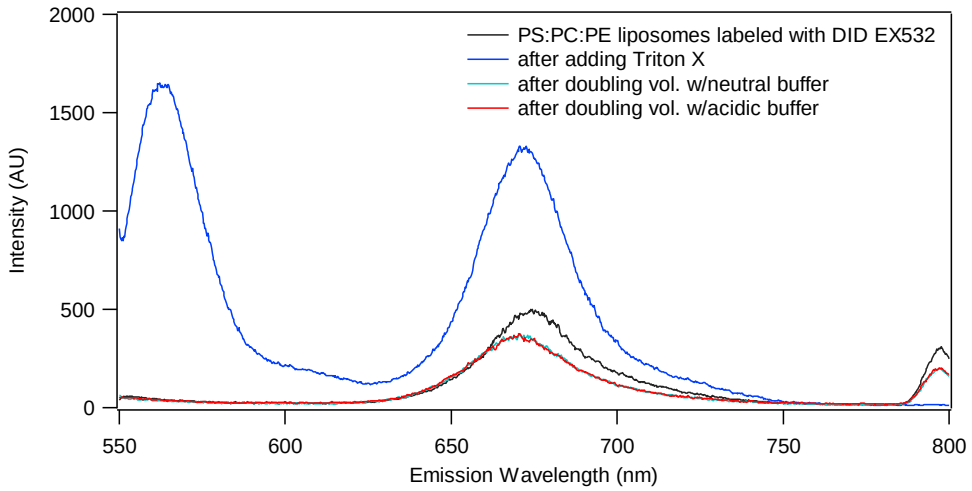

Figure 3.12. Under green lamp DID doesn't have a second emission peak. DiD dye is incorporated into PS:PC:PE liposomes and excited by 532 nm light. The dye is quenched in the bilayer as seen by the sudden increase in intensity when Triton-X is added. Triton-X is a detergent that dissolves the liposome's membrane, allowing the dye molecules to move away from each other. Triton-X fluoresces around 560 nm, accounting for the additional peak in the blue curve. The peaks around 800 nm are due to scattering of light from the liposomes. In later experiments a 540 LP filter was used to filter out these peaks.

3.3 Summary of Bulk Experiments

Incorporation of lipid membrane dye into liposomes doesn't have a detrimental affect on membrane fusion, unlike the encapsulation of calcein into the liposomes' aqueous compartments. These lipid dyes did not behave as expected when excited by laser light that is not part of the excitation spectrum. This can be problematic for designing single particle TIRFM experiments (described in the next chapter). The bulk fusion measurements showed osmotically balancing calcein dye with extravesicular buffer, incorporating gangliosides into the liposomes and removing CH from the lipid bilayer did not adversely affect fusion to influenza. For Sindbis virus CH must be in the bilayer. Gangliosides are not used with Sindbis virus fusion, but calcein must be osmotically balanced.

TIRFM EXPERIMENTS

In this chapter, I will describe results of experiments using a single particle fluorescence microscope (described in Chapter 2, section 2.4) to measure single virus particles of influenza and Sindbis fusing in response to low pH to a supported lipid bilayer and to immobile single liposomes.

4.1 Bilayer Experiments

4.1.1 Summary of Rapid Membrane Fusion of Individual Virus Particles with Supported Lipid Bilayers

Our experiments measuring fusion of single virus particles to supported lipid bilayers was published in the July 2007 issue of the Biophysical Journal. This entire publication is reproduced in the appendix of this dissertation. In this section I will briefly summarize the results described in that publication, which was the first experiment to make high-resolution measurements of the membrane fusion between enveloped virus particles and a supported lipid bilayer at single particle resolution and has since been adapted and extended by other research groups.

The lipid bilayer is a very simple model for a cell membrane but its benefit is that it allows high precision measurements not possible in living cell systems. This paper successfully demonstrated lipid membrane fusion between the outer membrane of the viral envelope and the glass substrate supported lipid bilayer. However creation of a fusion pore between the viral envelope and lipid bilayer could not be assessed with this assay. The dye used in the following assay, R18, has been shown by Wor Thongthai to inhibit infectivity of

Sindbis virus but not low pH triggered lipid mixing. (Thongthai 2008) [http://www.lib.ncsu.edu/theses/available/etd-07152008-151522/]

Data was collected using a fluorescence spectrometer for bulk fusion experiments (explained in section 2.3) and total internal reflection microscopy (TIRFM) (explained in section 2.4). Bulk fusion experiments have used dequenching of fluorescent dye molecules for over twenty years. TIRFM is a much newer experimental technique. Improvement in video capture via CCD cameras have allowed for higher and higher time resolutions, our camera allows for intensity measurements to be recorded at 67 frames/sec. By performing bulk fusion experiments, we were able to verify our virus and lipid compositions were consistent with previously published findings. By averaging our single molecule data collected from our TIRFM setup we were able to compare this data to the behavior of our virus in bulk measurements. Consistency between the two measurements proved our single molecule data was reliable. The single molecule approach to fusion of a virus particle to a lipid bilayer was attemped by Niles and Cohen in 1992 (Niles and others 1992), but they had neither the time nor spatial resolution of our system and were not able to measure the diffusion or time constants that we were able to achieve in this study.

Key results of this paper are the finding that the dynamics of lipid mixing during individual fusion events is faster than 30 msec. Although neither Sindibis nor influenza bind protein free bilayers at neutral pH, under acidic conditions the delay between binding and lipid mixing is less than 500 msec for nearly all conditions. The complex dependence of fusion of lipid composition was explored and is highlighted by the finding that the delay between binding and fusion is lengthened in a pH and cholesterol dependent manner for

Sindibis virus. Highlighting that the complex interaction between lipids, virus, and the environment all affect fusion.

This paper focuses on both influenza and Sindbis virus. Since Sindbis virus' cell receptor remains unknown it was important to find an assay that could compare the systems with equal conditions applied. It is well established, and verified in our study both in bulk measurements and via TIRFM, that preexposure of the virus to acid will inactivate the virus.(Gaudin 2000; Smit and others 2003) Therefore we used a motorized buffer exchange pump to introduce the virus and acid onto our bilayer simultaneously (see figure 2.3). When a virus particle attaches to the bilayer, it will either lose intensity as the R18 dye molecules photobleach, eventually disappearing, or it will suddenly increase in intensity due to an exchange of lipids between the viral membrane and the lipid bilayer. As the dye molecules spread into the bilayer, they diffuse at a rate of ~1.5-2 μm^2/sec. The measured diffusion rate agrees with previously published reports on the mobility of R18 dye molecules in a bilayer. Recording dequenching events at 67 frames/sec, it was found that the the sudden intensity increase of a fusion event occurs within a single time step. Thus the time for fusion of the viral membrane to the lipid bilayer occurs in 28 ms or less.

Not all the viruses bound to the bilayer and of those virues that did bind, not all fused. For Sindbus virus 60% of the bound virions fused, for influenza only 30% of the bound virions fused. This was consistent with bulk measurements where Sindbis virus always had higher fusion rates than influenza. Also consistent with bulk fusion measurements, cholesterol in the bilayer was required for Sindbis fusion to occur, but not necessary for

influenza to fuse to the bilayer. Using a single molecule approach it was found that the majority of fusions occur within the first minute of exposure.

The time between viral docking to the lipid bilayer, termed the residence time, and fusion was successfully measured at 0.2 seconds. This residence time was unique because the virus attached to the membrane was exposed to low pH prior to docking, thus the N-terminus was already exposed. In previous experiments using influenza, the virus was predocked to an RBC ghost, or a RBC ghost expressing HA was predocked to the cell, using influenza's known cell receptor. (Blumenthal and others 1996; Kemble and others 1994; Lowy and others 1990; Zimmerberg 1993)

Specific contributions of co-authors on this published work: In this study, Dominic Scimeca performed bulk experiments measuring the fusion of Sindbis virus to liposomes composed of liver extracted lipids. Mary Williard Elting helped construct the instrument, developed dye labeleing protocols for virus, developed experimental techniques, helped design experiments, analyze data and interpret results. Keith Weninger designed and assembled the experimental instrument, designed epxeirments, helped analyze data and interpret results, composed the literature review, helped write the paper and performed experimental calculations. Laura Wessels performed bulk experiments measuring fusion of Sindbis and influenza virus to liposomes of various compositions, performed all TIRFM experiments, designed experiments, analyzed data, performed experimental calculations and participated in writing the paper.

4.1.2 Rapid Membrane Fusion of Individual Virus Particles with Supported Lipid Bilayers

Available online at http://www.cell.com/biophysj/fulltext/S0006-3495(07)71305-X

or in Appendix A.

4.1.3 Supplemental Movie Legends

In addition to the printed journal article, two movies showing the single viral particle fusion events were made available to Biophysical Journal subscribers online: [www.cell.com/biophysj/supplemental/S0006-3495(07)71305-X]

Movie 1: Movie used to generate figure 3a and 3b showing the fusion of an individual Sindbis virus particle to a supported lipid bilayer (liver extract). The 8-second video from a 13 μm by 13 μm area shows binding, membrane fusion and R18 dye molecules diffusing in the bilayer away from the fusion site.

Movie 2: Multiple fusions. A single Sindbis virus spot exhibits three dequenching events separated by several seconds. The diffusion of dye away from the dequenching location confirms independent lipid mixing events. Some fluorescence remains even after the final fusion event. We speculate that this rare phenomenon arises from aggregates of multiple virus particles. The movie shows a 25 μm by 25 μm area from a supported lipid bilayer (liver extract) at pH 4.2.

4.1.4 Sindbis Virus Grown in Mosquito Cells

In addition to the studies in the published article where the cholesterol content of the liposomes was varied, we also made attempts to modify the amount of cholesterol in the viral membrane by growing SV in mosquito cells. Our goal was to create SV without cholesterol in the viral membrane. In the wild, SV virus alternates between mammalian and insect hosts so differences in the membranes of viruses derived from different hosts could be informative about the different disease outcomes in these organisms. Insect cells in the wild do not synthesize cholesterol (CH), although our cultured cells do contain CH due to their exposure to fetal bovine serum in the growth medium (Raquel Hernandez, NCSU Biochemistry Department, private communication). Independent from the CH issue, virus produced from BHK and U4.4 cells do have different physiological behavior as characterized by classical virology measurements.(Mudiganti and others 2006) Specifically, there is a greater cytopathic effect in mammalian cells not seen in invertebrate cells and less viral structural proteins were detected in the U4.4 cells by immunofluorescence.(Miller and Brown 1992) For our experiments we compared Sindbis virus produced from two different cell lines: Baby Hamster Kidney cells (BHK) and mosquito U4.4 cells.

We characterized the fusion properties of Sindbis virus from these two different hosts in our *in vitro* assay. As characterized by bulk florescence experiments and rates of fusion to supported lipid bilayers, Sindbis virus grown in BHK cells and U4.4 cells appears very similar. One interesting difference is that Sindbis virus grown in cultured mosquito cells has an increased interval between binding and fusion at pH below 5 that is not seen in BHK produced virus or in influenza (figure 4.1). This difference highlights the complexity of the

interplay between the composition of membranes and the pH dependence of the viral fusion proteins. There are also more fusions in these first 30 seconds for mosquito produced Sindbis virus, which makes outlying values more probable skewing the average (figure 4.2).

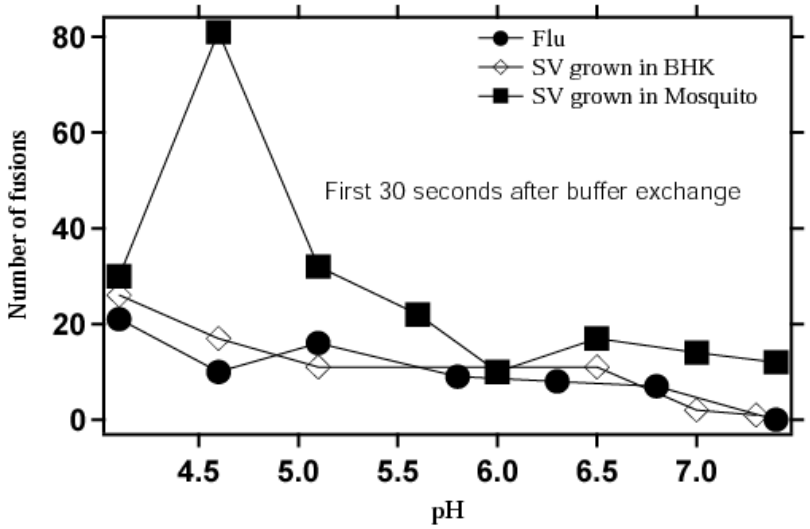

Figure 4.1. Fusions in the first 30 seconds for SV grown in BHK cells and Mosquito cells. The long solid line (filled squares) shows the increased number of fusions for SV grown in Mosquito cells at low pH compared to the near-constant residence time for SV grown in BHK cells, depicted by the solid line(open squares with crosshatch) and flu (filled circles).

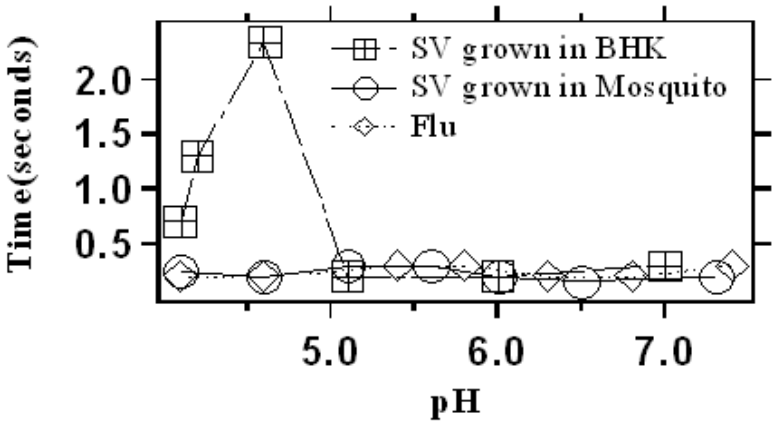

Figure 4.2. Residence Time for SV grown in BHK cells and Mosquito cells. The long dashed line (open squares with crosshatch) shows the increased median residence time for SV grown in BHK cells at low pH compared to the near-constant residence time for SV grown in Mosquito cells, depicted by the solid line(open circles) and flu (the dotted line, open diamonds).

4.1.5 Protein-free Experiments

I applied the single virus particle fusion assay that I developed to studies of protein-free fusion. Liposomes formed from liver extracted lipids were labeled with either lipid binding dyes or content dye and were injected over a lipid bilayer at either low or neutral pH. Lipid mixing of membrane dye (DiI) from liposomes to the supported bilayer was observed at pH 4.5 but not at pH 7.4. Content dye (calcein) containing liposomes did not fuse into the bilayer or spontaneously burst, but these liposomes did stick to the bilayer at pH 4.6. The localized liposomes did not diffuse in the plane of the bilayer. The DiI experiments indicated at least hemifusion between the liposomes and bilayer in which the outer leaflets of the liposome and substrate-supported bilayer merge. It is not possible from the calcein experiment to conclude if the inner leaflets fused. If they did fuse the calcien dye would be delivered through the supported bilayer but may not be able to diffuse laterally in the 1 nm gap between the bilayer and quartz surface. Calcien adsorbs to quartz so it likely will not diffuse away from a fusion site. Surface absorbed calcien photobleachs more quickly than when solubilized within the liposome.(Bowen and others 2004)

The ability of liposomes to fuse to lipid bilayers in response to low pH led to experiments to test fusion of virus particles in which the fusion proteins on the surface had been removed. We treated Sindbis virus with protease to cleave E1 & E2 proteins and dye labeled this ‘bald virus’ with DiI. At the lowest pH, this bald virus fused to a liver extracted lipid bilayer. Specifically 58% of virus particles that bound to the bilayer ended up fusing. This is similar to unaltered Sindbis virus (section 4.1.1). At neutral pH there was neither binding nor fusion.

4.2 Virus to Vesicle Fusion

4.2.1 General Overview

I developed a new assay to allow experimental observation of fusion of a single liposome to a single virus particle. Such fusion between equal sized objects will lead to a new membraneous structure. It is not clear whether the volume or the surface area of the original virus and liposome would be conserved. If the radius of each sphere is R_{old}, then the sum of both surface areas of two equal sphere is $2*4\pi R_{old}^{2}$. If it is assumed that the surface area is conserved when two spheres of equal size merge into a single sphere then the resulting sphere will have a radius of R_{new} where R_{new} is given by the relation $2*4\pi R_{old}^{2}=4\pi R_{new}^{2}$, which gives $R_{new}=1.4 * R_{old}$. Thus, the total volume is not the sum same as the sum of the volumes of the two original spheres, it is $(1.4 * R_{old})^{3} = 2.8 * R_{old}$ times larger. This will create a change in the internal pressure which can affect fusion, just as osmotic pressure affects fusion. Furthermore the assumption the surface area is conserved may not be accurate since the bilayers can stretch and compress. In fact the resulting object may not be spherical , which will affect the balance of the final energy state. The goal of my efforts to develop an assay to observe single virus-liposome fusion was to measure time resolved, simultaneous signals due to both content and lipid mixing. Such simultaneous time resolved information will address issues about the delay between formation of the hemifusion stalk (evidenced by lipid mixing) and formation of a fusion pore (evidenced by content mixing). Content mixing would provide definitive proof of pore formation that was hinted at but not established by membrane mixing alone as discussed in section 4.1.1. Although two

dye membrane fusion using FRET (discussed in section 5.1) has temporally resolved outer leaflet hemifusion and inner leaflet mixing using SNARE proteins (Yoon and others 2006) a direct content mixing signal is desirable.

For these experiments, cap Biotinyl PE lipids and gangliosides are incorporated into the liposome in order to anchor the liposome to the slide and the virus particle to the liposome as seen in figure 4.3. Gangliosides allow specific bindng of influenza to the liposomes. The anchored liposome-virus complex on the microscope slide surface is imaged with TIRFM as described in section 2.4.2. Fusion of a calcein containing liposome with an equal sized virus particle should result in an increase of emission intensity of calcein. Fusion will also increase the surface area available to the lipid dye and will result in dequenching of the membrane dye. With the multivalent nature of the binding of virus to the gangliosides containing liposomes, it is difficult to enforce a one virus to one liposome association. If there are many virus particles attached to a single liposome then the dequenching of the dye on the virus may not result in an intensity increase beyond signal noise.

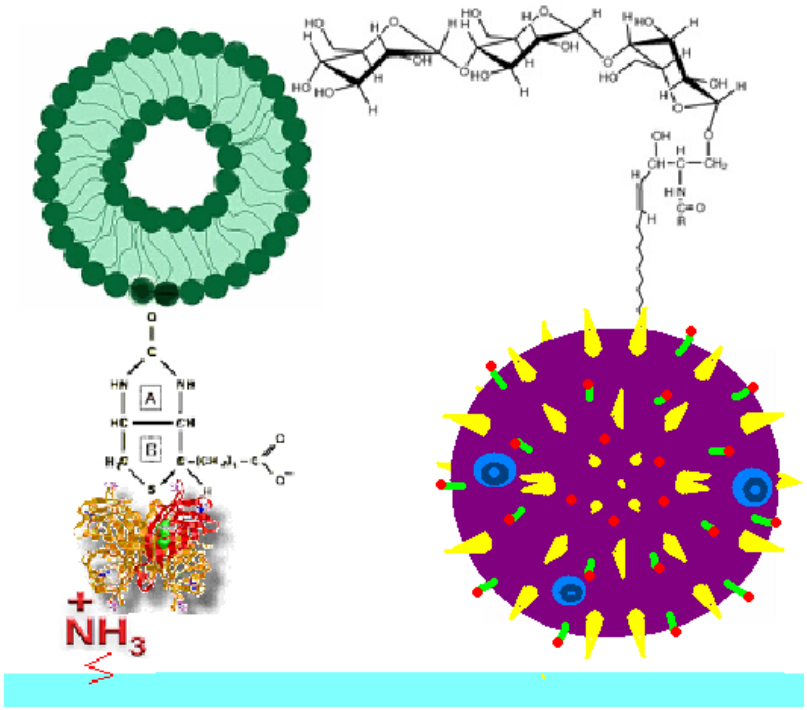

Figure 4.3. Anchoring liposome virus pair to slide. Biotin incorporated into liposomes attaches to streptavidin, which attaches to the amine incorporated into the slide's surface. Gangliosides are also incorporated into the liposome to provide a binding site for influenza.

4.2.2 Incorporating Gangliosides into the Liposomes

Gangliosides were added into the lipid bilayer to bind influenza's hemagglutinin (an antigenic glycoprotein) to the liposome so that when fusion is triggered by low pH the constituents are already in place on the slide (figure 4.3). Two different gangliosides were tested. Total ganglioside extract (Table 4.1) purchased from Avanti Polar Lipids (Alabaster, AL) and GD1a purchase from Sigma-Aldrich (St. Louis, MO).

Table 4.1. HPLC Analysis of Total Ganglioside Brain. High Performance Liquid Chromatography (HPLC), identifies, purifies, quantifies and separates compounds into their constituents. Data obtained from Avanti Polar Lipids website.

Ganglioside Structure	Measured in Absorbance Units
GM1	49.231 mAU
GM2	38.534 mAU
GM3	28.005 mAU
GD1a	56.647 mAU
GD1b	65.943 mAU
GD1d	70.054 mAU
GT1b	77.565 mAU
Others	16.024 mAU

Most experimenters in published reports use between 5-15% molar ratio for gangliosides. I have found that 1% gangliosides provides the best binding in my experiments (figure 4.4). In an assay that measured calcien leakage from liposomes fusing to Sendai virus(using an HA-NA receptor for attachment (Hoekstra and others 1989)) at 37^{o}C, leakage of calcien from liposomes with gangliosides peaks at 6.5% molar ratio for GD1a, 7.7% for GM1 and 3% for GT1b with as much as 30% leakage in some cases. The total ganglioside extract used in our lipid experiments contains all 3 of these gangliosides plus many more (Table 3), but in our experiments, GD1a alone binds influenza better than the total ganglioside extract.

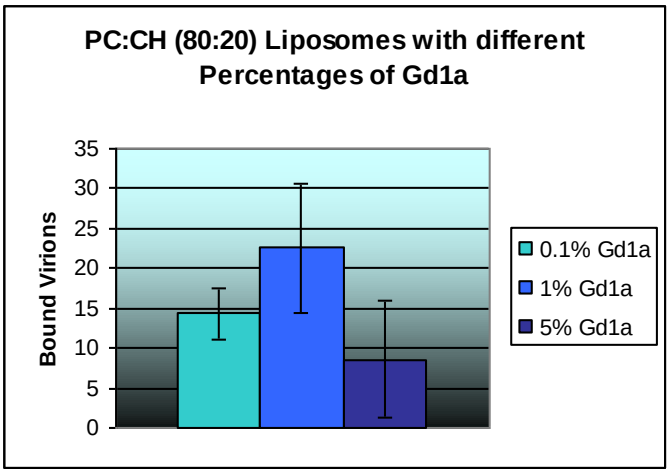

Figure 4.4. Molar Percentage of GD1a. Most papers recommend adding between 5-15% GD1a into a phospholipid bilayer for maximum binding of influenza, but my tests showed 1% to be the most effective.

Cholesterol is a requirement for membrane fusion in Sindbis virus. In influenza, cholesterol enhances fusion but is not required. We have demonstrated fusion of influenza to PS:PC:PE liposomes. Temperature can affect fusion by controlling the degree of fluidity of the lipid bilayer. In binding experiments with GD1a, we found temperature to be important (figure 4.5). We found more virus bound as the temperature increased.

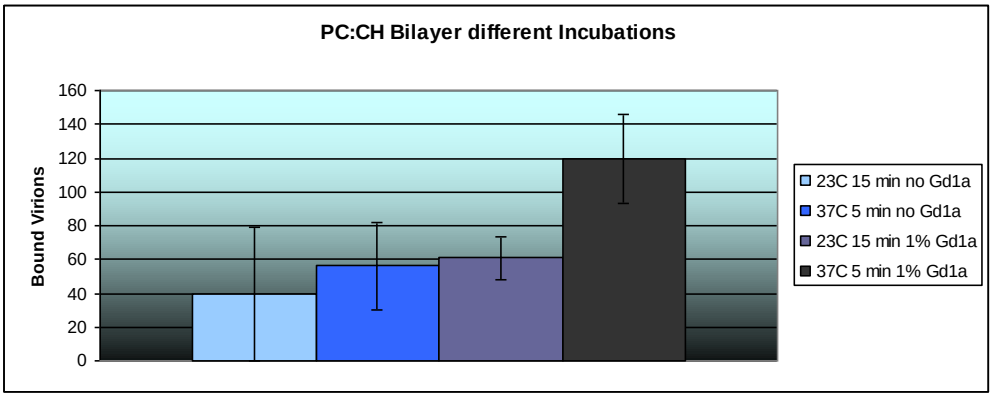

Figure 4.5. Influenza binds best at body temperature. Influenza binds at room temperature but even with longer incubation times it doesn't bind as well as at 37°C.

4.2.3 Dequenching of Calcein Encapsulated in Liposomes

An important aspect of experiments attempting to simultaneously measure dequenching of separate dyes in a two dye system is the capability to spectrally resolve each dye with confidence that the dyes are colocalized. The dualview imager uses a dichroic beam splitter to send wavelengths of 645 nm or higher to one half of the CCD and wavelengths below 645 nm or lower to the other half. The separate halves of the image are analyzed individually with a nonlinear mapping function used to map one spectral emission band to colocalized spots in the other spectral band. Images of broad emission band fluorescent microspheres are used to create the mapping function that is applied to the virus experiments. When these images are matched up, if a 'one liposome to one virus particle' relationship has been achieved than there should be 100% colocalization from both the longer wavelength side (usually the virus is labeled with fluorescent dyes that emit at 670 nm or more) and lower wavelength side (usually liposomes are loaded with calcien which emits around 510 nm). Realistically there are many gangliosides on a liposome and many receptors on a virus so the one-to-one association is not strictly maintained. For this reason we used a higher concentration of virus than liposomes so that every liposome is assured of a least one attached virus particle. An experimental challenge is the fact that the viruses stick non-specifically to the surface so that some virus particles do not match up with a liposome. For example, on a quartz slide where liposomes with biotin were prebound before influenza was introduced into the channel at a high concentration and allowed to incubate for 30 minutes at room tempature, 24 ± 1 % of the viruses could be matched up with a liposome, but 66 ± 33% of the liposomes matched up with a virus, indicating most of the virus in the channel was

simply stuck non-specifically to the surface. Of course having multiple virus particles attached to a single liposome will affect the intensity and number of dequenching events seen. Specifically since influenza particles vary in size and shape, and dye is absorbed differently by each virus particle the intensity of individual particles is not sufficient to quantitiatively identify viral aggregates. So in the virus to vesicle system the calcien dye on the liposome was examined on its own with undyed influenza and SV flowed in with low pH to categorize dequenching events.

Liver liposomes with 1% GD1a and 0.1% Cap biotin that were extruded in 55 mM calcien (concentration 0.0003 mg/ml) were bound to a quartz slide surface. For experiments with either virus, the double syringe pump was loaded with virus in one syringe and buffer in the other. High-salt HBS was used for both viruses. The low pH buffers also contained high salt to osmotically balance the calcein liposomes. 17 mM MES was used for low pH expeirments instead of Hepes, which was used in neutral control experiments.

Three types of behaviors of the calcein dye signal were observed in the fusion experiments. Some traces had an abrupt step-like increase in intensity indicating dequenching of the aqueous dye (figure 4.6 A). Some traces showed the exact opposite behavior of the intensity suddenly decreasing to zero (figure 4.6 B) indicating the liposome has left the evanescent field of view, likely indicating the liposome detached from the slide. Finally some traces showed a combination of this behavior where the liposome's intensity increases quickly but then decreases suddenly immediately afterwards (figure 4.6 C). The sudden loss of dye emission in figure 4.6 C could be due to the liposome spontaneously bursting or could indicate membrane lysis during fusion intermediates. If the liposome retains the content dye

after the initial intensity increase then the intensity should decrease slowly as a result of photobleaching. If dequenching occurs as well as lysis then there are several possibilites. The membrane may heal itself and after the sudden decrease in intensity, a slow decrease due to photobleaching may occur. The entire contents of the liposome may be lost so only background intensity will result, or the tear may not heal fully and a slow increase in intensity as content dye continues to dequench may occur. This final scenario is shown in figure 4.6 C. If the trace is due to bursting the sudden increase in intensity results from an expanding dye cloud that lasts for several frames as it expands isotropically out of the evanescent field while simultaneously photobleaching. As the dye cloud expands the concentration lessens and the photobleaching of calcien at lower concentrations happens more rapidly. (Bowen and others 2004)

Control experiments without virus found decreased frequencies of all three behaviors (figure 4.7). Lysis for both SV and influenza occurred at neutral pH, a condition where fusion should not occur. The bursting persisted despite adjusting the salt content of the buffer to osmotically balance the calcein dye indicating effects beyond osmotic pressure play a role in the system.

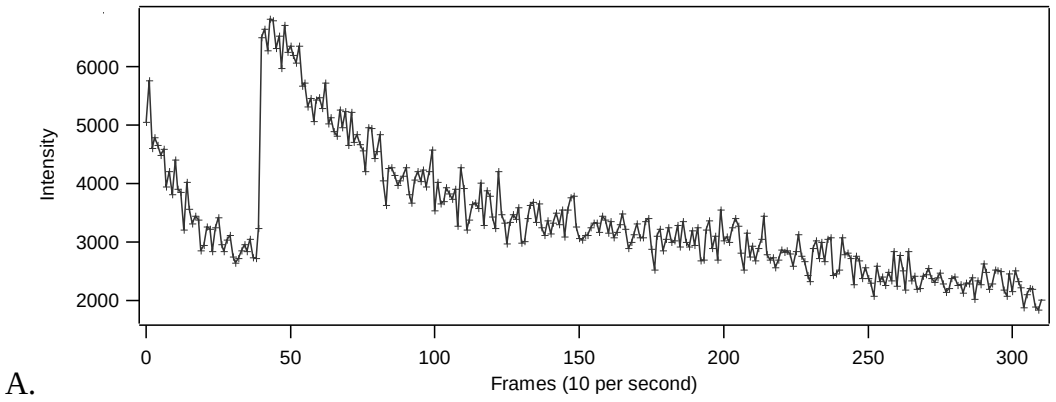

A.

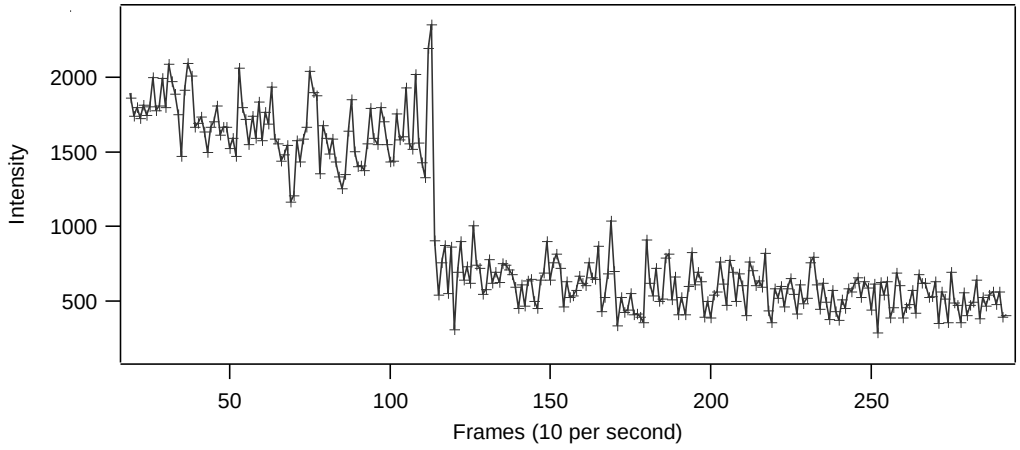

B.

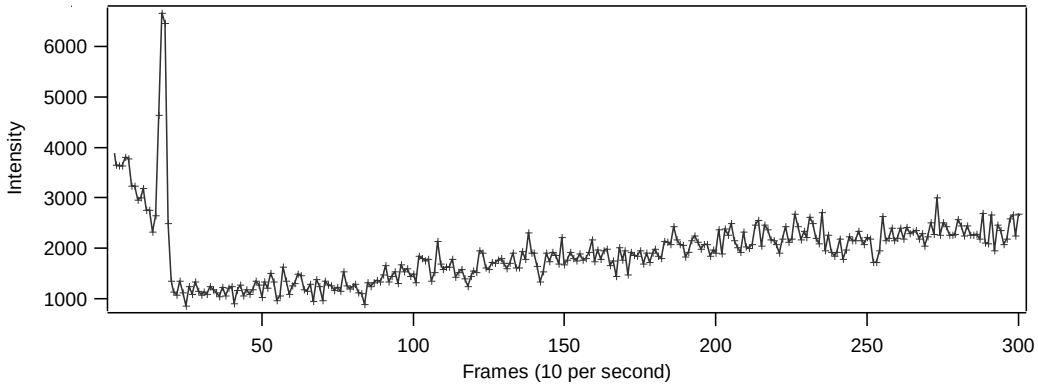

C.

Figure 4.6. Traces of calcien loaded liver liposomes. A. The dye in the liposome is dequenching. B. The liposome has become undocked from the quartz substrate. C. The liposome is undergoing lysis or bursting, resulting in a sudden release of the dye.

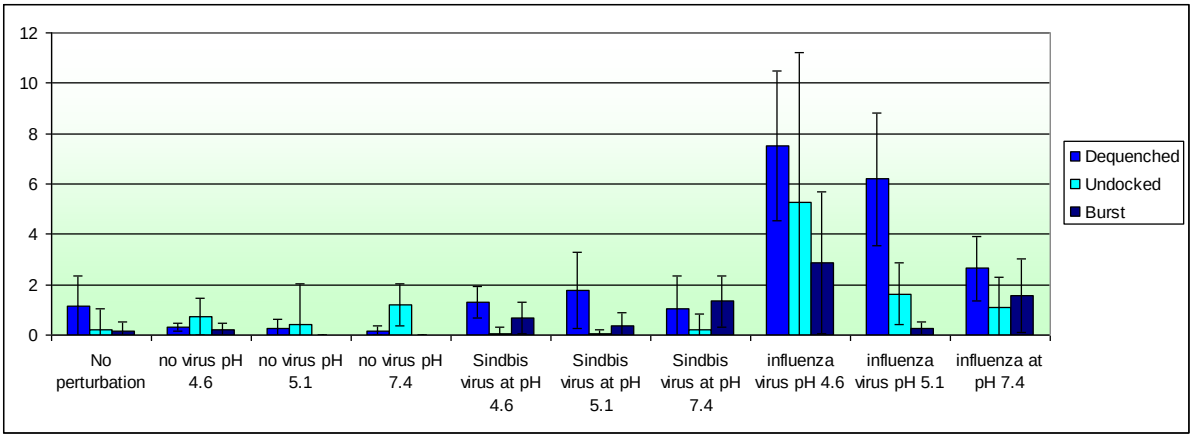

Figure 4.7. Fusion with Calcien loaded Liver Liposomes. In looking at the graph, no clear trend emerges. Without virus the lipsomes are fairly unperturbed. However at neutral pH the liposomes show more lysis than at lower pHs which is unexpected as neither Sindbis nor influenza fuse to cells at neutral pH.

4.2.4 Two Dye Emission

Attempts to incorporate DiD and calcien into the same liposomes failed due to a lack of co-solubility. Therefore, DiD was used to label the virus and calcein was loaded into liposomes. Liposomes docking to virus were mixed with flu being in excess. From bulk fusion and TIRFM bilayer experiments it was previously determined that 30% of flu particles were capable of fusing with liposomes. When dye is present in the liposomes and the virus, this percentage decreases by as much as 20% (see figure 3.9). When gangliosides are added this percentage is decreased from 30% to less than 5% (lowest efficiency conditions are gangliosides and biotin into calcein containing liposome with a single flu virus attached).

Experiments using DiD on the virus and calcein in the liposomes resulted in too little colocalization. Low colocalization resulted in less than 1% (0.33 ± 0.67) of liposomes sites exhibiting fusion behavior. We therefore designed a new assay using Rhodamine B a lipid dye molecule for detecting lipid mixing along with and calcein to indicate content mixing. These dyes were incorporated into the same liposome without difficulty. The virus was used

without dye in initial measurements, which allowed a very large excess of virus to be introduced. (Later work uses DiD to label the virus requiring 3 color detection.) Calcein was encapsulated into the liposomes at 111 mM concentration, while Rhodamine B was incorporated in the membrane at 5% (by weight). As expected, we observed that the occurance of fusion to a single liposome increases when using large excesses of unlabeled virus. A 473 nm laser excited both Rhodamine B and calcien (figure 4.8). Although there was significant emission by Rhodamine on both sides of the dichroic, this 'leakage' was systematically corrected by subtraction. During fusion both the content and membrane dye dequench simultaneously (figure 4.9 A).

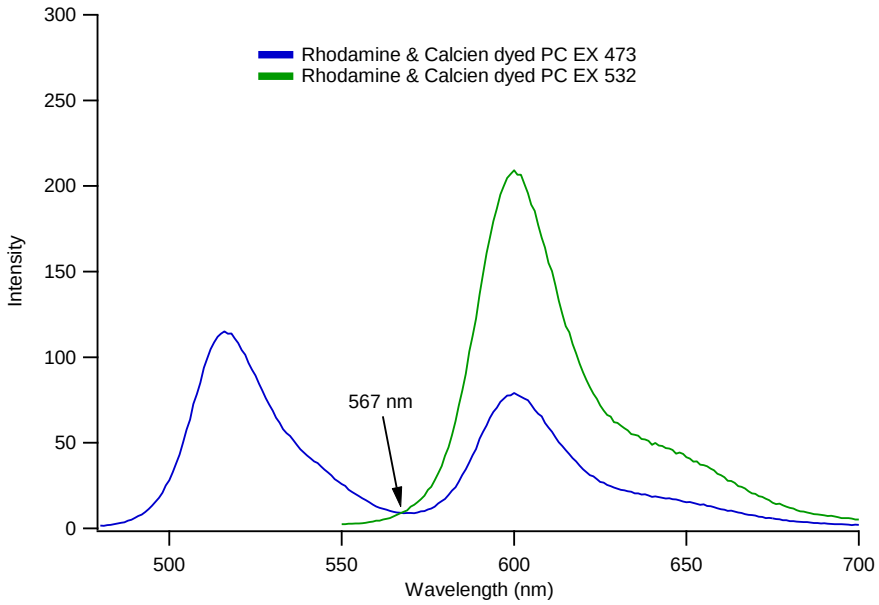

Figure 4.8. Emission curves for Rhodamine B and Calcien. Both Rhodamine B and Calcien are excited by 473nm light as evidenced by their emission curves which show strong peaks for both dyes. The Dualview has a dichroic splitter at 565 nm. It is clear that calcien will leak through the long wavelength side of the splitter as shown in the blue curve's second peak.

Our first experiments with this system were encouraging with fusion observed at about 3% of liposomes. Control experiments where either the virus is missing or the pH is

left at neutral had less than 1% fusion. However upon additional trials with this system the statistical difference between control experiments and low pH with virus was discernable. Since these double dequenching events were rare, no attempt was made to observe this type of fusion at high time resolution and thus a separation between dequenching curves was not observed. Such a separation is required to demonstrate whether inner or outer leaflet fusion occurs first.

A.

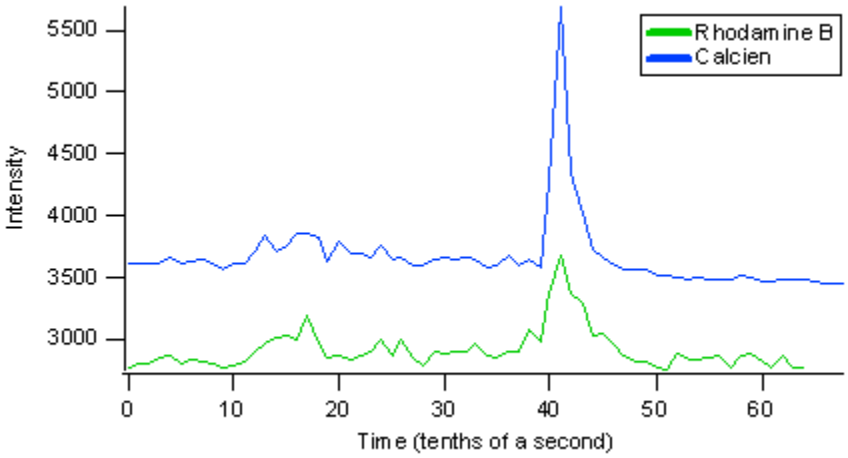

B.

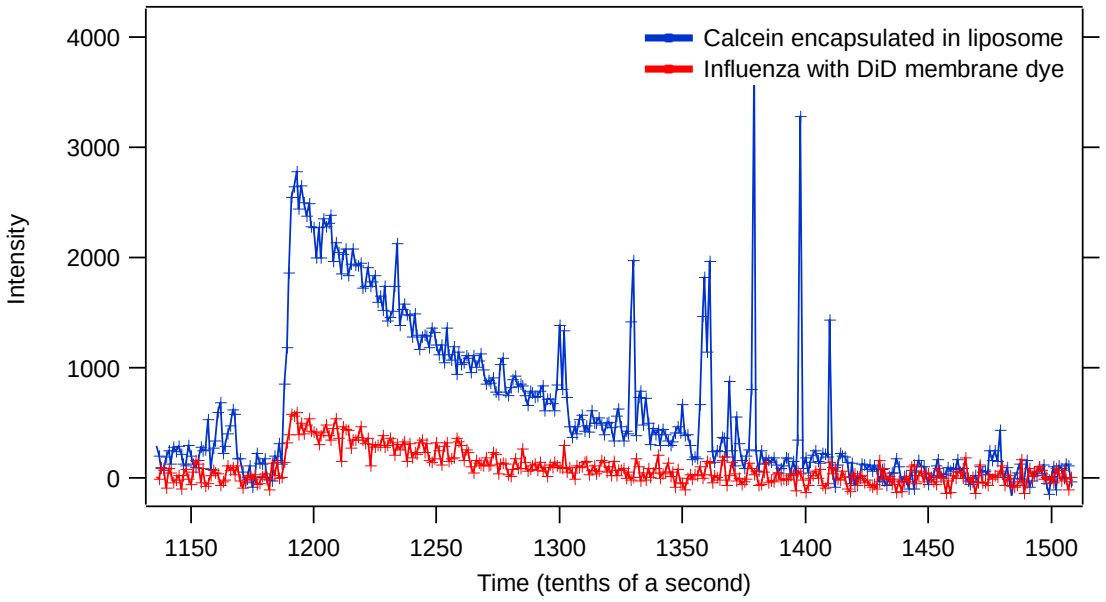

Figure 4.9. Time traces of a liposomes showing simultaneous dequenching. A. The liver-extracted liposome has two dye molecules, virus is undyed, Rhodamine B and Calcien, both of which are excited by a blue laser at 473 nm. The curves show simultaneous peaks around 4 seconds, indicating fusion with an undyed influenza virion. Leakage of Calcien into the longer wavelength register has been subtracted. B. In this trace DiD is incorporated into the viral membrane, calcein is encapsulated in the liposome. Background intensity has been subtracted for these curves.

4.3 Microfluidics

A microfluidic platform was developed to allow high-throughput observations of single virus-liposome fusion with a confocal microscope. This platform will allow time resolved measurements of membrane dye dequenching simultaneous with detection of content dye dequenching. In this way the interval between lipid mixing in the stalk and pore formation can be investigated. We have developed and characterized PDMS based microfluidic structures that are compatible with virus experiments. PDMS is an optically transparent, soft elastomer in which liquid handling devices incorporating pneumatically activated valves, mixers and pumps can be fabricated using soft lithography.(McDonald and others 2000) Affixing a microscope coverslip seals the channels in the polymer chip. Liposomes are anchored onto the coverslip surface as describe in section 2.4.2. At this level of microscale flow, the Reynolds number remains low so mixing of multiple components simultaneously introduced into the channels is completed via diffusion instead of turbulent mixing.(Fu and others 1999) Using capillary pressure in a pumping drop at the entrance of the channel to drive flow, we measured the rate of virus traveling through the channel is ~390 μm/sec with a deceleration of ~1 $\mu m/sec^2$. Fluorescently labeled virus was tracked in a fluorescence microscope as shown in figure 4.10. A pumping drop was first placed on the inlet hole of the microfluidic channel and the time required to cross the 80 μm screen was recorded. Virus particles were tracked until flow in the channel stopped (~50 seconds later) and the deceleration of the flow over that interval was calculated. In our tests neither the virus nor liposomes stuck to the surface of the PDMS channel (see side walls in figure 4.10). The drop was placed on the channel's inlet hole by hand via a pipet. (Walker and Beebe

2002) A motorized pump system will be used for future experiments. In general, flow through the channel proceeded rapidly and without air bubbles.

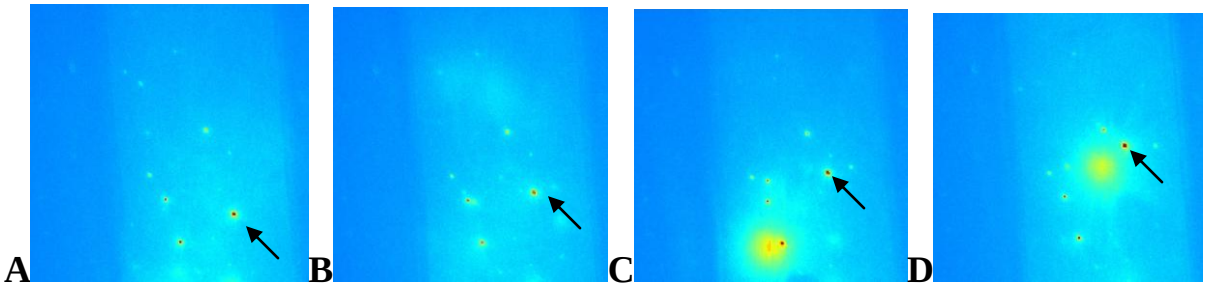

Figure 4.10 PDMS walls are free of liposomes and virus. An arrow follows the path of a virus moving through the channel in the direction of flow. It takes 15 seconds for the virus to move from one end of the screen to the other.

4.4 Summary of Liposome-Virus Fusion Studies

Using single molecule techniques we have observed lipid mixing during a fusion event and quite possibly the formation of a fusion pore. Measurements of the diffusion rate, residence time and number of binding events have been achieved. Further work must be done to time resolve the formation of the fusion pore. A better understanding of the properties of calcein dye and its effect on fusion as well as porting the experimental system over to a confocal microscope by employing PDMS channels will be necessary to make this measurement. Steps toward this goal include developing a binding system where a liposome-virus are held in place on the slide while fusion is triggered, making the flow channels and characterizing the membrane and content dyes used in the experiment.

CONCLUSION

5.1 Discussion

The study of viral membrane fusion has provided insight into a fundamental process that occurs widely in eukaryotic cell biology. The functional commonality among class I, II and III viral fusion proteins is surprising considering the diversity of structure they exhibit and the varied ways in which fusion is triggered. The current model of viral membrane fusion proposes a procedure for bringing two membranes into apposition requiring a conformational change in the fusion protein, which exposes a hydrophobic fusion peptide. This peptide extends outwards towards an apposing membrane. After this the fusion peptide inserts into the targeted membrane, the fusion protein folds back into a hairpin, which brings the two apposed membranes together. The fusion of these membranes is dependent on the lipid composition of the membranes as well as possible additional protein conformational changes, and cooperativity among several fusion proteins. The exact mechanisms that lead to lipid mixing are not known but the precise sequence of the fusion peptide along with the transmembrane domain of the viral fusion protein are indispensable. It is believed that an intermediate hemifusion stalk is formed that then expands into a diaphragm membrane structure. Finally a fusion pore forms within the diaphragm. The created fusion pore may be stable or may flicker repeatedly before expanding into an opening large enough to allow the genetic material of the virus to enter the cell. The exact nature of these intermediate structures is unknown.

TIRFM and bulk experiments were performed to distinguish between the hemifusion stalk and the fusion pore during viral membrane fusion. Using single molecule techniques the

time between when acidified viral particles first encountered a lipid bilayer and hemifusion occurred was measured for influenza, Sindbis virus grown in mammalian cells and Sindbis virus grown in mosquito cells. For each of these viruses, the optimal pH and lipid bilayer composition that best promoted fusion was determined. The actual hemifusion stalk formation occurred more quickly than the time resolution limit of the CCD camera could measure. This time resolution was sufficient to measure the diffusion constant of the lipid dye molecules as they diffused into the lipid bilayer after fusion. To move to the next step of determining when the fusion pore first opens, the properties of calcein were tested. It was discovered that to osmotically balance calcein's high ionic character required a high salt extravesicular buffer. Bulk fusion experiments showed that calcein could be incorporated into an otherwise fusogenic system without hindering fusion. It was also discovered that to prebind influenza to the lipid bilayer, GD1a incorporated at 1% molar worked best when employing a 5 minute incubation time at 37^{o}C.

Forster Resonance Energy Transfer (FRET) was another method considered for measuring fusion. FRET is a radiationless transfer of energy from one molecule to another. FRET can be used to measure distances in the 2-8 nm range between macromolecules, in our case lipid dye molecules.(Cardullo and Parpura 2003) The lipid dye molecules will only come close enough to transfer energy when they coexist within the same membrane, i.e. after membrane fusion has occurred. The donor molecule's emission spectrum must overlap the excitation spectrum of the acceptor molecule (figure 5.1). When the donor and acceptor are within approximately 5 nm of each other, energy is transferred between them. It was found that DiD was excited by 532 nm and that it produced two peaks under this excitation

wavelength which made it unusable for the FRET experiment since it's lower wavelength emission peak would incorrectly be interpreted as donor emission. Similar results were found using DiR membrane dye as well. Removing cholesterol from the bilayer removed the second emission peak. However in the FRET pair of a liposome to virus particle, the virus particle will always contain cholesterol.

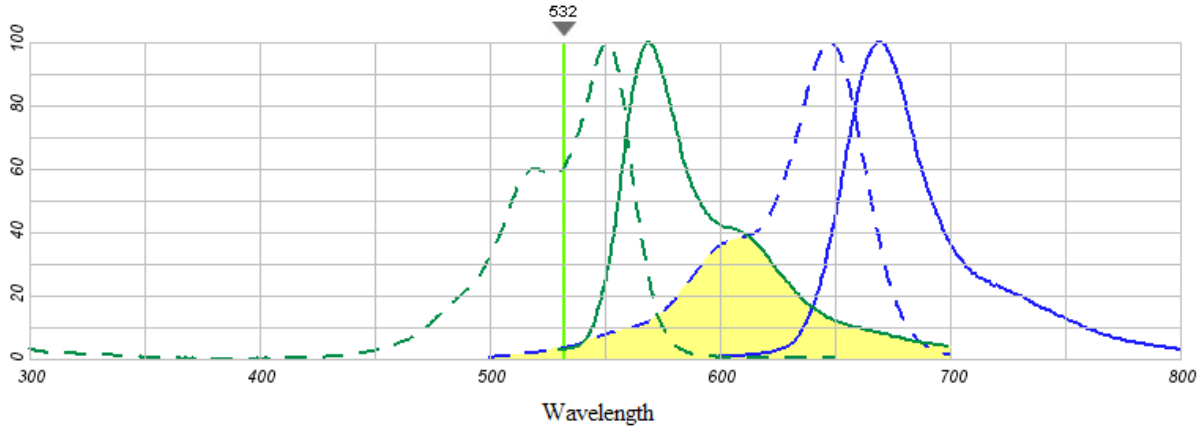

Figure 5.1. Overlap of DiI's emission spectrum with DiD's excitation spectrum. The solid green line shows the fluorescence emission spectrum of DiI while the dotted blue line shows the excitation spectrum of DiD both bound to phopholipid membrane bilayers. Between 575 and 650 nm these spectra overlap allowing FRET between the molecules to occur. A 565 dichroic separates the emission spectra of each dye into separate channels on the camera and a 585 bandpass filter removes the 532 nm laser while a 700 bandpass filter removes most of the DiI emission that crosses through the higher wavelength channel. (Source: Invitrogen Molecular Probes Spectraviewer)

In the TIRFM bilayer experimentes viral particles fusing to a bilayer were not sufficient in proving pore formation. Some viral particles appeared to dequech or fuse more than once. This could be indicative of either hemifusion followed by pore formation or aggregate viral particles hemifusing to the bilayer at the same place. Nonetheless bilayer fusion between the sphere and planar bilayer was successful under low pH conditions, so the sphere to sphere (i.e. liposome to virion) fusions were attempted next. A liposome with

content dye & a virus with membrane dye were exposed to low pH. When they fused both dyes dequenched simultaneously. This double dequenching only occurred in 3% of paired molecules, which is reasonable compared to other published results (Floyd and others 2008), however was not statistically significant compared to experimental controls. Since previous experiments with the membrane dye only were successful, the membrane dye was removed from the two dye system and focus was placed on the content dye. After osmotically balancing the intravesicular and extravesicular buffers and performing tests both in bulk and on the microscope, fusion was clearly observed, but no systematic pattern of variation in parameter space was discerned from the resulting data.

5.2 Future Directions

Although influenza has been studied extensively, the actual mechanism by which lipid bilayers merge is still unknown. The specific transitions and their exact energy cost between when the two bilayers are apposed to the final creation of a fusion pore have been theorized, but experimental evidence is still lacking. Sindbis has also been studied and it has been hypothesized that Sindbis mirrors influenza' infection pathway, however single particle tracking experiments that have shown influenza's endocytosis and fusion have not been successfully completed with Sindbis. Thus other infection pathways for Sindbis may be possible, including infection via a protein pore or penetration at the cell surface.

In vitro efforts to obtain high temporal resolution movies of both membrane dye dequenching and content dye dequenching would eliminate the endocytotic pathway of viral infection if the content dye dequenches prior to the membrane dye. If the content dye dequenches after the membrane dye then infection via a protein pore would not be a viable

infection pathway. Experiments using membrane dye allowed for the measurement of a residence time (time between the virus particle's attachment to the bilayer and fusion of the outer monolayers), bound virus' fusogencity at varying pHs and lipid compositions. Also, the cell receptor for Sindbis virus remains unknown, making it impossible to tether the virus onto a liposome. By only having liposomes tethered to the slide, the only guarantee that a Sindbis virus particle would encounter a tethered liposome was to inundate the channel with an extremely high concentration of virus particles. A two dye system was no longer feasible because individual virus particles were no longer distinguishable at such high concentrations.

Molecular dynamic simulations have addressed some of the questions surrounding membrane fusion. A course grain MD simulation of 2 vesicles fusing due to crosslinker tethering has shown membrane fusion between a pair of 14-nm-diameter vesicles on the hundred-microsecond time scale.(Kasson and others 2006) The crosslinker is analogous to the prefusion states of HIV gp41, influenza HA, or trans-SNARE complexes. The simulation showed fusion proceeding via a stalk-like intermediate state. About 20% of vesicles rapidly fuse from the stalk state. The remaining vesicles remained in a long-lived hemifusion intermediate that slowly converted to the fused state. The hemifused intermediate state had a decay half-life of 6.3 μs. In addition to being able to measure $t_{1/2}$, the free energy of the stalk-like state (ΔG of −3.3 kcal/mol) and fused state (ΔG of −6.0 kcal/mol) were determined. However a determination of the energy of fusion pore expansion did not result from this simulation.

The simulation of atomic force microscopy measurements on the viral capsid of cowpea chlorotic mottle virus (CCMV) provides an opportunity to study homogenous

changes in the capsid shell geometry and couple the global assembly response to local conformational changes.(Gibbons and Klug 2008) Although for most viruses the capsid is not involved in membrane fusion, alphaviruses and flaviviruses whose fusion proteins' conformational changes result in the rearrangement of the viral surface may benefit from a similar analysis.

Future studies are needed to determine how viral fusion proteins and membrane lipids interact to generate a membrane instability that is large enough to produce membrane fusion. *In vitro* systems in general must always answer the question: 'how closely does this system match real life conditions?' Using lipid bilayers removes much of the complexity that a truly cellular or endosomal membrane would contain, such as varying lipid composition and numerous proteins embedded in the bilayer. It is difficult to work with real systems as well. Cells autofluoresce. Researchers photobleach the cells to reduce the autofluorescence, but this damages the cells. The cell lines available for research are often very different from the cells that exist in nature because they are cells that are hearty in the unnatural conditions of a laboratory. Nonetheless single particle tracking using fluorescence microscopy has shown an influenza virion bind to a cell, become endocytosed, travel through the cell in both diffusive and directed motion and then fuse with the cell's endosome in close proximity to the cell nucleus where RNA transcription can take place. (Lakadamyali and others 2003) If the same observation can be made with Sindbis virus, a definitive answer to the virus' infection pathway can be obtained. Only membrane labeling is necessary in this experiment, so the difficulties encountered with obtaining a usable content dye can be avoided.

One impediment that the *in vivo* experiment has that was less consequential in the *in vitro* experiment is the dye photobleaching before the entire course of fusion is complete. On average it takes an influenza particle 8 minutes between binding to the cell and fusing with the endosome. (Lakadamyali and others 2003) Laser illumination of the dye molecules can be reduced through time lapse video capture but some information is lost when employing this method. Still if successful this experiment should provide a definitive answer to the question: ‘What is Sindbis virus’ infection pathway?

Bibliography

Aizaki H, Morikawa K, Fukasawa M, Hara H, Inoue Y, Tani H, Saito K, Nishijima M, Hanada K, Matsuura Y and others. 2008. Critical role of virion-associated cholesterol and sphingolipid in hepatitis C virus infection. J Virol 82(12):5715-24.

Antonin W, Fasshauer D, Becker S, Jahn R, Schneider TR. 2002. Crystal structure of the endosomal SNARE complex reveals common structural principles of all SNAREs. Nat Struct Biol 9(2):107-11.

Axelrod D. 1989. Total internal reflection fluorescence microscopy. Methods Cell Biol 30:245-70.

Basanez G. 2002. Membrane fusion: the process and its energy suppliers. Cell Mol Life Sci 59(9):1478-90.

Bergelson LD, Bukrinskaya AG, Prokazova NV, Shaposhnikova GI, Kocharov SL, Shevchenko VP, Kornilaeva GV, Fomina-Ageeva EV. 1982. Role of gangliosides in reception of influenza virus. Eur J Biochem 128(2-3):467-74.

Blumenthal R, Sarkar DP, Durell S, Howard DE, Morris SJ. 1996. Dilation of the influenza hemagglutinin fusion pore revealed by the kinetics of individual cell-cell fusion events. Journal of Cell Biology 135(1):63-71.

Bonnafous P, Stegmann T. 2003. Pore formation in target liposomes by viral fusion proteins. Methods Enzymol 372:408-18.

Boukobza E, Sonnenfeld A, Haran G. 2001. Immobilization in surface-tethered lipid vesicles as a new tool for single biomolecule spectroscopy. Journal of Physical Chemistry B 105(48):12165-12170.

Bowen ME, Weninger K, Brunger AT, Chu S. 2004. Single molecule observation of liposome-bilayer fusion thermally induced by soluble N-ethyl maleimide sensitive-factor attachment protein receptors (SNAREs). Biophys J 87(5):3569-84.

Brandenburg B, Lee LY, Lakadamyali M, Rust MJ, Zhuang X, Hogle JM. 2007. Imaging Poliovirus Entry in Live Cells. PLoS Biol 5(7):e183.

Brandenburg B, Zhuang X. 2007. Virus trafficking - learning from single-virus tracking. Nat Rev Microbiol 5(3):197-208.

Bressanelli S, Stiasny K, Allison SL, Stura EA, Duquerroy S, Lescar J, Heinz FX, Rey FA. 2004. Structure of a flavivirus envelope glycoprotein in its low-pH-induced membrane fusion conformation. Embo J 23(4):728-38.

Brunger AT. 2005. Structure and function of SNARE and SNARE-interacting proteins. Q Rev Biophys 38(1):1-47.

Bullough PA, Hughson FM, Skehel JJ, Wiley DC. 1994. Structure of influenza haemagglutinin at the pH of membrane fusion. Nature 371(6492):37-43.

Cardullo RA, Parpura V. 2003. Fluorescence resonance energy transfer microscopy: theory and instrumentation. Methods Cell Biol 72:415-30.

Carroll SM, Higa HH, Paulson JC. 1981. Different cell-surface receptor determinants of antigenically similar influenza virus hemagglutinins. J Biol Chem 256(16):8357-63.

Carter GC, Bernstone L, Sangani D, Bee JW, Harder T, James W. 2009. HIV entry in macrophages is dependent on intact lipid rafts. Virology.

Center RJ, Kobe B, Wilson KA, Teh T, Howlett GJ, Kemp BE, Poumbourios P. 1998. Crystallization of a trimeric human T cell leukemia virus type 1 gp21 ectodomain fragment as a chimera with maltose-binding protein. Protein Sci 7(7):1612-9.

Chen EH, Olson EN. 2005. Unveiling the mechanisms of cell-cell fusion. Science 308(5720):369-73.

Chen YD, Rubin RJ, Szabo A. 1993. Fluorescence dequenching kinetics of single cell-cell fusion complexes. Biophys J 65(1):325-33.

Chernomordik L, Chanturiya A, Green J, Zimmerberg J. 1995. The hemifusion intermediate and its conversion to complete fusion: regulation by membrane composition. Biophys J 69(3):922-9.

Chernomordik LV, Frolov VA, Leikina E, Bronk P, Zimmerberg J. 1998. The pathway of membrane fusion catalyzed by influenza hemagglutinin: Restriction of lipids, hemifusion, and lipidic fusion pore formation. Journal of Cell Biology 140(6):1369-1382.

Chernomordik LV, Kozlov MM. 2003. Protein-lipid interplay in fusion and fission of biological membranes. Annual Review of Biochemistry 72:175-207.

Chernomordik LV, Kozlov MM. 2005. Membrane hemifusion: crossing a chasm in two leaps. Cell 123(3):375-82.

Chernomordik LV, Kozlov MM. 2008. Mechanics of membrane fusion. Nat Struct Mol Biol 15(7):675-83.

Chernomordik LV, Vogel SS, Sokoloff A, Onaran HO, Leikina EA, Zimmerberg J. 1993. Lysolipids reversibly inhibit Ca(2+)-, GTP- and pH-dependent fusion of biological membranes. FEBS Lett 318(1):71-6.

Chizmadzhev YA. 2004. The mechanisms of lipid-protein rearrangements during viral infection. Bioelectrochemistry 63(1-2):129-36.

Citovsky V, Loyter A. 1985. Fusion of Sendai virions or reconstituted Sendai virus envelopes with liposomes or erythrocyte membranes lacking virus receptors. J Biol Chem 260(22):12072-7.

Cohen FS, Melikyan GB. 2004. The energetics of membrane fusion from binding, through hemifusion, pore formation, and pore enlargement. J Membr Biol 199(1):1-14.

Damm EM, Pelkmans L. 2006. Systems biology of virus entry in mammalian cells. Cell Microbiol 8(8):1219-27.

Dimitrov DS. 2004. Virus entry: molecular mechanisms and biomedical applications. Nat Rev Microbiol 2(2):109-22.

Duffus WA, Levy-Mintz P, Klimjack MR, Kielian M. 1995. Mutations in the putative fusion peptide of Semliki Forest virus affect spike protein oligomerization and virus assembly. J Virol 69(4):2471-9.

Earp LJ, Delos SE, Park HE, White JM. 2005. The many mechanisms of viral membrane fusion proteins. Curr Top Microbiol Immunol 285:25-66.

Earp LJ, Hernandez LD, Delos SE, White JM. 2003. Receptor-activated binding of viral fusion proteins to target membranes. Methods Enzymol 372:428-40.

Edwards KA, Baeumner AJ. 2006. Liposomes in analyses. Talanta 68(5):1421-31.

Engel A, Walter P. 2008. Membrane lysis during biological membrane fusion: collateral damage by misregulated fusion machines. Journal of Cell Biology 183(2):181-186.

Estes DJ, Lopez SR, Fuller AO, Mayer M. 2006. Triggering and visualizing the aggregation and fusion of lipid membranes in microfluidic chambers. Biophysical Journal 91(1):233-243.

Farge E, Devaux PF. 1992. Shape changes of giant liposomes induced by an asymmetric transmembrane distribution of phospholipids. Biophys J 61(2):347-57.

Farsad K, De Camilli P. 2003. Mechanisms of membrane deformation. Curr Opin Cell Biol 15(4):372-81.

Finke S, Brzozka K, Conzelmann KK. 2004. Tracking fluorescence-labeled rabies virus: enhanced green fluorescent protein-tagged phosphoprotein P supports virus gene expression and formation of infectious particles. J Virol 78(22):12333-43.

Floyd DL, Ragains JR, Skehel JJ, Harrison SC, van Oijen AM. 2008. Single-particle kinetics of influenza virus membrane fusion. Proc Natl Acad Sci U S A 105(40):15382-7.

Freed EO, Myers DJ, Risser R. 1990. Characterization of the fusion domain of the human immunodeficiency virus type 1 envelope glycoprotein gp41. Proc Natl Acad Sci U S A 87(12):4650-4.

Fu AY, Spence C, Scherer A, Arnold FH, Quake SR. 1999. A microfabricated fluorescence-activated cell sorter. Nat Biotechnol 17(11):1109-11.

Furuta RA, Wild CT, Weng Y, Weiss CD. 1998. Capture of an early fusion-active conformation of HIV-1 gp41. Nat Struct Biol 5(4):276-9.

Garrett G. 1998. Biochemistry: Brooks/Cole.

Gaudin Y. 2000. Rabies virus-induced membrane fusion pathway. J Cell Biol 150(3):601-12.

Gibbons DL, Vaney MC, Roussel A, Vigouroux A, Reilly B, Lepault J, Kielian M, Rey FA. 2004. Conformational change and protein-protein interactions of the fusion protein of Semliki Forest virus. Nature 427(6972):320-5.

Gibbons MM, Klug WS. 2008. Influence of nonuniform geometry on nanoindentation of viral capsids. Biophys J 95(8):3640-9.

Giocondi MC, Besson F, Dosset P, Milhiet PE, Le Grimellec C. 2007. Temperature-dependent localization of GPI-anchored intestinal alkaline phosphatase in model rafts. J Mol Recognit 20(6):531-7.

Greber UF, Way M. 2006. A superhighway to virus infection. Cell 124(4):741-54.

Gruner SM. 2002. Caught in the act. Science 297(5588):1817-1818.

Gunther-Ausborn S, Schoen P, Bartoldus I, Wilschut J, Stegmann T. 2000. Role of hemagglutinin surface density in the initial stages of influenza virus fusion: Lack of evidence for cooperativity. Journal of Virology 74(6):2714-2720.

Haluska CK, Riske KA, Marchi-Artzner V, Lehn JM, Lipowsky R, Dimova R. 2006. Time scales of membrane fusion revealed by direct imaging of vesicle fusion with high temporal resolution. Proc Natl Acad Sci U S A 103(43):15841-6.

Haque ME, Koppaka V, Axelsen PH, Lentz BR. 2005. Properties and structures of the influenza and HIV fusion peptides on lipid membranes: implications for a role in fusion. Biophys J 89(5):3183-94.

Harris A, Cardone G, Winkler DC, Heymann JB, Brecher M, White JM, Steven AC. 2006. Influenza virus pleiomorphy characterized by cryoelectron tomography. Proc Natl Acad Sci U S A 103(50):19123-7.

Harrison SC. 2008. Viral membrane fusion. Nat Struct Mol Biol 15(7):690-8.

Heldwein EE, Lou H, Bender FC, Cohen GH, Eisenberg RJ, Harrison SC. 2006. Crystal structure of glycoprotein B from herpes simplex virus 1. Science 313(5784):217-20.

Helenius A, Kartenbeck J, Simons K, Fries E. 1980. On the entry of Semliki forest virus into BHK-21 cells. J Cell Biol 84(2):404-20.

Hinterdorfer P, Baber G, Tamm LK. 1994. Reconstitution of membrane fusion sites. A total internal reflection fluorescence microscopy study of influenza hemagglutinin-mediated membrane fusion. J Biol Chem 269(32):20360-8.

Hoebe RA, Van Oven CH, Gadella TW, Jr., Dhonukshe PB, Van Noorden CJ, Manders EM. 2007. Controlled light-exposure microscopy reduces photobleaching and phototoxicity in fluorescence live-cell imaging. Nat Biotechnol 25(2):249-53.

Hoekstra D, de Boer T, Klappe K, Wilschut J. 1984. Fluorescence method for measuring the kinetics of fusion between biological membranes. Biochemistry 23(24):5675-81.

Hoekstra D, Klappe K, Hoff H, Nir S. 1989. Mechanism of fusion of Sendai virus: role of hydrophobic interactions and mobility constraints of viral membrane proteins. Effects of polyethylene glycol. J Biol Chem 264(12):6786-92.

Hoppins S, Nunnari J. 2009. The molecular mechanism of mitochondrial fusion. Biochim Biophys Acta 1793(1):20-6.

Hua Y, Scheller RH. 2001. Three SNARE complexes cooperate to mediate membrane fusion. Proc Natl Acad Sci U S A 98(14):8065-70.

Hung WC, Lee MT, Chen FY, Huang HW. 2007. The condensing effect of cholesterol in lipid bilayers. Biophys J 92(11):3960-7.

Jahn R, Scheller RH. 2006. SNAREs--engines for membrane fusion. Nat Rev Mol Cell Biol 7(9):631-43.

Jardetzky TS, Lamb RA. 2004. Virology: a class act. Nature 427(6972):307-8.

Kadlec J, Loureiro S, Abrescia NG, Stuart DI, Jones IM. 2008. The postfusion structure of baculovirus gp64 supports a unified view of viral fusion machines. Nat Struct Mol Biol 15(10):1024-30.

Kashiwada A, Matsuda K, Mizuno T, Tanaka T. 2008. Construction of a pH-responsive artificial membrane fusion system by using designed coiled-coil polypeptides. Chemistry 14(24):7343-50.

Kasson PM, Kelley NW, Singhal N, Vrljic M, Brunger AT, Pande VS. 2006. Ensemble molecular dynamics yields submillisecond kinetics and intermediates of membrane fusion. Proc Natl Acad Sci U S A 103(32):11916-21.

Kemble GW, Danieli T, White JM. 1994. Lipid-anchored influenza hemagglutinin promotes hemifusion, not complete fusion. Cell 76(2):383-91.

Kemble GW, Henis YI, White JM. 1993. GPI- and transmembrane-anchored influenza hemagglutinin differ in structure and receptor binding activity. J Cell Biol 122(6):1253-65.

Kielian M, Klimjack MR, Ghosh S, Duffus WA. 1996. Mechanisms of mutations inhibiting fusion and infection by Semliki Forest virus. J Cell Biol 134(4):863-72.

Kielian M, Rey FA. 2006. Virus membrane-fusion proteins: more than one way to make a hairpin. Nat Rev Microbiol 4(1):67-76.

Korte T, Ludwig K, Huang Q, Rachakonda PS, Herrmann A. 2007. Conformational change of influenza virus hemagglutinin is sensitive to ionic concentration. Eur Biophys J 36(4-5):327-35.

Kozlovsky Y, Chernomordik LV, Kozlov MM. 2002. Lipid intermediates in membrane fusion: formation, structure, and decay of hemifusion diaphragm. Biophys J 83(5):2634-51.

Kshirsagar NA, Pandya SK, Kirodian GB, Sanath S. 2005. Liposomal drug delivery system from laboratory to clinic. J Postgrad Med 51 Suppl 1:S5-15.

Kwong PD, Wyatt R, Robinson J, Sweet RW, Sodroski J, Hendrickson WA. 1998. Structure of an HIV gp120 envelope glycoprotein in complex with the CD4 receptor and a neutralizing human antibody. Nature 393(6686):648-659.

Lakadamyali M, Rust MJ, Babcock HP, Zhuang X. 2003. Visualizing infection of individual influenza viruses. Proc Natl Acad Sci U S A 100(16):9280-5.

Lakadamyali M, Rust MJ, Zhuang X. 2004. Endocytosis of influenza viruses. Microbes Infect 6(10):929-36.

Lang T, Halemani ND, Rammner B. 2008. Interplay between lipids and the proteinaceous membrane fusion machinery. Prog Lipid Res 47(6):461-9.

Lescar J, Roussel A, Wien MW, Navaza J, Fuller SD, Wengler G, Rey FA. 2001. The Fusion glycoprotein shell of Semliki Forest virus: an icosahedral assembly primed for fusogenic activation at endosomal pH. Cell 105(1):137-48.

Liu T, Wang T, Chapman ER, Weisshaar JC. 2008. Productive hemifusion intermediates in fast vesicle fusion driven by neuronal SNAREs. Biophysical Journal 94(4):1303-1314.

Lowy RJ, Sarkar DP, Chen Y, Blumenthal R. 1990. Observation of single influenza virus-cell fusion and measurement by fluorescence video microscopy. Proc Natl Acad Sci U S A 87(5):1850-4.

Malinin VS, Lentz BR. 2004. Energetics of vesicle fusion intermediates: comparison of calculations with observed effects of osmotic and curvature stresses. Biophys J 86(5):2951-64.

Markosyan RM, Cohen FS, Melikyan GB. 2005. Time-resolved imaging of HIV-1 Env-mediated lipid and content mixing between a single virion and cell membrane. Mol Biol Cell 16(12):5502-13.

Markovic I, Pulyaeva H, Sokoloff A, Chernomordik LV. 1998. Membrane fusion mediated by baculovirus gp64 involves assembly of stable gp64 trimers into multiprotein aggregates. Journal of Cell Biology 143(5):1155-1166.

Marsh M, Helenius A. 2006. Virus entry: open sesame. Cell 124(4):729-40.

Martens S, McMahon HT. 2008. Mechanisms of membrane fusion: disparate players and common principles. Nat Rev Mol Cell Biol 9(7):543-56.

McDonald JC, Duffy DC, Anderson JR, Chiu DT, Wu H, Schueller OJ, Whitesides GM. 2000. Fabrication of microfluidic systems in poly(dimethylsiloxane). Electrophoresis 21(1):27-40.

Melikyan GB, Barnard RJ, Abrahamyan LG, Mothes W, Young JA. 2005. Imaging individual retroviral fusion events: from hemifusion to pore formation and growth. Proc Natl Acad Sci U S A 102(24):8728-33.

Melikyan GB, White JM, Cohen FS. 1995. GPI-anchored influenza hemagglutinin induces hemifusion to both red blood cell and planar bilayer membranes. J Cell Biol 131(3):679-91.

Miller ML, Brown DT. 1992. Morphogenesis of Sindbis virus in three subclones of Aedes albopictus (mosquito) cells. J Virol 66(7):4180-90.

Modis Y, Ogata S, Clements D, Harrison SC. 2004. Structure of the dengue virus envelope protein after membrane fusion. Nature 427(6972):313-9.

Mudiganti U, Hernandez R, Ferreira D, Brown DT. 2006. Sindbis virus infection of two model insect cell systems--a comparative study. Virus Res 122(1-2):28-34.

Mukhopadhyay S, Zhang W, Gabler S, Chipman PR, Strauss EG, Strauss JH, Baker TS, Kuhn RJ, Rossmann MG. 2006. Mapping the structure and function of the E1 and E2 glycoproteins in alphaviruses. Structure 14(1):63-73.

Munoz-Barroso I, Durell S, Sakaguchi K, Appella E, Blumenthal R. 1998. Dilation of the human immunodeficiency virus-1 envelope glycoprotein fusion pore revealed by the inhibitory action of a synthetic peptide from gp41. J Cell Biol 140(2):315-23.

Nelson. 2004. Biological Physics Energy Information Life. New York: Freeman Company. 325-336 p.

Niles WD, Cohen FS. 1991. Fusion of influenza virions with a planar lipid membrane detected by video fluorescence microscopy. J Gen Physiol 97(6):1101-19.

Niles WD, Li Q, Cohen FS. 1992. Computer detection of the rapid diffusion of fluorescent membrane fusion markers in images observed with video microscopy. Biophys J 63(3):710-22.

Nunes-Correia I, Eulalio A, Nir S, Duzgunes N, Ramalho-Santos J, Pedroso de Lima MC. 2002. Fluorescent probes for monitoring virus fusion kinetics: comparative evaluation of reliability. Biochim Biophys Acta 1561(1):65-75.

Nybakken GE, Nelson CA, Chen BR, Diamond MS, Fremont DH. 2006. Crystal structure of the West Nile virus envelope glycoprotein. J Virol 80(23):11467-74.

Ohki S, Arnold K. 2008. Experimental evidence to support a theory of lipid membrane fusion. Colloids and Surfaces B-Biointerfaces 63(2):276-281.

Ohki S, Flanagan TD, Hoekstra D. 1998. Probe transfer with and without membrane fusion in a fluorescence fusion assay. Biochemistry 37(20):7496-503.

Paredes AM, Ferreira D, Horton M, Saad A, Tsuruta H, Johnston R, Klimstra W, Ryman K, Hernandez R, Chiu W and others. 2004. Conformational changes in Sindbis virions resulting from exposure to low pH and interactions with cells suggest that cell penetration may occur at the cell surface in the absence of membrane fusion. Virology 324(2):373-86.

Peisajovich SG, Shai Y. 2003. Liposomes in identification and characterization of viral fusogenic peptides. Methods Enzymol 372:361-73.

Pelkmans L, Helenius A. 2003. Insider information: what viruses tell us about endocytosis. Curr Opin Cell Biol 15(4):414-22.

Pritzen C, Herrmann A. 1988. Are osmotic forces involved in influenza virus-cell fusion? Biosci Rep 8(1):55-64.

Rawat SS, Viard M, Gallo SA, Rein A, Blumenthal R, Puri A. 2003. Modulation of entry of enveloped viruses by cholesterol and sphingolipids (Review). Mol Membr Biol 20(3):243-54.

Rawicz W, Smith BA, McIntosh TJ, Simon SA, Evans E. 2008. Elasticity, strength, and water permeability of bilayers that contain raft microdomain-forming lipids. Biophys J 94(12):4725-36.

Razinkov VI, HernandezJimenez EI, Mikhalyov II, Cohen FS, Molotkovsky JG. 1997. New fluorescent lysolipids: Preparation and selective labeling of inner liposome leaflet. Biochimica Et Biophysica Acta-Biomembranes 1329(1):149-158.

Reeves JD, Gallo SA, Ahmad N, Miamidian JL, Harvey PE, Sharron M, Pohlmann S, Sfakianos JN, Derdeyn CA, Blumenthal R and others. 2002. Sensitivity of HIV-1 to entry inhibitors correlates with envelope/coreceptor affinity, receptor density, and fusion kinetics. Proc Natl Acad Sci U S A 99(25):16249-54.

Reeves JD, Lee FH, Miamidian JL, Jabara CB, Juntilla MM, Doms RW. 2005. Enfuvirtide resistance mutations: impact on human immunodeficiency virus envelope function, entry inhibitor sensitivity, and virus neutralization. J Virol 79(8):4991-9.

Rey FA, Heinz FX, Mandl C, Kunz C, Harrison SC. 1995. The envelope glycoprotein from tick-borne encephalitis virus at 2 A resolution. Nature 375(6529):291-8.

Rimsky LT, Shugars DC, Matthews TJ. 1998. Determinants of human immunodeficiency virus type 1 resistance to gp41-derived inhibitory peptides. J Virol 72(2):986-93.

Rizo J, Rosenmund C. 2008. Synaptic vesicle fusion. Nat Struct Mol Biol 15(7):665-74.

Roche S, Bressanelli S, Rey FA, Gaudin Y. 2006. Crystal structure of the low-pH form of the vesicular stomatitis virus glycoprotein G. Science 313(5784):187-91.

Schibli DJ, Weissenhorn W. 2004. Class I and class II viral fusion protein structures reveal similar principles in membrane fusion (Review). Molecular Membrane Biology 21(6):361-371.

Schroth-Diez B, Ludwig K, Baljinnyam B, Kozerski C, Huang Q, Herrmann A. 2000. The role of the transmembrane and of the intraviral domain of glycoproteins in membrane fusion of enveloped viruses. Biosci Rep 20(6):571-95.

Sears C, Conrad and Stanitski. 1983. Chemistry for Health-related Sciences: Concepts and Correlations. NJ: Prentice-Hall Inc. 154-158 p.

Seisenberger G, Ried MU, Endress T, Buning H, Hallek M, Brauchle C. 2001. Real-time single-molecule imaging of the infection pathway of an adeno-associated virus. Science 294(5548):1929-32.

Sieczkarski SB, Whittaker GR. 2005. Viral entry. Curr Top Microbiol Immunol 285:1-23.

Simons K, Vaz WL. 2004. Model systems, lipid rafts, and cell membranes. Annu Rev Biophys Biomol Struct 33:269-95.

Skehel JJ, Wiley DC. 2000. Receptor binding and membrane fusion in virus entry: The influenza hemagglutinin. Annual Review of Biochemistry 69:531-569.

Sklodowaka A, Wozniak M, Matlakowska R. 1999. The method of contact angle measurements and estimation of work of adhesion in bioleaching of metals. Biol Proced Online 1:114-121.

Smit JM, Li G, Schoen P, Corver J, Bittman R, Lin KC, Wilschut J. 2002. Fusion of alphaviruses with liposomes is a non-leaky process. Febs Letters 521(1-3):62-66.

Smit JM, Waarts BL, Bittman R, Wilschut J. 2003. Liposomes as target membranes in the study of virus receptor interaction and membrane fusion. Methods Enzymol 372:374-92.

Sollner TH. 2004. Intracellular and viral membrane fusion: a uniting mechanism. Current Opinion in Cell Biology 16(4):429-435.

Struck DK, Hoekstra D, Pagano RE. 1981. Use of resonance energy transfer to monitor membrane fusion. Biochemistry 20(14):4093-9.

Sudhof TC, Rothman JE. 2009. Membrane fusion: grappling with SNARE and SM proteins. Science 323(5913):474-7.

Sutton RB, Fasshauer D, Jahn R, Brunger AT. 1998. Crystal structure of a SNARE complex involved in synaptic exocytosis at 2.4 A resolution. Nature 395(6700):347-53.

Suzuki T, Suzuki Y. 2006. Virus infection and lipid rafts. Biological & Pharmaceutical Bulletin 29(8):1538-1541.

Tamm LK. 2003. Hypothesis: spring-loaded boomerang mechanism of influenza hemagglutinin-mediated membrane fusion. Biochimica Et Biophysica Acta-Biomembranes 1614(1):14-23.

Thongthai W. 2008. Effects of Photobleaching on Membrane Fusion and Infectivity of Dye Labeled Sindbis Virus. Raleigh: North Carolina State University. 61 p.

Thongthai W, Weninger K. 2008. Photoinactivation of Sindbis Virus Infectivity Without Inhibition of Membrane Fusion. Photochem Photobiol.

Tsao YS, Huang L. 1985. Sendai virus induced leakage of liposomes containing gangliosides. Biochemistry 24(5):1092-8.

van der Schaar HM, Rust MJ, Waarts BL, van der Ende-Metselaar H, Kuhn RJ, Wilschut J, Zhuang X, Smit JM. 2007. Characterization of the early events in dengue virus cell entry by biochemical assays and single-virus tracking. J Virol 81(21):12019-28.

Vashishtha M, Phalen T, Marquardt MT, Ryu JS, Ng AC, Kielian M. 1998. A single point mutation controls the cholesterol dependence of Semliki Forest virus entry and exit. Journal of Cell Biology 140(1):91-99.

von Bonsdorff CH, Harrison SC. 1975. Sindbis virus glycoproteins form a regular icosahedral surface lattice. J Virol 16(1):141-5.

Vonderheit A, Helenius A. 2005. Rab7 associates with early endosomes to mediate sorting and transport of Semliki forest virus to late endosomes. PLoS Biol 3(7):e233.

Waarts BL, Bittman R, Wilschut J. 2002. Sphingolipid and cholesterol dependence of alphavirus membrane fusion. Lack of correlation with lipid raft formation in target liposomes. J Biol Chem 277(41):38141-7.

Walker GM, Beebe DJ. 2002. A passive pumping method for microfluidic devices. Lab Chip 2(3):131-4.

Wang G, Hernandez R, Weninger K, Brown DT. 2007. Infection of cells by Sindbis virus at low temperature. Virology 362(2):461-7.

Wassarman PM, Litscher ES. 2008. Mammalian fertilization is dependent on multiple membrane fusion events. Methods Mol Biol 475:99-113.

Weise K, Reed J. 2008. Fusion peptides and transmembrane domains of fusion proteins are characterized by different but specific structural properties. Chembiochem 9(6):934-943.

Weissenhorn W, Carfi A, Lee KH, Skehel JJ, Wiley DC. 1998. Crystal structure of the Ebola virus membrane fusion subunit, GP2, from the envelope glycoprotein ectodomain. Mol Cell 2(5):605-16.

Weissenhorn W, Hinz A, Gaudin Y. 2007. Virus membrane fusion. Febs Letters 581(11):2150-2155.

Wessels L, Elting MW, Scimeca D, Weninger K. 2007. Rapid membrane fusion of individual virus particles with supported lipid bilayers. Biophys J 93(2):526-38.

White J, Helenius A. 1980. pH-dependent fusion between the Semliki Forest virus membrane and liposomes. Proc Natl Acad Sci U S A 77(6):3273-7.

White JM, Delos SE, Brecher M, Schornberg K. 2008. Structures and mechanisms of viral membrane fusion proteins: multiple variations on a common theme. Crit Rev Biochem Mol Biol 43(3):189-219.

Wickner W, Schekman R. 2008. Membrane fusion. Nat Struct Mol Biol 15(7):658-64.

Wild CT, Shugars DC, Greenwell TK, McDanal CB, Matthews TJ. 1994. Peptides corresponding to a predictive alpha-helical domain of human immunodeficiency virus type 1 gp41 are potent inhibitors of virus infection. Proc Natl Acad Sci U S A 91(21):9770-4.

Wilson IA, Skehel JJ, Wiley DC. 1981. Structure of the haemagglutinin membrane glycoprotein of influenza virus at 3 A resolution. Nature 289(5796):366-73.

Yang L, Huang HW. 2002. Observation of a membrane fusion intermediate structure. Science 297(5588):1877-1879.

Yang ZN, Mueser TC, Kaufman J, Stahl SJ, Wingfield PT, Hyde CC. 1999. The crystal structure of the SIV gp41 ectodomain at 1.47 A resolution. J Struct Biol 126(2):131-44.

Yoon TY, Lu X, Diao J, Lee SM, Ha T, Shin YK. 2008. Complexin and Ca2+ stimulate SNARE-mediated membrane fusion. Nat Struct Mol Biol 15(7):707-13.

Yoon TY, Okumus B, Zhang F, Shin YK, Ha T. 2006. Multiple intermediates in SNARE-induced membrane fusion. Proc Natl Acad Sci U S A 103(52):19731-6.

Zaitseva E, Mittal A, Griffin DE, Chernomordik LV. 2005. Class II fusion protein of alphaviruses drives membrane fusion through the same pathway as class I proteins. J Cell Biol 169(1):167-77.

Zhang W, Mukhopadhyay S, Pletnev SV, Baker TS, Kuhn RJ, Rossmann MG. 2002. Placement of the structural proteins in Sindbis virus. Journal of Virology 76(22):11645-11658.

Zhou Y, Raphael RM. 2007. Solution pH alters mechanical and electrical properties of phosphatidylcholine membranes: relation between interfacial electrostatics, intramembrane potential, and bending elasticity. Biophys J 92(7):2451-62.

Zhukovsky MA, Leikina E, Markovic I, Bailey AL, Chernomordik LV. 2006. Heterogeneity of early intermediates in cell-liposome fusion mediated by influenza hemagglutinin. Biophysical Journal 91(9):3349-3358.

Zimmerberg J. 1993. Simultaneous electrical and optical measurements of individual membrane fusion events during exocytosis. Methods Enzymol 221:99-112.

Zimmerberg J, Kozlov MM. 2006. How proteins produce cellular membrane curvature. Nat Rev Mol Cell Biol 7(1):9-19.

APPENDIX

Rapid Membrane Fusion of Individual Virus Particles with Supported Lipid Bilayers

Laura Wessels, Mary Williard Elting, Dominic Scimeca, and Keith Weninger
Department of Physics, North Carolina State University, Raleigh, North Carolina

ABSTRACT Many enveloped viruses employ low-pH-triggered membrane fusion during cell penetration. Solution-based in vitro assays in which viruses fuse with liposomes have provided much of our current biochemical understanding of low-pH-triggered viral membrane fusion. Here, we extend this in vitro approach by introducing a fluorescence assay using single particle tracking to observe lipid mixing between individual virus particles (influenza or Sindbis) and supported lipid bilayers. Our single-particle experiments reproduce many of the observations of the solution assays. The single-particle approach naturally separates the processes of membrane binding and membrane fusion and therefore allows measurement of details that are not available in the bulk assays. We find that the dynamics of lipid mixing during individual Sindbis fusion events is faster than 30 ms. Although neither virus binds membranes at neutral pH, under acidic conditions, the delay between membrane binding and lipid mixing is less than half a second for nearly all virus-membrane combinations. The delay between binding and lipid mixing lengthened only for Sindbis virus at the lowest pH in a cholesterol-dependent manner, highlighting the complex interaction between lipids, virus proteins, and buffer conditions in membrane fusion.

INTRODUCTION

The boundaries of all living cells and their compartments are defined by lipid bilayers. Intracellular transport, cell entry, and secretion require vesicular lipid structures to fuse with target membranes. Membrane fusion proteins are involved in catalyzing almost every situation of biological membrane fusion. Despite decades of intense study, the precise molecular mechanism by which fusion proteins mediate membrane fusion remains a subject of much debate (1–11).

Among the best-studied membrane fusion protein machines are those present in enveloped viruses. Enveloped viruses have evolved highly efficient fusion proteins that allow the viral genome to penetrate targeted cells (12–18). For most enveloped viruses, environmental signals trigger these proteins to catalyze fusion of the viral membrane with the cell membrane. The decreased pH encountered along the endocytotic pathway is a common trigger for the fusion proteins of many enveloped viruses, most notably influenza (19,20). In a few cases, atomic resolution structures are available for viral fusion proteins under both neutral pH and low pH conditions (12) that have led to formulation of models of their molecular action (12,13).

Many enveloped viruses will fuse to protein free lipid bilayers (20–22). In vitro liposome fusion experiments have been extremely useful in characterizing the biochemical properties of viral fusion, including the pH and lipid species dependences (23,24). Bulk liposome measurements have also confirmed that viral fusion is often nonleaky and can fully mix both the lipids and the contents of fusing structures (25,26).

As valuable as these bulk assays have been in advancing our understanding of membrane fusion, they have limitations. Low-pH triggered viral membrane fusion occurs rapidly after acidification, with timescales measured in tens of seconds or minutes in the bulk liposome experiments(16,21). The stochastic nature of each occurrence of fusion prevents the precise synchronization of all of the individual virus-liposome fusion events within a cuvette-based bulk solution assay. These experimental challenges mask transient, intermediate states along the fusion pathway and obscure detailed analysis of the trajectory of the nonequilibrium processes driving the dynamics. Difficulty separating the linked processes of binding and fusion in bulk assays also complicates the interpretation of experimental results.

We have developed a fluorescence assay to make detailed measurements of the early stages of individual Sindbis and influenza virus particles fusing to supported lipid bilayers under acidic conditions. Our assay detects lipid mixing of octadecyl rhodamine (R18) between virus particles and the supported lipid bilayer. As R18 is known to ''flip-flop'' between the inner and outer leaflets of a labeled bilayer (27,28), this signal does not differentiate between hemifusion and full fusion. Throughout this article we will use hemifusion/fusion to indicate this ambiguity.

The supported lipid bilayer geometry is desirable for its compatibility with high-resolution optical measurements as well as its ease of integration with biotechnological instrumentation and sensors. Supported bilayers have been successfully applied in membrane fusion studies of SNARE proteins (29–31) and influenza virus (32–36). Illumination of the supported lipid bilayer by total internal refection yields a

Submitted September 14, 2006, and accepted for publication March 8, 2007.

Address reprint requests to Keith Weninger, Dept. of Physics, North Carolina State University, Raleigh, NC 27695. E-mail: keith_weninger@ncsu.edu.

Editor: Lukas K. Tamm.

0006-3495/07/07/526/13 $2.00

doi: 10.1529/biophysj.106.097485

signal/noise ratio sufficient for precise measurements of individual virus particles during fusion. Continued development of this single-particle approach will allow detection of the transient, stochastic intermediate states that are commonly averaged in liposome fusion assays.

We have verified that our supported bilayer assay reproduces the general trends seen in the bulk liposome experiments for these viruses (16,21,37). Although preexposure to low pH for several minutes inactivates the virus for fusion (21) and infection (38), our results show that virus exposed to low pH immediately before encountering the target membrane maintains fusion capacity. Observation of individual virus particles indicates that lipid mixing follows binding rapidly, in under a half second for most conditions, and that the dynamics of lipid mixing in individual fusion events is faster than our instrumental resolution limit of 30 ms.

Cholesterol in the target membrane enhances the final extent of fusion for Sindbis virus. Cholesterol forms microdomains, or lipid rafts, when combined with sphingomyelin in lipid bilayers (39–42). These microdomains are not required for Sindbis virus fusion and may actually inhibit fusion (41,43) by reducing lipid mobility (44–49). Here, we find that inclusion of cholesterol in the target membrane increases the interval between binding and lipid mixing at pH values <5 for Sindbis but not for influenza; a result that emphasizes the complex interactions between lipids and proteins in membrane fusion and may point to subtle differences between the mechanisms of fusion for type 1 and type 2 viral fusion proteins.

MATERIALS AND METHODS

Virus and dye labeling

Influenza (A, X:31, A Aichi/68, H3N2) grown in fertilized chicken eggs and purified by density-gradient ultracentrifugation was purchased from Charles River Laboratories (Wilmington, MA) and used as provided (2 mg/ml viral protein).

Sindbis was grown in baby hamster kidney cells (BHK-21) cultured by standard methods in minimal essential media with Earl's salts containing 10% fetal bovine serum, 5% tryptose phosphate broth, and 2 mM glutamine. Cells were inoculated with Sindbis virus and incubated for 12 h at 37°C. Supernatant was then collected and clarified by low-speed centrifugation.

Sindbis virus was purified from the clarified supernatant by ultracentrifugation on a step density gradient followed by a continuous density gradient in phosphate-buffered saline (PBS, 10 mM phosphate, 140 mM sodium chloride, pH 7.4), containing variable amounts (15–35%) of potassium tartrate to adjust the density. Purified Sindbis solutions were adjusted to a concentration of 2×10^{12} particles/ml as calibrated by BCA Assay (Pierce Biotechnology, Rockford, IL). Sindbis was used immediately or stored at –80°C without noticeable loss of fusion capacity (50).

Both Sindbis and influenza were dye-labeled with the hydrophobic fluorescent dye R18 (octadecyl rhodamine B chloride) from Molecular Probes (Invitrogen, Carlsbad, CA). Aliquots of virus (100 μl each, Sindbis at 2×10^{12} particles/ml, influenza at 0.2 or 2 mg/ml viral protein) were rapidly mixed at room temperature with 3 μl of dye dissolved in ethanol at 1.4 mM. The dye-virus mix was incubated on ice for 2 h. Virus was purified from unincorporated dye by gel filtration (NAP 5, G.E. Biosciences, Piscataway, NJ) at room temperature in PBS (for Sindbis) or Hepes-buffered saline (HBS, 45 mM Hepes, pH 7.4, 100 mM NaCl) (for influenza). We estimate that gel filtration in NAP 5 columns diluted the samples to ~⅓ the starting concentration (0.7×10^{12} particles/ml (Sindbis) or 0.07 or 0.7 mg/ml viral protein (influenza)).

Lipids, flow cells, bilayers, and buffer exchanger

All lipids (including total liver extract, brain phosphatidylethanolamine (PE), egg phosphatidylcholine (PC), brain sphingomyelin, and cholesterol) were purchased from Avanti Polar Lipids (Alabaster, AL). Chloroform was removed from solutions of lipids and cholesterol (mixed at ratios indicated in the text) under flowing argon leaving a film on the surface of a glass tube. The lipid films were placed in vacuum for at least 2 h and then hydrated with Tris-buffered saline (TBS, 25 mM Tris-HCL, pH 7.3, 150 mM NaCl) (51). Small unilamellar vesicles were prepared by extrusion through 100-nm-pore filters (miniextruder, Avanti Polar Lipids) at 5 mg/ml (liver extract), 4 mg/ml (mixes), or 20 mg/ml (PC).

Quartz microscope slides were cleaned with a sequence of bath sonication steps (soapy water, acetone, ethanol, 1 M potassium hydroxide, and water), and dried in a propane flame immediately before use. Flow-cell chambers were built by attaching glass coverslips to the quartz microscope slides, with channels defined by double-sided tape. The ends of the channels were sealed with 5-min epoxy. Fluid was introduced into the channel through holes drilled in the quartz slide at either end of the channel. To form supported bilayers on the walls of the channel, liposomes were incubated in the chamber for 5 min and then rinsed away. A second incubation with 20 mg/ml of PC liposomes for 1 h improved overall experimental reproducibility.

A home-built buffer exchanger pumped solutions through the flow cells during observations with the microscope. Virus and acidic buffers were contained in separate syringes and mixed in a tee immediately before injection into the flow cell. A variable-speed motor actuated the syringes. Enough solution was perfused to ensure that ~2.5 channel volumes were injected through the flow cell within ~5 s (~20 μl/s) during each experiment.

Sindbis virus will stick to many surfaces. We minimized surface adsorption by constructing the buffer exchange apparatus using PEEK (polyetheretherketone) tubing and fittings from Upchurch Scientific (Oak Harbor, WA) and disposable syringes (Norm-Ject, Henke Sass Wolf, Tuttlingen, Germany). Clear Tygon tubing was used immediately before the flow-cell entrance to diagnose the presence of air bubbles.

Lipid mixing hemifusion/fusion assays

For bulk measurements, equal volumes of liposome solution (concentrations as extruded, except for PC which was used at 4 mg/ml) and dye-labeled virus solution (~0.7×10^{12} particles/ml for Sindbis; 0.07 or 0.7 mg/ml viral protein for influenza) were mixed in a fluorescence cuvette. A fluorimeter (Shimadzu, Kyoto, Japan) detected fluorescence emission from the cuvette using excitation at 510 nm and emission at 570 nm. After the initial emission intensity (I_o) was recorded, the mixture was acidified by addition of an equal volume of an acidic buffer pretitrated to yield the desired final pH. The emission intensity (I) was recorded for 3–5 min, and at the end of the experiment, ~1% vol/vol of 100 mM dodecyl-maltoside was added to dissolve the samples and yield the unquenched intensity (I_f)(16,21,22). Dequenching was calculated as $(I - (I_o/2))/I_f$ and converted into a percentage for plotting.

Single virus particles were observed with a prism-type total internal reflection florescence microscope. Samples were illuminated with 8–10 mW laser light (532 nm). Fluorescence emission was collected by a water immersion objective lens (PlanApo 60×, NA 1.2, Olympus, Melville, NY), filtered by long-pass filter (HQ545lp, Chroma Technologies, Rockingham, VT), and detected with a CCD camera (Cascade 512B, Photometrics, Roper Scientific, Tucson, AZ) at 10 or 67 frames/s. Custom programs written in MATLAB (The MathWorks, Natik, MA) identified individual spots within movies representing individual virus particles. Intensity time traces were extracted from the movies at those locations by integrating the background-subtracted signal from a 7-pixel-diameter circle (1.8 μm in the sample plane)

centered on the identified spots and averaging by the integrated number of pixels. Virus solutions with low pH were injected into the flow cell while movies were recorded. For injection into flow cells, virus solution at neutral pH (~0.7×10^{12} particles/ml for Sindbis; 0.07 or 0.7 mg/ml viral protein for influenza) was contained in one syringe and acidic buffer was held in a second syringe. When injection was triggered, a motor activated both syringes. The two solutions mixed in a tee (mixing time <1 s) and then traveled to the entrance of the flow cell. We measured a 1-s delay between solution leaving the tee and appearing in the field of view in a flow cell mounted on the microscope. The virus was thus acidified 1–2 s before it was exposed to the lipid bilayer. Particles then encountered the bilayer at random times after their free diffusion in the flow cell.

Different acidification buffers were used depending on the virus and the desired final pH. For Sindbis experiments, 0.1 M Mes/0.2 M Acetic acid/145 mM NaCl was added to achieve the lowest final pH of 4.1. For all other final pH values, 100 mM Mes/150 mM NaCl buffer with pH adjusted with NaOH was diluted with variable amounts of TBS to yield a final pH as indicated in the text when mixed with virus samples in PBS. Control experiments at neutral pH used TBS (pH 7.3). For influenza experiments, the second syringe contained 500 mM Mes/145 mM NaCl adjusted to various pH to yield the indicated final pH when mixed with virus in HBS. HBS (pH 7.3) was used for the influenza control experiments. Both bulk and single-virus-particle experiments were performed at room temperature.

The precise values of our ensemble measurements of single-particle behavior (see Table 1, and Figs. 1, 2, and 6) were variable over the months of experimentation of this project. Different purifications of Sindbis virus or different manufacturer lots of influenza virus exhibit different infectivity and fusion capacity. Different substrates and different manufacturer lots of lipids generate heterogeneity in the properties and defects in the supported bilayers. To minimize the effects of the variability of our samples on the ensemble measurements presented here, all data for any given figure were acquired from the same sample, on the same day, on substrates prepared in batch with identical cleaning treatment and using the same supply of lipids.

To estimate the expected variability in the quantitative values from our experimental protocol, we simulated multi-experiment runs all in one day, but instead of scanning parameter space, as was done to generate the data in the figures of this article, we repeated one condition in parameter space many times. From these repeated measurements of a single parameter space point, we estimate the standard deviation for number of fusions at 44% (Sindbis) and 36% (influenza). Standard deviations for the median residence times are 25% (Sindbis) and 21% (influenza). The fact that both Sindbis virus and influenza have similar quantitative variability suggests that these effects are random. The spread in our parameter-space data generally agrees with this variability in regions of parameter space where previous bulk solution experiments suggest there should be no systematic variation. The main ensemble effects that we claim in this article (increased fusion at low pH and increased residence time for Sindbis at pH below 5 for cholesterol containing target membranes) are effects substantially larger than these random run-run variations. The standard deviation of the final dequenching percentages, upon multiple attempts at identical bulk solution virus-liposome fusion experiments, was ~10% for both viruses in our lab.

RESULTS

Bulk solution experiments

Fusion of virus with liposomes in bulk solution has been studied with fluorescence dequenching for many years. Before developing a single-particle fusion assay, we confirmed that our Sindbis and influenza viruses exhibit fusion behavior consistent with this large body of past work. In bulk assays, samples of virus labeled with self-quenching concentrations of lipophilic, fluorescent dyes are mixed in a fluorescence cuvette with liposomes. Upon acidification of the solution in the cuvette, virus particles fuse with liposomes, resulting in dilution of the fluorescent dye and release of the self-quenching of the fluorescent dye. The intensity increase due to the dequenching of most of the lipophilic dyes used in these bulk fusion experiments (as well as our single-particle assay described below) only reports lipid mixing, but this signal has correlated with content mixing in some cases (21,25,37).

The release of the self-quenching of membrane dye during bulk fusion experiments leads to an increase in the fluorescence emission intensity that reaches a steady value typically within a few minutes. The emission is scaled to the completely de-quenched value measured upon addition of detergent to completely dissolve the vesicular structures in the cuvette. Time courses of typical bulk fusion experiments using our Sindbis virus are displayed as the continuous traces in Fig. 1. Similar results are found when using influenza. No de-quenching from membrane fusion is detected in control experiments where the pH is maintained near neutral (Fig. 1, *lowest curve*).

Fig. 2 (*solid symbols*) displays the pH dependence of the final extent of the dequenching signal resulting from fusion for Sindbis and influenza viruses, as deduced from bulk measurements with liposomes. In agreement with previous published work, we find that fusion with a physiological blend of lipids in liposomes (total liver extract) is rapid and nearly complete for Sindbis virus for pH <~6.5, whereas

TABLE 1 Hemifusion/fusion of Sindbis virus with bilayers formed from mixtures of purified lipids

Membrane composition	Molar ratio	Final % dequenching (bulk solution) pH 4.6	Final % dequenching (bulk solution) pH 5.5	Residence time single virus: bilayer pH 4.6
PC/PE	1:1	0	0	0.2 s
PC/PE/SM	1:1:1	1	0	0.26 s
PC/PE/CH	1:1:1.5	17	2	0.75 s
PC/PE/SM/CH	1:1:1:1.5	20	8	0.5 s

Liposomes of the indicated mixtures of lipids (*CH*, cholesterol; *SM*, sphingomyelin) were used in bulk solution assays or to form supported lipid bilayers for single particle studies. The final extent of dequenching from bulk fusion experiments illustrates the strict cholesterol requirement for fusion with Sindbis virus. The essential nature of sphingomyelin is evident at pH 5.5 but is reduced at pH 4.6. The column of residence times is from single-particle bilayer experiments at pH 4.6. In the absence of cholesterol, there were fewer events in agreement with the lower final dequenching extent in the bulk studies, but residence times could be determined from the few events that did occur. The residence time increased in the presence of cholesterol only for experiments with pH <5.

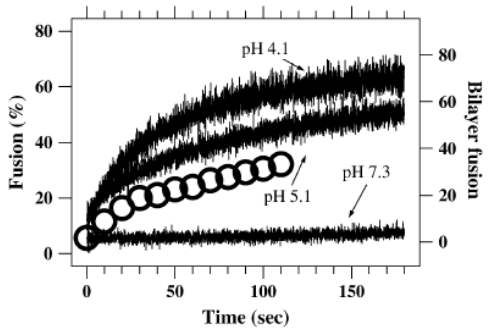

FIGURE 1 Bulk solution hemifusion/fusion of Sindbis virus with liposomes formed from total liver extract triggered by low-pH conditions. The continuous lines show how fluorescence emission from self-quenched dye in the virus membrane increases after hemifusion/fusion to liposomes dilutes the dye. Buffer is added at time zero to change the pH to the indicated final value. Lipid mixing does not occur at neutral pH. The large circles are the accumulated number of dequenching events as a function of time during the single-particle bilayer experiment from Fig. 5 *B*. Similar ensemble kinetics are observed in the bulk experiments and the single-particle bilayer experiments.

influenza requires a lower pH of <6.0 to reach highly efficient fusion with the same type of liposomes (16,20,21,52,53). Table 1, columns 3 and 4, contains results of bulk fusion experiments where the composition of the target liposome is varied. Again consistent with previous work (21), we find an enhancement of fusion efficiency for Sindbis virus when the target membrane contains both cholesterol and sphingomyelin. The data in Table 1 only include a small region of the parameter space relevant to fusion. For example, it is clear that the composition of the target membrane determines the optimal pH for fusion, as demonstrated by the observation that influenza can fuse to liposomes at neutral pH when

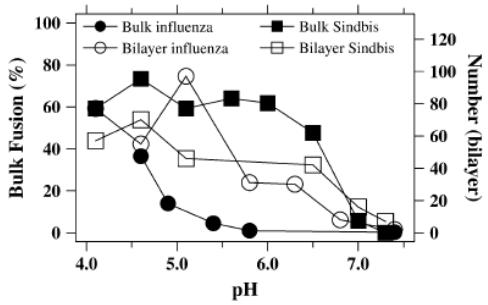

FIGURE 2 Comparison of bulk solution to supported lipid bilayer measurements of the pH response of membrane hemifusion/fusion for Sindbis and influenza viruses. The final extents of dye dequenching from bulk solution measurements with liposomes as in Fig. 1 (liver extract) are plotted against the left axis. Plotted on the right axis is the total number of individual dequenching events on a 100 μm × 100 μm area within 12 min after injection of virus and acidic buffer in supported lipid bilayer experiments (liver extract).

specific blends of lipids are used to form target membranes (54). The agreement between these bulk studies using virus in our lab and the published work of other labs validates our starting point to design a single-particle assay for viral membrane fusion.

Single-virus assay

To exploit the advantages afforded by the single-particle experimental approach (55,56), we developed an assay to observe individual Sindbis and influenza virus particles fusing to a supported lipid bilayer. For this assay, we formed a bilayer on a quartz surface within a liquid flow cell. The bilayer was illuminated with total internal reflection of laser light, which results in fluorescence emission only from dye-labeled virus particles that are less than a few hundred nanometers from the bilayer. We observed the illuminated region of the bilayer with a sensitive fluorescence microscope capable of single-molecule detection.

Membrane fusion is triggered by low pH for both Sindbis and influenza viruses. The priming of the particles for fusion upon low-pH exposure is transient and within a few minutes of initial acidification they are rendered incompetent for fusion. We therefore built a two-chamber buffer exchange system to change the pH of the virus solution immediately before it was pumped into the flow cell. Virus was contained at neutral pH in one chamber, separate from the low-pH solution in the other chamber. Upon activation, the buffer exchanger mixed the solutions in a tee and pumped the mixture into the flow cell containing the supported lipid bilayer while the flow cell was being observed with the microscope. The pumping was slow to allow mixing of the solutions in the tee. The delay between solutions leaving the mixing tee and arriving in the flow chamber was ~1 s (~30 μl in the connecting lines and tee).

Virus samples were labeled with self-quenching concentrations of fluorescent membrane dyes in the same manner as in the bulk fusion studies. After injection of the virus sample into the flow cell, individual particles were detected around the bilayer as their Brownian motion took them into the evanescent light field that extends 100–200 nm beyond the supported bilayer. Individual particles diffused into the illuminated region and then back into bulk solution in control experiments using neutral pH (pH 7.3). Sindbis and influenza virus did not bind to the protein free lipid bilayers at neutral pH. For those few particles that did bind the bilayer, hemifusion/fusion was very rare at neutral pH for either virus. Of the few bound particles, only 3% of Sindbis and 7% of influenza eventually hemifused/fused when the pH was >7.0.

When the final pH was in the range 4.1–6.5, both viruses quickly bound to and efficiently hemifused/fused with the supported bilayer. We found that 60% of bound Sindbis hemifused/fused, whereas 30% of bound influenza hemifused/fused in the low-pH experiments. (These values are determined by averaging the ratio of hemifused/fused

particles to total bound particles for experiments in Fig. 2 that lie between pH 4.1 and 6.5. We find (hemifused/fused)/(total bound) = 0.6 (SD 0.05) for Sindbis and (hemifused/fused)/(total bound) = 0.30 (SD 0.12) for influenza.) This value for influenza efficiency agrees with published reports using the same influenza product from the identical supplier that found ''two-thirds of the viruses were intrinsically fusion defective'' (19).

Background-subtracted time courses of emission intensity integrated over a 1.7-μm-diameter spot centered on two Sindbis virus particles that bind to the bilayer at low pH are displayed in Fig. 3, *B* and *C*. Binding of a virus particle from solution leads to a small, localized emission emerging from the background. In the absence of lipid mixing, these particles appear as diffraction-limited spots with very low mobility. The intensity of a bound and unfused virus particle remains localized and stable for minutes (Fig. 3 *C*), unbinding only in rare cases.

Hemifusion/fusion of a bound virus particle leads to lipid mixing between the viral membrane and the bilayer. The dilution of the membrane-incorporated dye as it diffuses into the supported bilayer is reported by sudden dequenching of the dye emission by a factor of ~10. In Fig. 3, *A* and *B*, the small intensity increase due to binding of a Sindbis particle is followed by a larger intensity increase 0.2 s later that is due to membrane hemifusion/fusion (see Fig. 3 *B*, *inset*). Influenza hemifusion/fusion was similar to Sindbis (Fig. 3 *D*). Hemifusion/fusion is confirmed by the observation in the two-dimensional image data of free diffusion of the lipid dye isotropically into the bilayer away from the site of binding after the large dequenching (Fig. 3 *A* and Supplementary Material, Movie 1). The motion of the dye in the bilayer was generally consistent with diffusion using a diffusivity of ~1–2 $\mu m^2/s$ for all events measured. (Diffusion after the sudden dequenching is discussed in detail below.) In all measurements described below we confirmed hemifusion/fusion events by verifying both the sudden dequenching of the integrated intensity and visualization of the subsequent radial spreading of the membrane dye as it diffused into the supported bilayer.

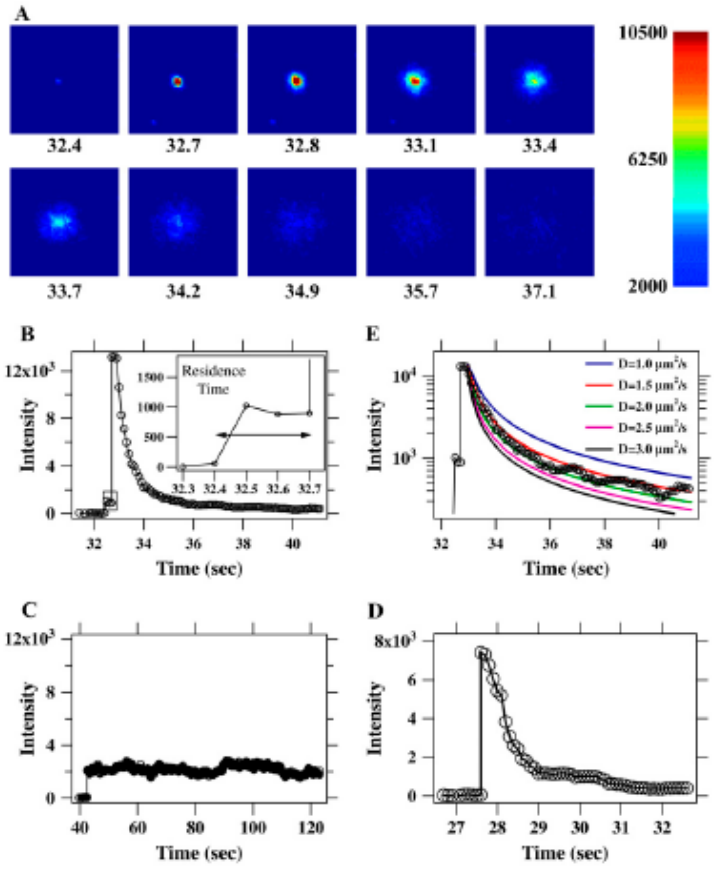

FIGURE 3 Single-particle hemifusion/fusion events. (*A*) Images extracted from a 10 frames/s movie (Movie S1) of a single Sindbis virus particle labeled with R18 dye hemifusing/fusing with a supported lipid bilayer (liver extract). The pH is 5.5 and virus has been in solution in the flow cell for ~30 s. Time in seconds is indicated under each frame. Individual dye molecules are visible in the later images as they diffuse away from the initial fusion site. The edges of the squares are 13 μm long. The image is uncorrected camera output values that have been false-colored using the jet color table (MATLAB) with the indicated pixel value mapping. (*B*) Background-subtracted intensity time course for the particle in *A*. The particle binds the supported bilayer at ~32.5 s. The particle remains attached but unfused for less than a third of a second. The interval between binding and hemifusion/fusion is indicated by a rectangle, zoomed in the inset, and denoted as the residence time. The sudden increase in intensity arises from the dequenching of the membrane dye label as it mixes with the supported bilayer after hemifusion/fusion. The dye disperses by diffusion away from the hemifusion/fusion site, leading to the slower intensity decrease. The smooth line connects the data points to guide the eye. (*C*) Intensity time course for a Sindbis virus particle on a supported lipid bilayer (liver extract) at pH 5.0 that binds but does not hemifuse/fuse. The intensity from virus particles that do not fuse is stable for much longer than is required for the dye to diffuse away after fusion events. (*D*) Intensity time course for a hemifusing/fusing influenza virus particle on a supported lipid bilayer (liver extract) at pH 4.6. (*E*) Logarithmic plot of the event from *B* overlaid with theoretical diffusion curves (see text) for varying diffusion constants, *D*. $D \approx 1.5$–$2.0\ \mu m^2/s$ fits the data.

Dynamics of sudden R18 dequenching due to lipid mixing during individual events

Lipids mixed quickly during individual hemifusion/fusion events. Using our 10-Hz imaging mode, the sudden dequenching of dye emission due to lipid mixing during fusion occurred within a single 100-ms time bin for all Sindbis fusion events. Seventy-five percent of influenza events were consistent with dequenching within a single 100-ms bin, whereas the remaining 25% extended up to three time bins (300 ms). As no lipid dye remained at the docking site after hemifusion/fusion (with the exception of a few very rare cases described below and in Movie S2), the sudden dequenching indicates that lipid mixing of the membranes occurs in <100 ms.

To further constrain the dynamics of lipid mixing during individual hemifusion/fusion events we increased the data rate to 67 frames/s (our current instrumental limit). Laser illumination intensity was increased by a factor of 3 above the value used in the 10-Hz movies to increase dye emission levels and maintain an acceptable signal/noise ratio. The brighter illumination increased the photobleaching rate. For these measurements, focusing on the short interval between binding and hemifusion/fusion, photobleaching was not a limiting factor. An example of a fusion event recorded at the 67 frames/s rate is shown in Fig. 4 *A*. Even when using 15-ms time steps, dequenching for this Sindbis virus event occurred in two frames (Fig. 4 *B*). The dequenching intervals for many events are plotted as a histogram in Fig. 4 *B*. All of these events dequenched to approximately the same final intensity as illustrated in the inset of Fig. 4 *B*. The events in this graph were derived from 10 movies using five independently prepared experiments. Only 2 out of the 51 total events exceeded the 0.2-s interval plotted here.

Following Liu et al. (29), we note that for fast kinetics the lack of synchronization of fusion events with the edge of a time bin in the detector reduces the number of events observed to transition within one time bin. Dequenching transitions due to fusion that start close to the end of one detector integration interval may finish during the following integration interval. Such events will thus span two time bins even if the inherent dynamics are faster than one time bin. Such a suppression of the first 15 ms bin in the distribution of dequenching transition times is clear in Fig. 4 *B*. The remaining bins of the histogram match a simple exponential decay with a time constant of 28 ms (or ~2 time bins). Due to the similarity of the observed dynamics to our experimental resolution, we conclude that our observation of the lifetime of states leading to lipid mixing during membrane fusion in these viral systems remains instrument-limited and that 30 ms is an upper bound.

Virus particles appeared to undergo multiple fusions in a few rare cases. These viruses would hemifuse/fuse to the bilayer, leaving behind a smaller, but still bright, center after the initial burst of diffusing dye in the bilayer dispersed and faded. Another sudden dequenching event followed by diffusion of membrane dye into the bilayer occurred a few seconds later from that bright center. In a few cases, a third hemifusion/fusion event occurred from the same spot (Movie S2). We interpret these multiple hemifusion/fusion events as being caused by aggregates of virus in which different virus particles in the aggregate hemifused/fused at different moments. It has also been suggested that aggregation may explain the observation of multiple fusions at single sites for SNARE-driven fusion of liposomes to supported bilayers (29).

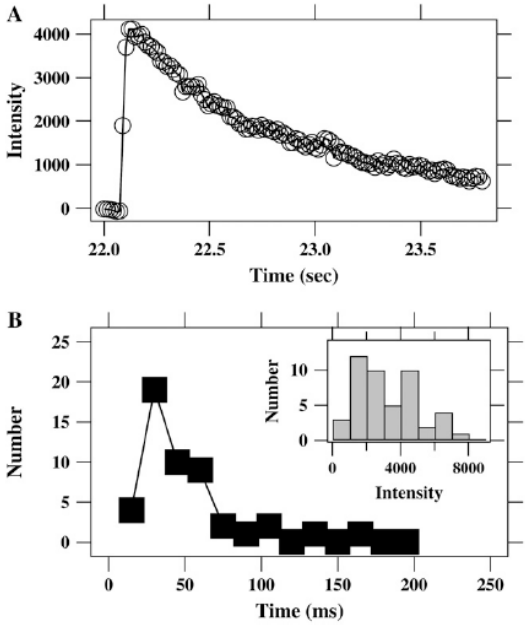

FIGURE 4 Measurements of the dynamics of lipid mixing between individual virus particles and a supported bilayer, at 15 ms/frame. (*A*) The intensity versus time for a single R18-labeled Sindbis virus particle on a supported lipid bilayer (liver extract). The particle binds the supported bilayer, then hemifuses/fuses in less than two 15-ms time steps. (*B*) A histogram of dequenching times (10–90%) for 49 of 51 fusion events taken over 10 movies from five slides (two were >200 ms). Most events occur in two time steps. Some events that are fast enough to be completed within one time bin will be counted in the group requiring two time bins, because those events may begin toward the end of one time bin and finish during the next bin. An exponential fit omitting the first time bin yields a time constant of 28 ms. The histogram in the inset displays the maximum intensity after dequenching for the fusion events analyzed in *B*. The distribution in the inset shows that the events used to measure the initial dequenching rate did not vary by more than a factor of 3–4 in final intensity, although there is some heterogeneity in the efficiency of particle labeling.

Diffusion of R18 in the supported bilayer after sudden dequenching

After sudden dequenching of the dye within the virus particles, we observed that the R18 dye spread in the supported

bilayer uniformly away from the fusion site. The concentration (number of dyes per area), $C(r,t)$, of R18 in a two-dimensional bilayer that spreads from a sudden point source of N_o molecules of dye deposited at $r = 0$ and $t = 0$ is described by $C(r,t) = (N_o/4\pi Dt)e^{-r^2/4Dt}$, where D is the diffusivity of R18 in the bilayer (57). Integration of this concentration over a circle of radius R around the initial fusion site yields a function proportional to the intensity we observe in the time traces (Fig. 3, *B* and *D*) in our experiment, $I(t) = I(0)[1 - e^{-R^2/4Dt}]$. This function is plotted in Fig. 3 *E* for $R = 1.2$ μm (our experimental parameter), along with the data from Fig. 3 *B*, as a log-linear plot for values of D ranging from 1 to 3 $\mu m^2/s$. $D \approx 1.5$–2.0 $\mu m^2/s$ fits the data well, capturing the nonexponential behavior. This diffusivity agrees with published reports of R18 mobility in bilayers (33), with our measurements of R18 diffusivity in bilayers using single-particle tracking and fluorescence recovery after photobleaching (data not shown), and also with the mobility of many different fluorescent lipid analogs in purified lipid bilayers (58,59).

We often observed a delay between the sudden dequenching due to initial lipid mixing and the eventual spreading of lipid dye by free diffusion. Such a delay is evident in Fig. 3 *B*, where a nearly constant intensity is observed for 0.3 s (three time bins) between the sudden dequenching rise and the eventual spread of dye into the bilayer by diffusion. Not all fusion events showed this sort of delay; for example, Fig. 3 *D* does not have a measurable delay between dequenching and free diffusion. Several fusion events (55% of Sindbis events and 44% of influenza events) did not have the delay at the top, whereas the remaining events showed a subdiffusive pause after the sudden dequenching. These pauses were of variable duration, with the most common delays ~0.2–0.5 s (2–5 time bins), but a few pauses extended up to ~1 s. This delay may indicate that the viral fusion proteins at a site of hemifusion/fusion alter the free flow of lipids between the viral particle and the target bilayer (60–63).

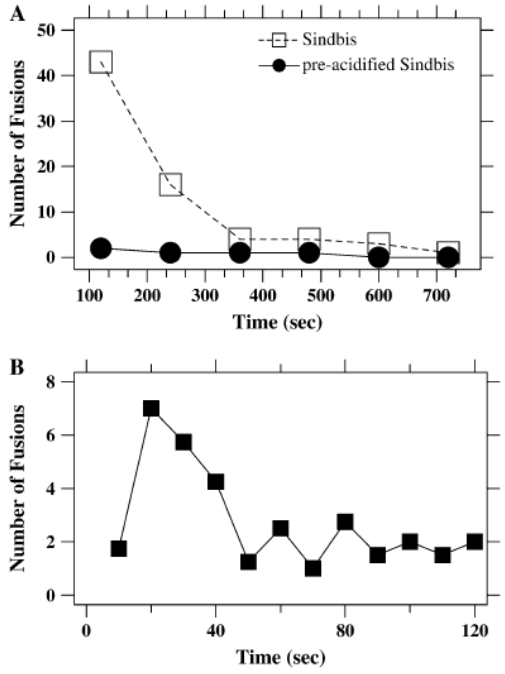

FIGURE 5 Time course of single particle-bilayer experiments. (*A*) Each of the open symbols (*dashed line*) corresponds to the total number of hemifusions/fusions observed in the preceding 2-min interval for Sindbis virus interacting with supported lipid bilayers (liver extract) at pH 4.6. Virus was introduced into the flow cell at time zero. The solid line (*solid symbols*) reports an identical measurement of virus that was exposed to pH 4.6 for 6 min before the injection into the flow cell. Sindbis loses its fusion capacity quickly after exposure to acidic conditions. (*B*) Results from a different experiment at pH 5.5 (without acid exposure to the virus before injection to the flow cell) binned into events within the preceding 10 s illustrates that the majority of lipid mixing events takes place within the first minute of the experiment. The large circles in Fig. 1 plot this same data as the cumulative number of hemifusion/fusions as a function of time.

The ensemble of particles in solution

Immediately after acidification and injection into the flow cell, we observed a burst of activity, with virus particles binding and hemifusing/fusing with the supported bilayers. After continued exposure to acidic conditions for only 1–2 min, the frequency of events leading to lipid mixing declined. Sporadic events were detected out to 12 min. By recording the time of each fusion event relative to the initial introduction of virus into the flow cell, we were able to compare the time course and parameter dependence of fusion in our bilayer assay with bulk fusion assays. As shown in Fig. 5 *A*, almost all of the fusion activity of Sindbis virus was completed within 4 min, in agreement with bulk fusion studies (21). Fig. 5 *B* displays the rate of fusion for earlier times, demonstrating that there is a burst of activity within the first half-minute of exposure to acidic conditions. In Fig. 1, the accumulation of dequenching events from the data in Fig. 5 *B* is plotted as large circles along with the bulk solution experiments. Similar overall kinetics is observed in the bulk solution and bilayer experiments, with most fusion being completed in the first minute or two although there is a small amount of fusion continuing for several more minutes.

The total number of individual hemifusion/fusion events occurring on supported bilayers within 12 min (analogous to the final extent of dequenching in bulk solution experiments) for experiments at varying pH is reported in Fig. 2 (*open symbols*). The integrated activity in bilayer experiments matches the trends observed in the final extent of dequenching for bulk fusion experiments despite the substantial difference in curvature of vesicles and supported bilayers.

The decline of the hemifusion/fusion rate is due to both the overall depletion of virus from solution due to hemifusion/fusion, as well as unfused virus in solution losing its fusion

competence after incubation in acidic conditions. In control experiments where virus was mixed with low pH for 6 min before being introduced onto the bilayer, fusion was almost completely eliminated (Fig. 5 *A*, *solid symbols*). In control experiments at neutral pH, the rate of binding and lipid-mixing events was much lower, although the few individual events that did occur could be analyzed for their detailed behavior as described in Figs. 2 and 6.

The residence time: the interval between membrane binding and membrane fusion for individual virus particles

The single-particle approach allowed us to measure the time interval between binding of an individual virus particle to the bilayer and the hemifusion/fusion of that particle to the bilayer (Fig. 3 *B*, *inset*, *arrow*). Measurements of the median of this time interval, which we call the residence time, for ensembles of fusing influenza and Sindbis particles are plotted in Fig. 6 for varying pH. Note that in our assay, viral priming and activation processes due to acidic exposure are completed before the membrane is engaged by the particles. Therefore, our residence time is not equivalent to the delay time reported in experiments where influenza fusion proteins (hemagglutinin (HA)) are prebound to a target membrane by receptor interactions at neutral pH. Those delay times, which are longer, include low-pH priming and activation steps (see Discussion). At pH near 6.9, fusion events were rare, but we were able to calculate median residence times from the few events that were observed. In most cases, hemifusion/fusion follows quickly after each virus particle binds the bilayer. Particles that hemifuse/fuse spend a median time of only ~0.2 s on the bilayer. A few virions remain stably docked on the bilayer for half a minute or longer before eventually hemifusing/fusing.

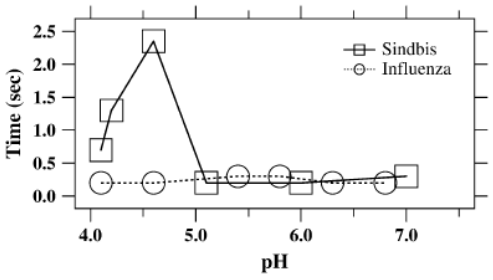

FIGURE 6 Residence times for Sindbis and influenza virus as a function of pH. The median residence time (as defined in Fig. 3 *B* and the text) accumulated from many experiments for Sindbis virus increases sharply by a factor of 10 at low pH compared to the near-constant residence time for influenza. Note that most events occur quickly after virus binds to the bilayer. No pH dependence was observed for influenza, but at the lowest pH values, the residence time for Sindbis virus increased by more than a factor of three.

The surprising exception to the short residence time is evident in Fig. 6 for Sindbis virus fusing with total liver extract bilayers below pH 5. In this particular system, the residence time was longer by more than a factor of 10. The only other condition in which longer residence times were observed was in the hemifusion/fusion to blends of purified lipids (Table 1, *last column*). The inclusion of cholesterol and sphingomyelin into mixtures of PC and PE lipids increase the residence time of Sindbis virus by a factor of 2–3 for pH 4.9.

DISCUSSION

Membrane fusion is a rapid, nonequilibrium process, and high-resolution observations of its dynamics will greatly advance our understanding of the mechanics underlying this important biological phenomenon. Membrane fusion is often described as triggerable by environmental conditions; for instance, neurotransmitter release is triggered by calcium influx during action potentials, or many viruses fuse membranes upon acidification of endosomes. In actuality, triggering is only a change of the probability (sometimes dramatically) that membranes will fuse. Even under highly promoting conditions, the occurrence of any single fusion event is still stochastically distributed. The single-particle approach is well suited to reveal the mechanistic details about protein-mediated membrane fusion because single-particle analysis avoids averaging the behavior of ensembles of particles and is therefore sensitive to the transient dynamics during membrane fusion.

Here, we describe an in vitro assay for high-precision measurements of lipid mixing during early stages of individual viruses fusing with supported lipid bilayers in response to low pH. In our assay, an ensemble of virus labeled with quenched fluorescent dye is acidified and immediately introduced into a flow cell with a protein-free, supported lipid bilayer on its surface. Particles encountered the bilayer by diffusion, so we used a fluorescence microscope to observe the bilayer for up to 12 min (Fig. 5). When particles encountered the bilayer, many bound and hemifused/fused. Lipid mixing commenced around a quarter-second after binding (Fig. 6). The sudden dequenching transitions during individual lipid mixing events were resolution-limited at 30 ms (Figs. 3 and 4). As the ensemble was monitored for the 12-min interval, the rate of individual hemifusion/fusion events decreased, largely due to the loss of fusion capacity after acidification of the virus (Fig. 5). Our assay has reproduced many results previously found in bulk solution experiments, including the pH dependence of fusion for Sindbis and influenza, the inactivation of fusion capacity by preexposure to acidic conditions, and the requirement for cholesterol and sphingomyelin in Sindbis fusion (37,39–43,45).

Our supported lipid bilayer assay differs from the bulk-solution-based fusion assays in several important aspects. In the bilayer experiments, it is clear that the virus is exposed to

low pH before encountering the target membrane. In bulk fusion experiments, this distinction is difficult to verify. The successful crystallization of low pH conformations of trimers of type 2 fusion proteins, as are present in Sindbis, required the presence of liposomes and lipidlike detergents(64,65). This biochemical result suggests that the virus might require exposure to lipids before the acidification. Our single-particle approach allows the sequence of acidification, binding, and hemifusion/fusion to be observed, and demonstrates that acidification of virus particles before lipid exposure maintains hemifusion/fusion capacity.

Criticisms of spontaneous dye transfer between virus and target membranes independent of membrane fusion (66) are avoided in our assay. Such spontaneous transfer is easily rejected in our data analysis, as it is much slower than the dequenching due to fusion (67) and also involves a much smaller percentage of dye than our complete particle fusion signals (25,26).

In bulk experiments, fusion typically occurs between virus particles and highly curved, small liposomes. Supported lipid bilayers have zero curvature and more closely approximate the geometry of physiological situations where viruses fuse to larger structures. Different energetic concerns arise related to supported lipid bilayers. Fusion of a virus particle to a supported lipid bilayer requires compression of the bilayer to accommodate the extra lipids. Also, interactions with the supporting surface will alter the energy balance between the virus particle and the target membrane. It is not clear how relevant any of these considerations are to the in vivo situation of viral entry in living cells, but the rapid, efficient hemifusion/fusion observed in our experiments suggests that these effects are not substantial barriers.

Our assay only diagnoses hemifusion between the supported lipid bilayer and the virus particle. R18 rapidly flips between the inner and outer leaflet of a labeled bilayer membrane, and therefore the complete lipid mixing between individual virus particles and the supported bilayer that we observe is expected for either arrested hemifusion or full fusion. The geometry of the supported bilayer clearly prevents the late stages of fusion from progressing naturally, as there is not room to accommodate the viral capsid between the bilayer and the solid support. It is possible that this restriction will prevent formation of the final fusion pore and limit this assay to studies of the initial lipid mixing aspects of protein-mediated membrane fusion. Further experiments will attempt to confirm full membrane continuity using an aqueous content dye or a lipid dye that asymmetrically differentiates between the inner and outer leaflets. Adaptation of our single-virus-particle assay to fusion with immobilized liposomes (our unpublished results and Yoon et al. (68)) will also address the issue of hemifusion versus full fusion in this assay.

Imaging individual events allows us to measure kinetic features of the rapid transitions during the hemifusion/fusion process. By recording time trajectories for each particle we can synchronize fusion dynamics for many particles after the data have been recorded. In this way, we directly confirm that lipid mixing occurs during individual Sindbis virus fusion events faster than 30 ms and that hemifusion/fusion rapidly follows membrane binding. Influenza hemifuses/fuses with similarly fast kinetics. Lipid mixing is complete, with no dye remaining at the fusion site after the dispersal by diffusion into the bilayer after a few seconds. Niles and Cohen (33) imaged fusion of individual influenza particles with planar lipid bilayers with results that are consistent with our measurements. They observed the initial sudden dequenching to be complete on the order of 0.1 s and the dye to radially disperse in a few seconds. Niles and Cohen also observed that the overall rate of fusion declined to zero over 3–5 min after injection into the low-pH solution around the bilayer. Our higher resolution allowed us to further constrain the upper limit of the dequenching event to 30 ms and to determine the intensity trajectory of fusion events for quantitative comparison to diffusion theory.

Diffusion theory accurately described the radial transport of the dye in the bilayer away from the initial particle attachment site after the sudden dequenching due to a lipid mixing event (Fig. 3 *E*). Careful examination of the data for the few tenths of a second between the sudden dequenching and the eventual diffusive flow revealed subdiffusive lipid spreading (Fig. 3 *B*). Other published work examining lipid mixing during membrane fusion of HA cells to red blood cells (RBC) or fusion of influenza virus to RBC (32,60,63) have also found subdiffusive lipid dye mixing. Those experiments using RBC as the target membrane saw dequenching and lipid mixing that continued for minutes. Studies of the fusion of influenza virus with protein-free bilayers found less restriction of lipid transfer than the RBC experiments, with the lipid dye dispersing at a speed consistent with free diffusion in the bilayer in a matter of seconds (33). These results led to the suggestion that the viral proteins could restrict lipid flow at a fusion site (61–63).

Our observation of a brief, subdiffusive pause between initial lipid dequenching and subsequent diffusive lipid spread in the bilayer using influenza hemifusing/fusing with protein free bilayers supports the idea that HA restricts lipid flow at a fusion site. That we observed roughly half of hemifusion/fusion events for both Sindbis virus and influenza virus with similar subdiffusive, subsecond pauses suggests that the restriction of lipid mixing by fusion proteins occurs for both type1 fusion proteins and type 2 fusion proteins, and thus supports the idea that the mechanisms of action for type 1 and type 2 fusion proteins are similar (64,65).

As a result of many different types of experimentation, a unified model of the sequence of events underlying influenza-HA-mediated membrane fusion is emerging (13,14,69,70). At neutral pH, HA on the influenza particle bind their receptor, sialic acid, which is present on glangliosides and proteins in a targeted cell membrane. After acidification of the

medium around this receptor-HA complex, HA molecules undergo conformational rearrangement into a primed, or activated, state. This activated state is metastable, and after tens of seconds to a few minutes, in the absence of membrane fusion, HA decays to a dead-end state incapable of catalyzing fusion. It is expected that activated HA trimers must aggregate until a threshold density (estimated to be ~3–8 molecules per fusion site (71,72)) is achieved that is capable of catalyzing fusion through further conformational changes. In the event that the rapid fusion transition is triggered, a number of transient intermediate structures form, including small pores capable of conducting ionic currents, hemifused stalks permitting lipid mixing between the membranes, and full fusion pore formation capable of transferring larger molecules between the two fusing compartments (10,73).

Different assays applied to influenza-HA-mediated membrane fusion are sensitive to different aspects of this overall progression. The most common assays detect fluorescence dequenching or ionic current when whole influenza virus (18,33,60,74), mammalian cells engineered to express HA on their surface (HA cells) (32,63,74–76), or purified HA reconstituted into liposomes (77) fuse with target membranes in liposomes, planar lipid bilayers, or, commonly, RBCs. Experimental configurations detect fusion of either in bulk solution or spatially resolved individual viruses or individual cells.

In assays where virus is not prebound to a target membrane, the diffusional search for a virus to encounter a target membrane typically limits fusion rates. Many assays that use neutral-pH prebinding of virus or HA-expressing cells to a target membrane via receptor interactions have found a delay between acidification and fusion, often called the lag time. The lag time is found to be ~1–5 s by stopped-flow measurements (74) or single fusion imaging of whole influenza virus fusing with RBCs (60) but lengthens to the range of 20 s to several minutes for HA cells fusing with RBCs (18,60,63,74,76). A series of experiments varying the levels of HA expression in transfected cell lines found shorter lag times as the concentration of functional HA in the membrane increased. These results led to the conclusion that at least some part of the lag time is due to diffusion and oligomerization of primed fusion proteins to a sufficient density to catalyze the fusion transition. The lag time depends upon the composition of the target membrane (52,74), the temperature (18,63), and pH (74), suggesting that the lag time may be a convolution of several different kinetic processes.

In our assay, virus is not prebound to the target bilayer. For influenza, the supported bilayer assay is easily extendable to allow prebinding by incorporating its receptor molecule, sialic acid on glycolipids, into the bilayer (18,33,34,36,75). In contrast, Sindbis cannot be prebound because the relevant receptor molecule is unconfirmed. (In the event that the receptor molecule is identified, it could likely be incorporated into a single virus bilayer fusion assay.) To allow direct comparison to Sindbis virus, we did not include influenza receptor in the bilayers. Thus, unlike the prebound experiments, virus in our assay is exposed to low pH before encountering the membrane.

We measured the time interval between bilayer binding and hemifusion/fusion for many individual virus particles. In Fig. 3 *B*, we denote this interval as the residence time. Our residence time differs from the previously described delay time for prebound experiments, because in our assay we expect that low-pH priming reactions occur while the virus is in solution. Under most conditions, for both viruses, we find that the residence time is around a quarter-second. Measurement of the residence time for Sindbis virus interacting with liposomes has previously been attempted using coflotation during density-gradient centrifugation (21). Our results qualitatively agree with these earlier experiments that found that not all virus binds to liposome, and additionally not all of the bound virus will fuse with the bilayer. However, our assay measured a much shorter delay between the binding and lipid mixing than was determined with the bulk assay. The inherent delay and insensitivity to weak binding of the centrifugation measurements may account for these differences.

The delay time observed in prebound experiments is longer than our residence time. The prebound virus experiments measure the additional delays of protonation and priming after acidification that in our assay occur before particles encounter the targeted membrane. In all cases, the dynamic transition from a primed and membrane-engaged fusion complex to lipid mixing is rapid and remains temporally unresolved by any experiment. We emphasize that our assay primes virus particles before they are bound to the membrane, the opposite of the situation in assays where virus is prebound to the target membrane at neutral pH by receptor interactions.

The residence time for Sindbis virus increased in the presence of cholesterol at the lowest pH values tested. The role of cholesterol and sphingomyelin in virus entry is complex (41). The combination of cholesterol and sphingomyelin in sufficient concentrations in membranes is known to cluster into microdomains, or lipid rafts (78,79), that some viruses including Ebola and human immunodeficiency virus (HIV) require in the target membrane for infection (80,81). Membrane fusion by influenza does not require cholesterol in the target membrane (20), although cholesterol in the viral membrane has recently been implicated to be important for HA trimerization (82). We did not observe any cholesterol dependent change in the residence time of influenza comparable to what we observed with Sindbis.

Fusion by Sindbis and other alphaviruses strictly requires cholesterol and sphingomyelin in the target membrane (21,83–85), but lipid raft formation is not relevant to this property (43). Rather, the 3β-OH group on cholesterol has been shown to be essential for low-pH binding to membranes (85), possibly by interacting with the alphavirus fusion protein E1 to stabilize an uncharacterized intermediate conformation that is essential for membrane binding (42). Any sterol with the 3β-OH group substitutes for cholesterol, and further-

more, a point mutation in E1 can eliminate this requirement, presumably by stabilizing the necessary intermediates without the sterol involvement (86,87). Although the 3β-OH group plays a specific role in binding, a fusogenic role for cholesterol cannot be ruled out (44,88).

Studies around pH 5.5 have found that small amounts (a few percent) of sphingomyelin are required in the target membrane for fusion, but not for binding of alphaviruses (89). It is also postulated that sphingomyelin interacts with E1 to facilitate conformational changes leading to membrane fusion (90). We observe that Sindbis virus fusion increases in the absence of sphingomyelin for pH well below the optimal acidic levels (Table 1). We have found that pH below the optimal partially overcomes the strict requirement for sphingomyelin to mediate fusion, but under these conditions the delay between binding and fusion increases. The specific mechanisms responsible for the delicate interplay between the fusion proteins, the lipids, and the buffer remain unknown, but the pH dependence supports the model that certain lipid species have specific interactions with the fusion proteins.

In this work, we have compared the fusion behavior of influenza and Sindbis viruses, prototypical examples of the type 1 and type 2 viral fusion protein families. In their neutral pH conformations, type 1 and type 2 proteins show little organizational similarity, but recent structural studies at low pH have led to the suggestion that these two families of proteins achieve membrane fusion by a unified mechanism (12). In our experiments, we find that the rapid lipid mixing kinetics, the residence time and a subdiffusive lipid mixing pause during hemifusion/fusion of Sindbis and influenza are similar for most conditions, supporting a common mechanism for the action of type 1 and type 2 fusion proteins. We have also identified a region of parameter space with the lowest pH and cholesterol where the delay between binding and fusion is lengthened for Sindbis but not for influenza.

To conclude, the single-particle approach is well suited for studies of membrane fusion because it overcomes difficulties associated with high-precision synchronization of independent fusion events. Continued improvements of single-particle membrane fusion assays will allow experimental access to the dynamics of transient, intermediate states that occur during any individual event. Our results on the fusion of influenza and Sindbis virus with supported bilayers emphasize the importance of quantitative, high-resolution data, as from single-particle experiments, in helping to unravel the molecular mechanisms of membrane fusion.

SUPPLEMENTARY MATERIAL

To view all of the supplemental files associated with this article, visit www.biophysj.org.

We thank Dennis Brown, Raquel Hernandez, and Gongbo Wang for assistance in producing Sindbis virus and for useful discussions.

Keith Weninger is partially supported by a Ralph E. Powe Award from Oak Ridge Associated Universities, and a Career Award at the Scientific Interface from the Burroughs Wellcome fund.

REFERENCES

1. Chen, E. H., and E. N. Olson. 2005. Unveiling the mechanisms of cell-cell fusion. *Science.* 308:369–373.
2. Chernomordik, L. V., and M. M. Kozlov. 2005. Membrane hemifusion: crossing a chasm in two leaps. *Cell.* 123:375–382.
3. Cohen, F. S., and G. B. Melikyan. 2004. The energetics of membrane fusion from binding, through hemifusion, pore formation, and pore enlargement. *J. Membr. Biol.* 199:1–14.
4. Jahn, R., T. Lang, and T. C. Sudhof. 2003. Membrane fusion. *Cell.* 112:519–533.
5. Kozlovsky, Y., and M. M. Kozlov. 2002. Stalk model of membrane fusion: solution of energy crisis. *Biophys. J.* 82:882–895.
6. Lentz, B. R., and J. K. Lee. 1999. Poly(ethylene glycol) (PEG)-mediated fusion between pure lipid bilayers: a mechanism in common with viral fusion and secretory vesicle release? *Mol. Membr. Biol.* 16:279–296.
7. Markin, V. S., and J. P. Albanesi. 2002. Membrane fusion: stalk model revisited. *Biophys. J.* 82:693–712.
8. Muller, M., K. Katsov, and M. Schick. 2003. A new mechanism of model membrane fusion determined from Monte Carlo simulation. *Biophys. J.* 85:1611–1623.
9. Siegel, D. P. 1993. Energetics of intermediates in membrane fusion: comparison of stalk and inverted micellar intermediate mechanisms. *Biophys. J.* 65:2124–2140.
10. Sollner, T. H. 2004. Intracellular and viral membrane fusion: a uniting mechanism. *Curr. Opin. Cell Biol.* 16:429–435.
11. Yang, L., and H. W. Huang. 2002. Observation of a membrane fusion intermediate structure. *Science.* 297:1877–1879.
12. Schibli, D. J., and W. Weissenhorn. 2004. Class I and class II viral fusion protein structures reveal similar principles in membrane fusion. *Mol. Membr. Biol.* 21:361–371.
13. Earp, L. J., S. E. Delos, H. E. Park, and J. M. White. 2005. The many mechanisms of viral membrane fusion proteins. *Curr. Top. Microbiol. Immunol.* 285:25–66.
14. Kielian, M., and F. A. Rey. 2006. Virus membrane-fusion proteins: more than one way to make a hairpin. *Nat. Rev. Microbiol.* 4:67–76.
15. Sieczkarski, S. B., and G. R. Whittaker. 2005. Viral entry. *Curr. Top. Microbiol. Immunol.* 285:1–23.
16. Stegmann, T., D. Hoekstra, G. Scherphof, and J. Wilschut. 1986. Fusion activity of influenza virus. A comparison between biological and artificial target membrane vesicles. *J. Biol. Chem.* 261:10966–10969.
17. Stegmann, T., I. Bartoldus, and J. Zumbrunn. 1995. Influenza hemagglutinin-mediated membrane fusion: influence of receptor binding on the lag phase preceding fusion. *Biochemistry.* 34:1825–1832.
18. Stegmann, T., J. M. White, and A. Helenius. 1990. Intermediates in influenza induced membrane fusion. *EMBO J.* 9:4231–4241.
19. Lakadamyali, M., M. J. Rust, H. P. Babcock, and X. Zhuang. 2003. Visualizing infection of individual influenza viruses. *Proc. Natl. Acad. Sci. USA.* 100:9280–9285.
20. White, J., J. Kartenbeck, and A. Helenius. 1982. Membrane fusion activity of influenza virus. *EMBO J.* 1:217–222.
21. Smit, J. M., R. Bittman, and J. Wilschut. 1999. Low-pH-dependent fusion of Sindbis virus with receptor-free cholesterol- and sphingolipid-containing liposomes. *J. Virol.* 73:8476–8484.
22. Haywood, A. M., and B. P. Boyer. 1982. Sendai virus membrane fusion: time course and effect of temperature, pH, calcium, and receptor concentration. *Biochemistry.* 21:6041–6046.
23. White, J., and A. Helenius. 1980. pH-dependent fusion between the Semliki Forest virus membrane and liposomes. *Proc. Natl. Acad. Sci. USA.* 77:3273–3277.

24. Maeda, T., K. Kawasaki, and S. Ohnishi. 1981. Interaction of influenza virus hemagglutinin with target membrane lipids is a key step in virus-induced hemolysis and fusion at pH 5.2. *Proc. Natl. Acad. Sci. USA.* 78:4133–4137.

25. Smit, J. M., G. Li, P. Schoen, J. Corver, R. Bittman, K. C. Lin, and J. Wilschut. 2002. Fusion of alphaviruses with liposomes is a non-leaky process. *FEBS Lett.* 521:62–66.

26. Hoekstra, D., T. de Boer, K. Klappe, and J. Wilschut. 1984. Fluorescence method for measuring the kinetics of fusion between biological membranes. *Biochemistry.* 23:5675–5681.

27. Melikyan, G. B., B. N. Deriy, D. C. Ok, and F. S. Cohen. 1996. Voltage-dependent translocation of R18 and DiI across lipid bilayers leads to fluorescence changes. *Biophys. J.* 71:2680–2691.

28. Leenhouts, J. M., and B. De Kruijff. 1995. Membrane potential-driven translocation of a lipid-conjugated rhodamine. *Biochim. Biophys. Acta.* 1237:121–126.

29. Liu, T., W. C. Tucker, A. Bhalla, E. R. Chapman, and J. C. Weisshaar. 2005. SNARE-driven, 25-millisecond vesicle fusion in vitro. *Biophys. J.* 89:2458–2472.

30. Fix, M., T. J. Melia, J. K. Jaiswal, J. Z. Rappoport, D. You, T. H. Sollner, J. E. Rothman, and S. M. Simon. 2004. Imaging single membrane fusion events mediated by SNARE proteins. *Proc. Natl. Acad. Sci. USA.* 101:7311–7316.

31. Bowen, M. E., K. Weninger, A. T. Brunger, and S. Chu. 2004. Single molecule observation of liposome-bilayer fusion thermally induced by soluble N-ethyl maleimide sensitive-factor attachment protein receptors (SNAREs). *Biophys. J.* 87:3569–3584.

32. Chernomordik, L. V., V. A. Frolov, E. Leikina, P. Bronk, and J. Zimmerberg. 1998. The pathway of membrane fusion catalyzed by influenza hemagglutinin: restriction of lipids, hemifusion, and lipidic fusion pore formation. *J. Cell Biol.* 140:1369–1382.

33. Niles, W. D., and F. S. Cohen. 1991. Fusion of influenza virions with a planar lipid membrane detected by video fluorescence microscopy. *J. Gen. Physiol.* 97:1101–1119.

34. Niles, W. D., and F. S. Cohen. 1991. The role of N-acetylneuraminic (sialic) acid in the pH dependence of influenza virion fusion with planar phospholipid membranes. *J. Gen. Physiol.* 97:1121–1140.

35. Melikyan, G. B., J. M. White, and F. S. Cohen. 1995. GPI-anchored influenza hemagglutinin induces hemifusion to both red blood cell and planar bilayer membranes. *J. Cell Biol.* 131:679–691.

36. Hinterdorfer, P., G. Baber, and L. K. Tamm. 1994. Reconstitution of membrane fusion sites. A total internal reflection fluorescence microscopy study of influenza hemagglutinin-mediated membrane fusion. *J. Biol. Chem.* 269:20360–20368.

37. Smit, J. M., B. L. Waarts, R. Bittman, and J. Wilschut. 2003. Liposomes as target membranes in the study of virus receptor interaction and membrane fusion. *Methods Enzymol.* 372:374–392.

38. Edwards, J., E. Mann, and D. T. Brown. 1983. Conformational changes in Sindbis virus envelope proteins accompanying exposure to low pH. *J. Virol.* 45:1090–1097.

39. Yeagle, P. L. 1985. Cholesterol and the cell membrane. *Biochim. Biophys. Acta.* 822:267–287.

40. Demel, R. A., and B. De Kruyff. 1976. The function of sterols in membranes. *Biochim. Biophys. Acta.* 457:109–132.

41. Rawat, S. S., M. Viard, S. A. Gallo, A. Rein, R. Blumenthal, and A. Puri. 2003. Modulation of entry of enveloped viruses by cholesterol and sphingolipids (Review). *Mol. Membr. Biol.* 20:243–254.

42. Chatterjee, P. K., M. Vashishtha, and M. Kielian. 2000. Biochemical consequences of a mutation that controls the cholesterol dependence of Semliki Forest virus fusion. *J. Virol.* 74:1623–1631.

43. Waarts, B. L., R. Bittman, and J. Wilschut. 2002. Sphingolipid and cholesterol dependence of alphavirus membrane fusion. Lack of correlation with lipid raft formation in target liposomes. *J. Biol. Chem.* 277:38141–38147.

44. Tenchov, B. G., R. C. Macdonald, and D. P. Siegel. 2006. Cubic phases in phosphatidylcholine-cholesterol mixtures: cholesterol as membrane ''fusogen''. *Biophys. J.* 91:2508–2516.

45. van Duyl, B. Y., D. Ganchev, V. Chupin, B. de Kruijff, and J. A. Killian. 2003. Sphingomyelin is much more effective than saturated phosphatidylcholine in excluding unsaturated phosphatidylcholine from domains formed with cholesterol. *FEBS Lett.* 547:101–106.

46. Wassall, S. R., M. R. Brzustowicz, S. R. Shaikh, V. Cherezov, M. Caffrey, and W. Stillwell. 2004. Order from disorder, corralling cholesterol with chaotic lipids. The role of polyunsaturated lipids in membrane raft formation. *Chem. Phys. Lipids.* 132:79–88.

47. Shaikh, S. R., A. C. Dumaual, A. Castillo, D. LoCascio, R. A. Siddiqui, W. Stillwell, and S. R. Wassall. 2004. Oleic and docosahexaenoic acid differentially phase separate from lipid raft molecules: a comparative NMR, DSC, AFM, and detergent extraction study. *Biophys. J.* 87:1752–1766.

48. Crane, J. M., and L. K. Tamm. 2004. Role of cholesterol in the formation and nature of lipid rafts in planar and spherical model membranes. *Biophys. J.* 86:2965–2979.

49. Veatch, S. L., I. V. Polozov, K. Gawrisch, and S. L. Keller. 2004. Liquid domains in vesicles investigated by NMR and fluorescence microscopy. *Biophys. J.* 86:2910–2922.

50. Paredes, A. M., D. Ferreira, M. Horton, A. Saad, H. Tsuruta, R. Johnston, W. Klimstra, K. Ryman, R. Hernandez, W. Chiu, and D. T. Brown. 2004. Conformational changes in Sindbis virions resulting from exposure to low pH and interactions with cells suggest that cell penetration may occur at the cell surface in the absence of membrane fusion. *Virology.* 324:373–386.

51. Bangham, A. D., M. M. Standish, and J. C. Watkins. 1965. Diffusion of univalent ions across the lamellae of swollen phospholipids. *J. Mol. Biol.* 13:238–252.

52. Bailey, A., M. Zhukovsky, A. Gliozzi, and L. V. Chernomordik. 2005. Liposome composition effects on lipid mixing between cells expressing influenza virus hemagglutinin and bound liposomes. *Arch. Biochem. Biophys.* 439:211–221.

53. Stegmann, T., S. Nir, and J. Wilschut. 1989. Membrane fusion activity of influenza virus. Effects of gangliosides and negatively charged phospholipids in target liposomes. *Biochemistry.* 28:1698–1704.

54. Haywood, A. M., and B. P. Boyer. 1985. Fusion of influenza virus membranes with liposomes at pH 7.5. *Proc. Natl. Acad. Sci. USA.* 82:4611–4615.

55. Chu, S. 2003. Biology and polymer physics at the single-molecule level. *Philos. Transact. A Math. Phys. Eng. Sci.* 361:689–698.

56. Weiss, S. 2000. Measuring conformational dynamics of biomolecules by single molecule fluorescence spectroscopy. *Nat. Struct. Biol.* 7:724–729.

57. Landau, L. D., and E. M. Lifshitz. 1987. Fluid Mechanics, 2nd ed. (Course of Theoretical Physics, Vol. 6). Pergamon Press, London.

58. Derzko, Z., and K. Jacobson. 1980. Comparative lateral diffusion of fluorescent lipid analogues in phospholipid multibilayers. *Biochemistry.* 19:6050–6057.

59. Kusumi, A., C. Nakada, K. Ritchie, K. Murase, K. Suzuki, H. Murakoshi, R. S. Kasai, J. Kondo, and T. Fujiwara. 2005. Paradigm shift of the plasma membrane concept from the two-dimensional continuum fluid to the partitioned fluid: high-speed single-molecule tracking of membrane molecules. *Annu. Rev. Biophys. Biomol. Struct.* 34:351–378.

60. Lowy, R. J., D. P. Sarkar, Y. Chen, and R. Blumenthal. 1990. Observation of single influenza virus-cell fusion and measurement by fluorescence video microscopy. *Proc. Natl. Acad. Sci. USA.* 87:1850–1854.

61. Kemble, G. W., T. Danieli, and J. M. White. 1994. Lipid-anchored influenza hemagglutinin promotes hemifusion, not complete fusion. *Cell.* 76:383–391.

62. Zimmerberg, J., R. Blumenthal, D. P. Sarkar, M. Curran, and S. J. Morris. 1994. Restricted movement of lipid and aqueous dyes through pores formed by influenza hemagglutinin during cell fusion. *J. Cell Biol.* 127:1885–1894.

63. Blumenthal, R., D. P. Sarkar, S. Durell, D. E. Howard, and S. J. Morris. 1996. Dilation of the influenza hemagglutinin fusion pore revealed by the kinetics of individual cell-cell fusion events. *J. Cell Biol.* 135: 63–71.

64. Gibbons, D. L., M. C. Vaney, A. Roussel, A. Vigouroux, B. Reilly, J. Lepault, M. Kielian, and F. A. Rey. 2004. Conformational change and protein-protein interactions of the fusion protein of Semliki Forest virus. *Nature.* 427:320–325.

65. Modis, Y., S. Ogata, D. Clements, and S. C. Harrison. 2004. Structure of the dengue virus envelope protein after membrane fusion. *Nature.* 427:313–319.

66. Ohki, S., T. D. Flanagan, and D. Hoekstra. 1998. Probe transfer with and without membrane fusion in a fluorescence fusion assay. *Biochemistry.* 37:7496–7503.

67. Nunes-Correia, I., A. Eulalio, S. Nir, N. Duzgunes, J. Ramalho-Santos, and M. C. Pedroso de Lima. 2002. Fluorescent probes for monitoring virus fusion kinetics: comparative evaluation of reliability. *Biochim. Biophys. Acta.* 1561:65–75.

68. Yoon, T. Y., B. Okumus, F. Zhang, Y. K. Shin, and T. Ha. 2006. Multiple intermediates in SNARE-induced membrane fusion. *Proc. Natl. Acad. Sci. USA.* 103:19731–19736.

69. Skehel, J. J., and D. C. Wiley. 2000. Receptor binding and membrane fusion in virus entry: the influenza hemagglutinin. *Annu. Rev. Biochem.* 69:531–569.

70. Lakadamyali, M., M. J. Rust, and X. Zhuang. 2004. Endocytosis of influenza viruses. *Microbes Infect.* 6:929–936.

71. Yang, X., S. Kurteva, X. Ren, S. Lee, and J. Sodroski. 2006. Subunit stoichiometry of human immunodeficiency virus type 1 envelope glycoprotein trimers during virus entry into host cells. *J. Virol.* 80:4388–4395.

72. Bentz, J. 2000. Minimal aggregate size and minimal fusion unit for the first fusion pore of influenza hemagglutinin-mediated membrane fusion. *Biophys. J.* 78:227–245.

73. Chernomordik, L. V., and M. M. Kozlov. 2003. Protein-lipid interplay in fusion and fission of biological membranes. *Annu. Rev. Biochem.* 72:175–207.

74. Clague, M. J., C. Schoch, and R. Blumenthal. 1991. Delay time for influenza virus hemagglutinin-induced membrane fusion depends on hemagglutinin surface density. *J. Virol.* 65:2402–2407.

75. Razinkov, V. I., G. B. Melikyan, and F. S. Cohen. 1999. Hemifusion between cells expressing hemagglutinin of influenza virus and planar membranes can precede the formation of fusion pores that subsequently fully enlarge. *Biophys. J.* 77:3144–3151.

76. Mittal, A., E. Leikina, J. Bentz, and L. V. Chernomordik. 2002. Kinetics of influenza hemagglutinin-mediated membrane fusion as a function of technique. *Anal. Biochem.* 303:145–152.

77. Imai, M., T. Mizuno, and K. Kawasaki. 2006. Membrane fusion by single influenza hemagglutinin trimers. Kinetic evidence from image analysis of hemagglutinin-reconstituted vesicles. *J. Biol. Chem.* 281:12729–12735.

78. Kenworthy, A. K. 2005. Fleeting glimpses of lipid rafts: how biophysics is being used to track them. *J. Investig. Med.* 53:312–317.

79. Rajendran, L., and K. Simons. 2005. Lipid rafts and membrane dynamics. *J. Cell Sci.* 118:1099–1102.

80. Suzuki, T., and Y. Suzuki. 2006. Virus infection and lipid rafts. *Biol. Pharm. Bull.* 29:1538–1541.

81. Nayak, D. P., and E. K. Hui. 2004. The role of lipid microdomains in virus biology. *Subcell. Biochem.* 37:443–491.

82. Sun, X., and G. R. Whittaker. 2003. Role for influenza virus envelope cholesterol in virus entry and infection. *J. Virol.* 77:12543–12551.

83. Mooney, J. J., J. M. Dalrymple, C. R. Alving, and P. K. Russell. 1975. Interaction of Sindbis virus with liposomal model membranes. *J. Virol.* 15:225–231.

84. Scheule, R. K. 1987. Fusion of Sindbis virus with model membranes containing phosphatidylethanolamine: implications for protein-induced membrane fusion. *Biochim. Biophys. Acta.* 899:185–195.

85. Kielian, M. C., and A. Helenius. 1984. Role of cholesterol in fusion of Semliki Forest virus with membranes. *J. Virol.* 52:281–283.

86. Vashishtha, M., T. Phalen, M. T. Marquardt, J. S. Ryu, A. C. Ng, and M. Kielian. 1998. A single point mutation controls the cholesterol dependence of Semliki Forest virus entry and exit. *J. Cell Biol.* 140: 91–99.

87. Lu, Y. E., T. Cassese, and M. Kielian. 1999. The cholesterol requirement for sindbis virus entry and exit and characterization of a spike protein region involved in cholesterol dependence. *J. Virol.* 73:4272–4278.

88. Chen, Z., and R. P. Rand. 1997. The influence of cholesterol on phospholipid membrane curvature and bending elasticity. *Biophys. J.* 73:267–276.

89. Nieva, J. L., R. Bron, J. Corver, and J. Wilschut. 1994. Membrane fusion of Semliki Forest virus requires sphingolipids in the target membrane. *EMBO J.* 13:2797–2804.

90. Samsonov, A. V., P. K. Chatterjee, V. I. Razinkov, C. H. Eng, M. Kielian, and F. S. Cohen. 2002. Effects of membrane potential and sphingolipid structures on fusion of Semliki Forest virus. *J. Virol.* 76:12691–12702.